5-2004

Space-Time Codes Concatenated with Turbo Codes over Fading Channels

Junghoon Suh
University of Tennessee - Knoxville

To the Graduate Council:

I am submitting herewith a dissertation written by Junghoon Suh entitled "Space-Time Codes Concatenated with Turbo Codes over Fading Channels." I have examined the final electronic copy of this dissertation for form and content and recommend that it be accepted in partial fulfillment of the requirements for the degree of Doctor of Philosophy, with a major in Electrical Engineering.

Mostofa K. Howlader, Major Professor

We have read this dissertation and recommend its acceptance:

Mongi A. Abidi, Paul B. Crilly, Daniel B. Koch. Jan Rosinski

Accepted for the Council:
Dixie L. Thompson

Vice Provost and Dean of the Graduate School

(Original signatures are on file with official student records.)

To the Graduate Council:

I am submitting herewith a dissertation written by Junghoon Suh entitled "Space-Time Codes Concatenated with Turbo Codes over Fading Channels." I have examined the final electronic copy of this dissertation for form and content and recommend that it be accepted in partial fulfillment of the requirements for the degree of Doctor of Philosophy, with a major in Electrical Engineering.

Mostofa K. Howlader
Major Professor

We have read this dissertation
and recommend its acceptance:
Mongi A. Abidi
Paul B. Crilly
Daniel B. Koch
Jan Rosinski

Accepted for the Council:
Anne Mayhew
Vice Chancellor and
Dean of Graduate Studies

(Original signatures are on file with official student records.)

Space-Time Codes Concatenated with Turbo Codes over Fading Channels

A Dissertation Presented for the
Doctor of Philosophy Degree
The University of Tennessee, Knoxville

Junghoon Suh
May 2004

Acknowledgments

There is no doubt that numerous contributions by people other than the Ph.D. candidate are necessary to accomplish any effort as big as a Ph.D. dissertation research. This dissertation is not an exception, as there are several people that should be acknowledged. First of all, I'd like to thank Dr. Howlader for all his technical and financial support during the course of my Ph.D. research. I also thank Dr. Koch for helping me settle down when I first came to the department and teaching me the communication knowledge during the course work study and the research. I also owe a large debt of gratitude to everyone else on my Ph.D. committee, Dr. Abidi, Dr. Crilly, and Dr. Rosinski who contributed many technical criticism and suggestions that found their way into the final dissertation.

My gratitude goes to close friends, Gi-dong Kim, Peter Koh, and many other church members who lavished sincere and honest advice on me whenever I asked for comfort and encouragement both in personal and professional life.

There are a couple of financial sponsor groups. I would like to thank the Wireless Communications Research Group in our department, RF Systems Group, and Spallation Neutron Source (SNS) in Oak Ridge National Lab. (ORNL) for funding my research.

My deepest gratitude and sincerest love go to my late mother, Hyunsook who prayed every day and night together with my father, Hotaek who still prays for my successful completion. I also like to acknowledge my wife as well. Without the help of my wife, Seenjung who managed to survive living in the midst of all kinds of difficulty, I would have not come this far. Finally, I thank my Lord, Jesus Christ who listened to their prayer and endowed me the strength not to give up under any circumstances.

Abstract

The uses of space-time code (STC) and iterative processing have enabled robust communications over fading channels at previously unachievable signal-to-noise ratios. Maintaining desired transmission rate while improving the diversity from STC is challenging, and the performance of the STC suffers considerably due to lack of channel state information (CSI). This dissertation research addresses issues of considerable importance in the design of STC with emphasis on efficient concatenation of channel coding and STC with theoretical bound derivation of the proposed schemes, iterative space-time trellis coding (STTC), and differential space-time codes.

First, we concatenate space-time block code (STBC) with turbo code for improving diversity gain as well as coding gain. Proper soft-information sharing is indispensable to the iterative decoding process. We derive the required soft outputs from STBC decoders for passing to outer turbo code. Traditionally, the performance of STBC schemes has been evaluated under perfect channel estimation. For fast time-varying channel, obtaining the CSI is tedious if not impossible. We introduce a scheme of calculating the CSI at the receiver from the received signal without the explicit channel estimation.

The encoder of STTC, which is generally decoded using Viterbi like algorithm, is based on a trellis structure. This trellis structure provides an inherent advantage for the STTC scheme that an iterative decoding is feasible with the minimal addition computational complexity. An iteratively decoded space-time trellis coding (ISTTC) is proposed in this dissertation, where the STTC schemes are used as constituent codes of turbo code. Then, the performance upper bound of the proposed ISTTC is derived.

Finally, for implementing STBC without channel estimation and maintaining transmission rate, we concatenate differential space-time block codes (DSTBC) with ISTTC. The serial concatenation of DSTBC or STBC with ISTTC offers improving performance, even without an outer channel code. These schemes reduce the system complexity compared to the standalone ISTTC and increase the transmission rate under the same SNR condition. Detailed design procedures of these proposed schemes are analyzed.

Contents

List of Tables

List of Figures

Chapter 1

Introduction

In the design of modern digital communication systems, the importance of coding technology has been more and more recognized among researchers in the communication field. The energy efficiency is greatly improved by the coding scheme, although the overall data rate is impaired from adding redundant parity bits into the original data line. This spectral efficiency issue can be improved by a joint coded modulation technology [1]-[4], because the design of a trellis code is built on the set partitioning scheme [2][3]. Deploying multiple antennas is another way of enhancing the data transmission rate [5][6]. The capacity grows at least linearly with the number of transmit antennas, as long as the number of receive antennas is less than or equal to the number of transmit antennas [7]. The reliable communication over fading channels is another challenge of current digital communications, especially in wireless communications. The wireless communication channel is subject to time-varying impairment such as noise, interference and multi paths, which make it hard for the receiver to reliably determine the transmitted signal unless some less attenuated replica of the signal are provided to the receiver [8]. Transmitting the replica of the signal is called diversity, which is implemented in time, frequency and space. Several diversity techniques have been proposed and employed in wireless communication systems for reliable communication over fading channels [5][7]. The research of our dissertation is focused on achieving the reliable communication and

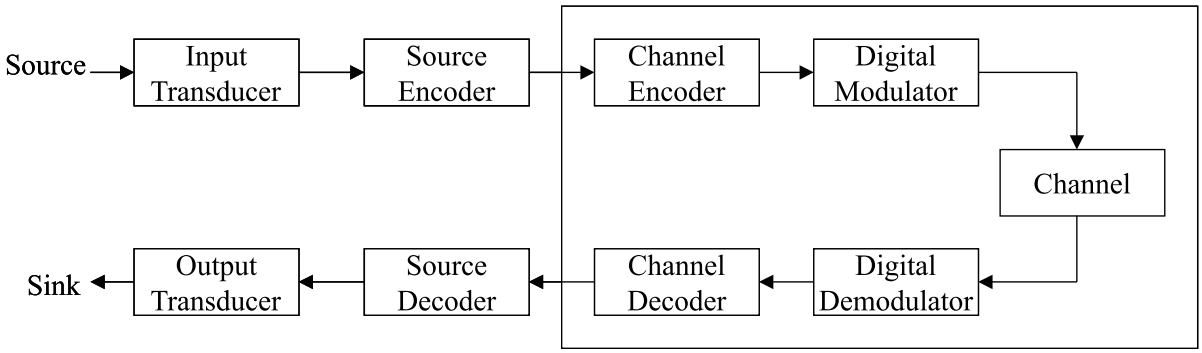

Figure 1.1: Block diagram of a digital communication system.

eventually improving the energy efficiency without affecting the bandwidth resources and system complexity.

1.1 Components of Modern Digital Communication Systems

When a digital communication system is designed, three factors, spectral efficiency, energy efficiency, and the system complexity are taken into account for trade-off. Figure 1.1 shows a simple block diagram for digital communication systems. Source and channel coding improve the energy efficiency. The spectral efficiency is improved by employing a higher order modulation scheme. The major concern of system design is to keep the optimal performance utilizing the provided power and bandwidth resources, while keeping the system complexity simple enough to minimize the cost.

Note that, for the analog sources, we assume that those have been digitized. Usually, sources are not random and contain significant amounts of redundancy. The role of source coding is to randomize these sources, that is, it eliminates the redundant information in an efficient way. A measure of randomness is entropy. The source coding increases the entropy of source information. On the other hand, some redundancy is

added to the source encoder outputs by channel coding. The channel encoder introduced an error correction capability into the source encoder output to combat channel transmission errors. But this redundancy added by channel codes are different from the original redundancy which was in the source information, in that the redundancy we add to the message by channel codes is controlled and the receiver has knowledge of the structure of this redundancy [4]. The channel coding is a good method of achieving the reliable transmission with limited transmission resources, such as power, bandwidth, and the cost of system design. Since digital bits are not appropriate for transmission over a physical channel, the digital modulator is used to transform them into a continuous waveform in time. The modulation is composed of symbol mapping, pulse shaping, and carrier multiplication. Whatever the channel medium is, the transmitted signal will be distorted in a random manner by, e.g., the thermal noise generated by electronic devices or the cosmic noise picked up by antennas [9]. The demodulator is the inverse of the modulation process, and the channel decoder detects and corrects errors occurred during the transmission over the channel. The source decoder reconstructs the original information using the knowledge of the source encoder structure. Although coding and modulation are usually treated together to improve spectral efficiency using trellis coded modulation [1]-[3], coding and modulation are normally treated separately in energy-limited wireless systems [9].

1.2 Evolution of Wireless Cellular Communications

The congestion of radio spectrum led to the proposal of cellular telephony concept. The cellular telephone systems break the whole service area into small coverage regions called 'cells'. Each cell is assigned a certain portion of total spectrum available for service and those portions of spectrum are designed to be reused, when cells using the same spectrum are located far enough. The first commercial cellular service in the United States began in Chicago in 1983 with the Advanced Mobile Phone System (AMPS), which was placed

in service by Ameritech [10][11]. The cellular telephony systems can provide service to any number of customers in theory by dividing cells into smaller and smaller areas through the process of 'cell-splitting' [12]. But, in practical and economical reason, it is impossible to build a base station each cell, and further more, the network architecture gets complicated from too frequent hand-over from one cell to another. Advances in integrated circuit design technology enabled digital communications to be employed in cellular telephony systems, which allowed greater spectral efficiency by implementing coding technology. Especially, the channel coding provides error correction capability and results in some resistance to interference that plagues analog systems.

It is around this time, early 1990's when the second generation cellular systems began services. Different from the digital cellular systems whose carrier frequency is 860 MHz, new spectrum around 1.8 GHz became available in U.S. for service. These new systems were called Personal Communication Systems (PCS), which are also implemented in digital communications. The only difference between 860 MHz digital cellular systems and PCS was the carrier frequency. Thus, 860 MHz band digital cellular systems and 1.8 GHz band PCS were in direct competition in this era with minimal service quality difference. Three multiple access standards were available for the second generation systems. Northern American Time Division Multiple Access (NA-TDMA) which has been directly evolved from AMPS was adopted as the multiple access standard by AT&T. The NA-TDMA was designed to share the same frequencies, frequency reuse plan and base stations of AMPS, so that dual mode base station equipment could support backward capability [13]. The pan European digital cellular standard, known as the Global System Mobile (GSM) was deployed in Europe in 1991. The GSM uses frequency division duplexing and a combination of 8 slots TDMA, with frequency hopping implemented to provide frequency diversity [13]. On the other hand, since the code division multiple access (CDMA) systems which Qualcomm has the original patent for were successfully employed for commercial services in Korea, the occupation of CDMA standard has been

growing fast over the world. All users transmit simultaneously at the same time and frequency in CDMA, but each user is assigned with his unique code that performs spreading of the original information spectrum. Even though all users share the same spectrum, users can be separated from each other at the receiver by the fact that all users appear to be orthogonal with one another.

The needs for the integration of these three different multiple access standards led to the conception of the third generation (3G) personal communication systems, which, we hoped, would eventually enable the global roaming and much faster data transmission rate. But, those three standards, NA-TDMA, GSM, and CDMA have evolved into UWC-136 (Universal Wireless Communications - 136), WCDMA (Wideband CDMA), and cdma2000, respectively.

There are six major service providers, Verizon, Sprint, Cingular, AT&T Wireless, Nextel, and VoiceStream (Now it is changed to T-mobile) in U.S. and majority stockholders of some of the providers are European and Japanese carriers who have already adopted W-CDMA as their 3G standard. Thus, 3G in U.S. may be heading toward both W-CDMA and cdma2000 as the platform for the next generation of mobile applications [14]. Five out of those six major carriers except for Sprint are likely to adopt W-CDMA as 3G standard. Even though Verizon implemented CDMA for 2G systems, British worldwide carrier Vodafone, which owns about 45% of Verizon would encourage Verizon to switch to W-CDMA. Shortage of spectrum may seriously undermine 3G implementation in the United States. The frequency band between 2.520 and 2.670 GHz has already been identified for 3G. However, this means that the six big carriers will have an average of somewhere between 25 MHz and 35 MHz of spectrum. In marked contrast, the big European carriers have about 90 MHz. As a result, many feel that the United States does not currently have adequate spectrum for a full-fledged nationwide implementation of 3G mobile services. The FCC has been discussing the possible allocation of the 1.710 to 1.755 GHz band, primarily used by the U.S. Department of Defense, and the 2.110 to

2.150 GHz band, which is used by schools and health care centers [14]. But, because of enormous cost required for moving these spectrum, the rollout of 3G in U.S. is getting delayed.

1.3 Space-Time Codes

Different from the Additive White Gaussian Noise (AWGN) channel, fading effect of wireless communication channels introduces serious performance degradation to digital communication systems. Under the limited resources such as the transmitter power or the size of antennas, the diversity that some less attenuated replica of the signal are provided to the receiver is the solution to combat the fading channel effect. The diversity system is implemented in time, frequency, and space. Time diversity makes the same information-bearing signal transmitted in several different time slots, where the separation between successive time slots equals or exceeds the coherence time of the channel, whereas in frequency diversity method, the same information-bearing signal is transmitted on several carriers, where the separation between successive carriers equals or exceeds the coherence bandwidth of the channel [15]. The fact that signals transmitted over different carriers induce different multipath structures and independent fading provides frequency diversity. The transmitter and/or receiver uses multiple antennas that are separated for transmission and/or reception to create independent fading channels in space diversity [5]. Recently, transmit diversity has been heavily studied to combat the signal distortion caused from the channel multipath fading effect. The same information-bearing signals are linearly arranged to be transmitted in different time slots and in multiple antennas using transmit diversity. The number of transmitters for transmit diversity is limited to two, but space-time block codes (STBC) introduces a general implementation method for any number of transmitters to obtain certain diversity gain with the help of mathematics of orthogonal design. The terms diversity gain, diversity advantage, or diversity order is used often in this dissertation, which represents

the degree of a diversity system. That is, for the same BER, the difference of SNR in decibels between the system with diversity and without the diversity. The diversity only mitigates small scale fading effects, since all diversity channels are affected identically by the large scale fading [13].

As for the space-time trellis codes (STTC), the same information-bearing signal is transmitted in space and time along a trellis and is decoded at the receiver using a Viterbi algorithm. Since STTC can be viewed as the combination of channel codes with symbol mapping onto multiple transmit antennas, it achieves the diversity gain as well as some coding gains [7]. The STTC can be used as the constituent codes of turbo codes owing to its inherent trellis coding property [16]-[18]. In this dissertation, we propose a similar scheme, the iteratively decoded space-time trellis codes (ISTTC), and derive the performance upper bound on BER. When the STTC is implemented together with STBC in series, the performance improvement is observed without changing the rate over the system with STTC only. Therefore, we also apply the iterative decoding principle into the STTC-STBC scheme (ISTTC-STBC) to achieve the improvement in both the rate and performance. Whereas the ISTTC or ISTTC-STBC are designed for flat fading channels, we combine OFDM in series with the ISTTC or ISTTC-STBC (ISTTC-OFDM with or without STBC) to overcome the frequency selective channel environment. The performance of an OFDM system under the assumption of perfect channel estimation was shown in [19]. We propose to design the ISTTC-OFDM with or without STBC under the perfect channel estimation assumption.

Reference [20] shows various ways of designing STBC from the classical mathematical framework of orthogonal designs in terms of diversity order and transmission rate. The numbers of transmit antennas are limited to 3, 5, 6 and 7 based on the full rate orthogonal design [20]. Transmission rate (R) is defined to be $R = K/T$, where K is the number of constellation symbols and T is the number of time slots, and it is called the full rate when R is 1. The number of transmit antennas is limited to 2 for the

complex orthogonal design proposed in [21] to obtain the full rate and the full diversity simultaneously, where the full diversity is defined to be the number of transmit antenna times the number of receiver antenna [7][20]. Reference [22] proposed a new design method, quasi-orthogonal design method for STBC providing higher transmission rate while sacrificing the diversity order. The complex orthogonal designs in [20] are trying to achieve the full diversity (order, 1), though they sacrifice the transmission rate. Full transmission rate is more important for very low SNR (Signal to Noise Ratio) and high BER (Bit Error Rate), whereas the full diversity is the right choice for high SNR and low BER [22].

The space-time codes (STC) require accurate channel state information (CSI) for a proper operation, but obtaining CSI is not an easy job, since fading channels are so fast variant that it is difficult to get an optimal channel model. Reference [23] proposed a transmit diversity with no channel estimation (TDNC) and [24] introduces a STBC with no channel estimation (STBCNC) for any number of transmitters. Overall system complexity will be reduced without the channel estimation. The normalized Doppler frequency, $f_d T_s$ is restricted to be less than 10^{-4} for STBCNC to work optimally, when the optimal performance is defined as 3 dB performance degradation for the system without channel estimation over the coherent system, but the concatenation of turbo codes to STBC is observed to loosen the restriction on $f_d T_s$, with the help of the interleaver in turbo codes [23]-[25]. In spite of all these benefits, the STBCNC in [23] requires the transmission of symbols known to the receiver at the beginning and hence is not truly differential. But, recently, differential space-time block coding (DSTBC) was proposed to achieve diversity gain with no channel estimation [27]-[30]. We review a DSTBC scheme according to [27] and combine it with ISTTC in this dissertation to provide diversity and considerable coding gains to the system over fading channels without extra channel codes and channel estimation.

Concatenated codes provide the desired error performance with a relatively lower overall

implementation complexity than what should be required by a single code. Therefore, we propose to concatenate turbo codes with STBC designed in various methods to obtain an improvement in coding gains in this dissertation.

1.4 Channel Codes

On the contrary to two way systems between transmitters and receivers in which automatic repeat request (ARQ) is available for error detection and retransmission, the error control scheme for one way systems is forward error correction (FEC), which detects and corrects errors at the receiver. The channel coding block in Figure 1.1 represents the FEC. The FEC has been developed from the late 1940's, based on the Shannon's mathematical ground works that set forth the theoretical basis for channel coding, better known as 'Information Theory' [31]. Whereas Shannon's 'Information Theory' puts ground works on the theoretical limits of reliable communications, the first practical FEC scheme was developed by Hamming and Golay [32][33]. The early Hamming codes collect groups of 4 information bits and map them into 7 bits codewords. But it was not efficient to add three redundant check bits for every four information bits. The binary Golay scheme gathers 12 bits and then computes 11 parity bits, which is capable of correcting up to three bits in the 23 bit codeword. Golay also proposed the ternary Golay code, which operates on ternary numbers instead of binary [34]. Thus, the general approach of Hamming and Golay codes were to group q-ary symbols (binary bits for Hamming codes) into blocks of k and then add n-k parity symbols to produce n symbol codeword [11]. The next development in FEC is 'cyclic codes'. The Hamming and Golay codes were linear codes, that is, the modulo-q sum of any two codewords is itself a codeword. Likewise, cyclic codes are linear block codes, since any cyclic shift of a codeword is also a codeword. The advantages of cyclic codes against Hamming and Golay codes are in the reduced complexity of encoders and decoders, and a simple representation of codewords by 'generator polynomial'. An important subclass of the cyclic

codes was discovered by Bose and Ray-Chaudhuri, which is known as BCH codes [35]. The binary BCH codes include Hamming and Golay codes whose correctable number of errors is bounded by $t < (2^m - 1)/2$. BCH codes were extended to non-binary case by Reed and Solomon [36]. However, Reed Solomon (RS) codes could not find practical applications until Berlekamp-Massey algorithm was proposed as an efficient decoding algorithm for RS codes [37]-[41].

Block codes have several drawbacks. Fist of all, because of the frame oriented nature of block codes, the entire codeword should be received before decoding can begin. The next drawback is that frame synchronization is required. The last drawback is hard-bit decision outputs out of block code decoders. The output of the channel is taken to be binary with hard-decision decoding, whereas the channel output is continuous-valued with soft-decision decoding. Therefore, a continuous-valued channel output is required to achieve the performance bound predicted by Shannon. Different approach from block codes, convolutional codes were introduced to overcome these drawbacks [42]. Convolutional encoders,instead of grouping data into a frame, add redundancy to a continuous stream of input data by using a shift register whose mapping from k information bits to n code bits is a function of the past data bits. Convolutional codes did not see many applications until the Viterbi algorithm (VA), the most efficient decoding algorithm of convolutional codes, had been introduced [43]. As an alternative to the maximum likelihood algorithm, VA, the maximum a posteriori (MAP) algorithm better known as BCJR algorithm named after the acronym of authors was proposed in [44].

The BCJR algorithm could not draw much attention due to its complexity only to achieve the similar performance to VA, until turbo codes were proposed by Berrou *et al.* in [45]. Turbo codes achieve the performance close to the Shannon bound with the combination of two or more convolutional codes, interleavers, and MAP iterative decoding algorithms. Several modified decoding algorithms such as soft-output VA (SOVA), or Max-Log-MAP, *etc.* have been introduced [46][47]. The claimed performance in [45] was so good that

people reacted with skepticism initially, but recently many researchers around the world have been able to reproduce and even improve the results. After the discovery of turbo codes, parallel concatenated convolutional codes, some other implementation schemes such as serial concatenated convolutional codes or hybrid concatenated convolutional codes were proposed [48]. Those schemes in [48] performs better than the parallel concatenated convolutional codes over high SNR area due to its superior distance profile, which result in lowering the error floor of turbo codes.

1.5 Outline of Dissertation

The research of this dissertation began from the fundamental ground works of STC in [7][8][20]-[23], and iterative channel codes, turbo codes. The step by step implementation of VA, and MAP decoding algorithm led to the successful implementation of turbo codes, which were effective channel codes for AWGN channel. The diversity gain obtained from STC effectively overcomes the Rayleigh fading channels, which virtually turns the fading channels into AWGN channels. At this point, our research proposed the serial concatenation of turbo codes with STC to improve coding gain of the overall system. The STTC, different from STBC, achieves slight coding gain in addition to the substantial diversity gain. The STTC will be iteratively implemented to result in much improved coding gains as well as diversity gain. For frequency selective channels, we combine the iteratively implemented STTC with OFDM.

This dissertation is organized in the order from the background research to the most recent research outcomes including the future works. In Chapter 2, we provide basic review of STC and reproduce simulation results. We study channel codes in Chapter 3 emphasizing convolutional codes and turbo codes. In Chapter 4, turbo codes are serially concatenated with STBC designed in various different schemes. We derive the soft decision equations for those STBC schemes in this Chapter. In Chapter 5, we propose new STBC schemes with no channel estimation, and also concatenate them with turbo

codes. In Chapter 6, the iteratively decoded STTC (ISTTC) are described using the STTC as an constituent code. The performance bound on BER for the ISTTC is derived in the chapter. The iterative decoding principle is applied for STTC-STBC in Chapter 7. In Chapter 8, we review the DSTBC schemes and combine them with ISTTC to achieve diversity and coding gains without channel estimation and channel codes. We combined an OFDM with the ISTTC in series to combat frequency selective channels in Chapter 9. Research contributions and future works are discussed in Chapter 10.

Chapter 2

Space-Time Codes

Recent information of the spatial and temporal characteristics on the multiple-input multiple output (MIMO) channel spawns a new type of codes, space-time codes (STC) providing improvements in system capacity and reliable communication. Several schemes using the MIMO channel model have been proposed over the last several years, among which the main classes are: Space-Time Block Codes (STBC), proposed by Alamouti [21], Space-Time Trellis Codes (STTC), proposed by Tarokh et. al. [7], and Bell Labs Layered Space-Time Architecture (BLAST), proposed by Foschini et. al. [49].
Encoding and Decoding schemes of STBC are obtained through the help of the mathematics of orthogonal design, which limits the number of transmitters and receivers to achieve full diversity at the cost of the rate. The biggest advantage of STBC is in the simplicity of system which uses only linear processing at the decoder end. Also STBC is easy to concatenate with some other forward error correction codes like convolutional codes to enhance the coding gain, even though the diversity is gained from STBC. On the other hand, STTC, itself is the combination of channel codes with symbol mapping onto multiple transmit antennas. Therefore, STTC achieves the same diversity gain as the Maximal Ratio Receive Combining (MRRC) scheme as well as some coding gains [7]. Let us delve more into these STBC and STTC schemes, starting from the flat fading MIMO channel in this chapter.

2.1 Flat Fading MIMO Channel

The flat fading MIMO channel is modeled by an NxM channel matrix A whose element represents the complex fade coefficient (channel path gains, $\alpha_{n,m}$) from the nth transmitter to the mth receiver, where N and M are the number of transmitters and receivers, respectively. In this dissertation, $\alpha_{n,m}$s are assumed to be independent with one another, and follows the Clarke's model for simulation [50][51]. The flat fading channel implies no channel induced ISI among multiple antenna elements. The fading coefficients are Rayleigh distributed, which is formed from a large number of scattering channel environments. The channel is sometimes assumed to be quasi-static such that its time coherence is greater than the duration of a symbol period. Except for the decoding algorithm without channel estimation, it is also assumed that the channel is estimated perfectly at the receiver end, that is, $\alpha_{n,m}$s are available at the receiver for decoding. The total transmit power is divided uniformly across multiple transmit antennas. The capacity of MIMO channels are originally given by Foschini and Gans [6], which is,

$$C = log_2 \det \left[I_M + (SNR/N) A^H A \right], \tag{2.1}$$

where A^H corresponds to the hermitian matrix of A, and SNR is the signal-to-noise ratio at the mth receiver. I_M is an MxM identity matrix. The following sub-sections address the details of (2.1) and the Clarke's model.

2.1.1 Capacity of Flat Fading MIMO Channels

A. Single-Input Single-Output Channel Since N and M are one, respectively, A in (2.1) is a complex scalar. Thus, the channel capacity becomes

$$C = log_2(1 + SNR|A|^2), \tag{2.2}$$

where $|A|^2$ is the normalized power characteristic of channel. The famous Shannon capacity formula in [31] for AWGN is obtained by putting A to be one.

B. Single-Input Multiple-Output Channel with MRRC For an optimal maximal ratio receiver combining (MRRC), the receiver employs linear combining with the channel fade coefficients as weights in order to maximize the SNR at the output of the combining stage. That is, while the signal components are coherently combined, the noise terms are not added coherently (noise terms across multiple receive elements are independent) [13][51]. Hence, the channel capacity for this case is

$$C = log_2 \left[1 + SNR \sum_{m=1}^{M} |\alpha_m|^2 \right], \tag{2.3}$$

where α_m is the channel path coefficient at the mth receiver.

C. Multiple-Input Single-Output Channel This channel corresponds to transmit diversity, and the channel capacity is

$$C = log_2 \left[1 + (SNR/N) \sum_{n=1}^{N} |\alpha_n|^2 \right]. \tag{2.4}$$

Here, we assume that the total transmit power is divided uniformly over N transmitters.

D. Multiple-Input Multiple-Output Channel For N=M elements, the multiple-input multiple-output (MIMO) channel corresponds to the case of N parallel channels, each of which has line-of-sight (LOS) between the nth transmitter and the mth receiver of m=n. That is, the channel matrix is the diagonal identity matrix, A=I_N. Thus, the capacity becomes,

$$C = N log_2 \left(1 + (SNR/N)\right). \tag{2.5}$$

The channel capacity of each aforementioned case increases as we go from case A to D, MIMO channel, and the channel capacity also increases in accordance with the number of transmitter and receiver [6]. The high channel capacity is indispensable for the high data transmission. Hence, the MIMO channel provides fundamental ground to design

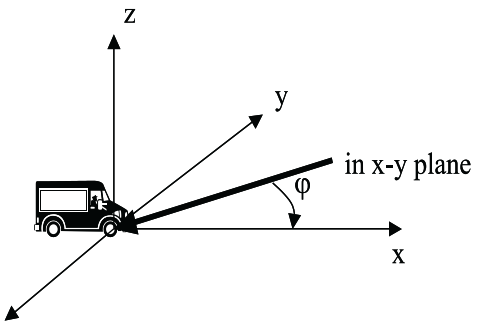

Figure 2.1: Plane waves arriving at random angles.

new coding technology for achieving our design goals of wireless communication, the high spectral efficiency (data rate, capacity), the high energy efficiency (error correction capability), and the simple system design complexity.

Before we describe the new coding technology, STC, let us go over the Clarke's model for flat fading channels.

2.1.2 Clarke's Model for Flat Fading

A flat fading channel model where the statistical characteristics of the electromagnetic fields of the received signal at the mobile are deduced from scattering is developed by Clarke [50][51]. There are several assumptions for this model. The field incident on the mobile antenna is composed of K azimuthal plane waves with arbitrary carrier phases, arbitrary azimuthal angles of arrival, and each wave having equal average amplitude, which is based on the fact that the scattered components arriving at a receiver will experience similar attenuation over small-scale distances in the absence of a direct line-of-sight path. The other one is the flat fading assumption that no excess delay due to multipath is assumed for any of the waves.

Figure 2.1 shows a diagram of plane waves incident on a mobile traveling at a velocity v, in the x-direction. The angle of arrival is measured in the x-y plane with respect to the

direction of motion. For the jth wave arriving at an angle φ_j to the x-axis, the Doppler shift in Hertz is given by

$$f_j = \frac{v}{\lambda} cos\varphi_j, \tag{2.6}$$

where λ is the wavelength of the incident wave.

The E and H field components for the incident plane waves are

$$\begin{array}{rcl} E_z & = & E_0 \sum_{j=1}^{K} C_j cos(2\pi f_c t + \theta_j), \\ H_x & = & -\frac{E_0}{\eta} \sum_{j=1}^{K} C_j sin\varphi_j cos(2\pi f_c t + \theta_j), \\ H_y & = & -\frac{E_0}{\eta} \sum_{j=1}^{K} C_j cos\varphi_j cos(2\pi f_c t + \theta_j), \end{array} \tag{2.7}$$

where E_0 is the real amplitude of local average E-field (constant), C_j is a real random variable representing the amplitude of individual waves, η is the intrinsic impedance of free space, and f_c is the carrier frequency. The random phase of the nth arriving component θ_j is given by

$$\theta_j = 2\pi f_j t + \phi_j. \tag{2.8}$$

Based on the analysis of Rice [52][53], the E-field in (2.7) can be expressed in an in-phase and quadrature form

$$E_z = T_c(t) cos(2\pi f_c t) - T_s(t) sin(2\pi f_c t), \tag{2.9}$$

where $T_c(t)$ and $T_s(t)$ are $E_0 \sum_{j=1}^{K} C_j cos(2\pi f_j t + \phi_j)$ and $E_0 \sum_{j=1}^{K} C_j sin(2\pi f_j t + \phi_j)$, respectively. The envelope of the E-field in (2.9) is given by

$$|E_z| = \sqrt{T_c^2(t) + T_s^2(t)} = r(t). \tag{2.10}$$

Since $T_c(t)$ and $T_s(t)$ are Gaussian random processes, the random received signal envelope r has a Rayleigh distribution given through a Jacobean transformation as

$$p(r) = \begin{cases} \frac{r}{\sigma^2} exp\left(-\frac{r^2}{2\sigma^2}\right) & 0 \leq r \leq \infty \\ 0 & r < 0 \end{cases} \tag{2.11}$$

where $\sigma^2 = E_0^2/2$.

A spectrum analysis for Clarke's model was developed by Gans in [54]. The spectrum

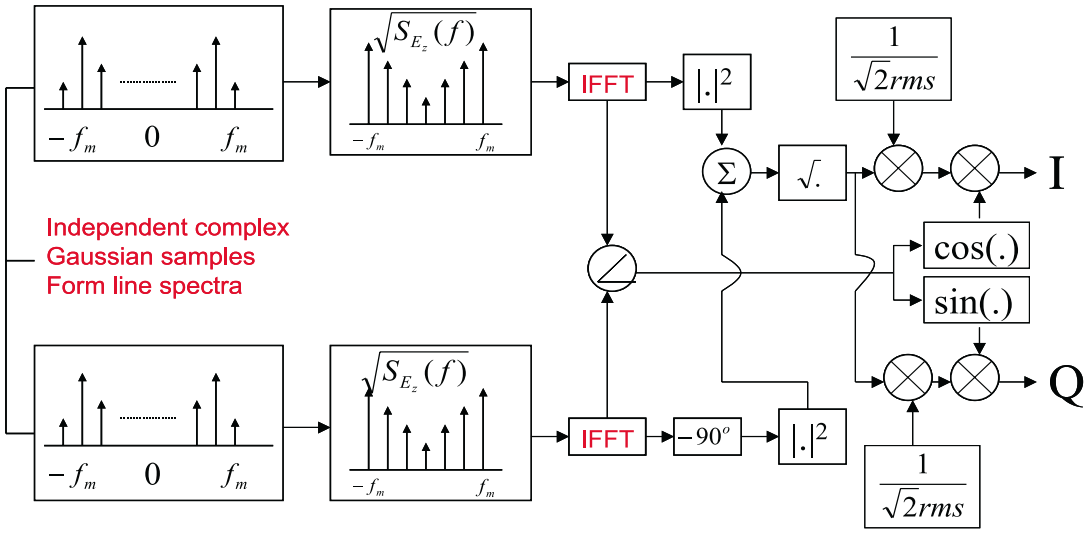

Figure 2.2: Frequency domain implementation of a Rayleigh fading simulator at baseband.

is centered on the carrier frequency and is zero outside the limits of $f_c \pm f_m$, where f_m is the maximum Doppler frequency shift. For the case of a vertical $\lambda/4$ antenna, and a uniform distribution of power $p(\varphi) = 1/2\pi$ over 0 to 2π, the output spectrum is given as [51]

$$S_{E_z}(f) = \frac{1.5}{\pi f_m \sqrt{1 - \left(\frac{f - f_c}{f_m}\right)^2}}. \tag{2.12}$$

A computer simulation program implementing flat fading channels with Doppler frequency effect was demonstrated by Smith in [55]. A complex Gaussian random number generator produces a baseband line spectrum with complex weights, and then multiplied with a discrete frequency representation of $\sqrt{S_{E_z}(f)}$. To implement the simulator shown in Figure 2.2, the following procedures are used:

A. Specify the number of frequency domain points (N_s) used to represent $\sqrt{S_{E_z}(f)}$ and the maximum Doppler frequency shift (f_m). The value N_s is usually a power of 2.

B. Compute the frequency spacing between adjacent spectral lines as $\Delta f = 2f_m/(N_s - 1)$. This defines the time duration of a fading waveform, $T = 1/\Delta f$.

C. Generate complex Gaussian random variables for each of the $N_s/2$ positive frequency components of the noise source.

D. Construct the negative frequency components of the noise source by conjugating positive frequency values and assigning these at negative frequency values.

E. Multiply the in-phase and quadrature noise sources by the fading spectrum $\sqrt{S_{E_z}(f)}$.

F-a. Perform an IFFT on the resulting frequency domain signals from the in-phase and quadrature arms to get two N_s-length time series, and add the squares of each signal point in time to create an N_s-point time series like under the radical of equation (2.10).

F-b. Since the upper flow and the lower flow in Figure 2.2 are in-phase and quadrature phase with each other, we take the angle between two components per each point.

G. Take the square root of the sum obtained in step **F-a** to obtain an N_s point time series of a simulated Rayleigh fading signal with the proper Doppler spread and time correlation.

H. Multiply $1/(\sqrt{2}rms)$ to the outputs of step **G**, where rms is the root mean square value of each output of step **G**.

I. Take a *cos* of each angle point obtained out of the step **F-b**, and multiply it to the output of step **H** to get the in-phase component of Rayleigh fading channel coefficient. Take a *sin* of each angle point obtained out of the step **F-b**, and multiply it to the output of step **H** to get the quadrature phase component of Rayleigh fading channel coefficient. The I and Q in Figure 2.2 represent the in-phase and quadrature phase components of Rayleigh fading simulation outputs.

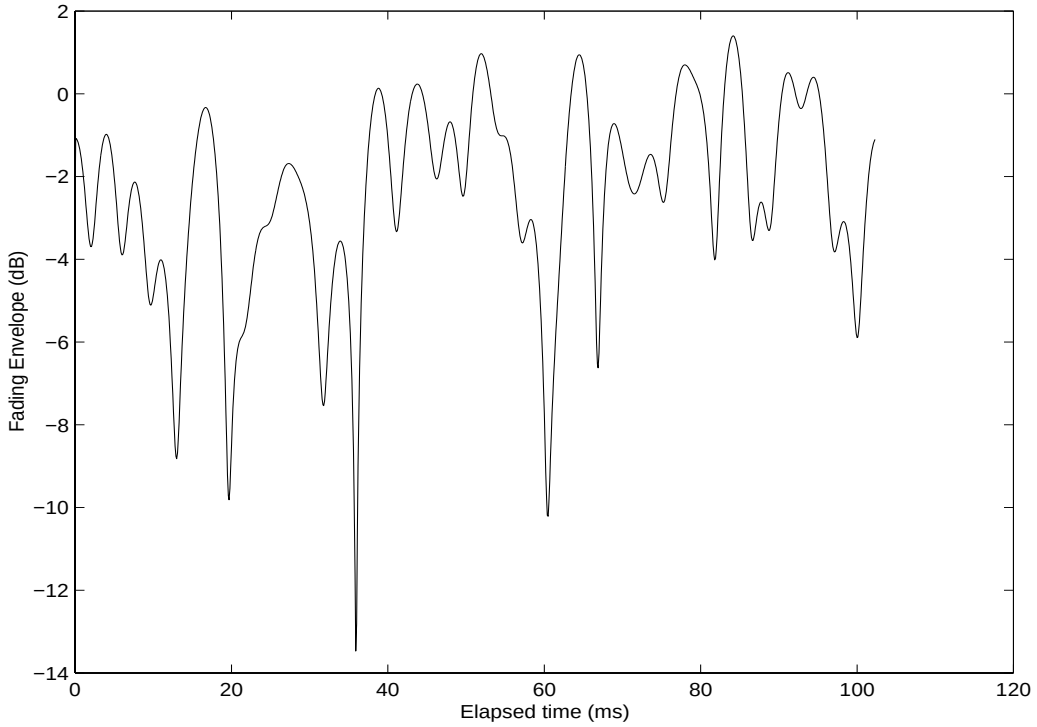

Figure 2.3: A typical Rayleigh fading envelope with $f_d T_s$, 0.01.

A simulation result according to the aforementioned simulation procedure is shown in Figure 2.3. A Rayleigh fading envelope in dB is plotted over the elapsed time in *ms*. The parameters for this simulation in Figure 2.3 are the normalized Doppler frequency $f_d T_s$, 0.01, sampling points N_s, 10^3, and sampling frequency f_s, 10^4.

2.2 Space-Time Block Codes

A space-time block codes (STBC) can be generally represented by a TxN transmission matrix G, where T is the number of time slots for transmitting one block of symbols and N is the number of transmit antennas. In this chapter, various STBC design schemes will be introduced through the help of orthogonal design mathematics. Since the transmit diversity is a special case of STBC, let us begin this chapter by reviewing the transmit

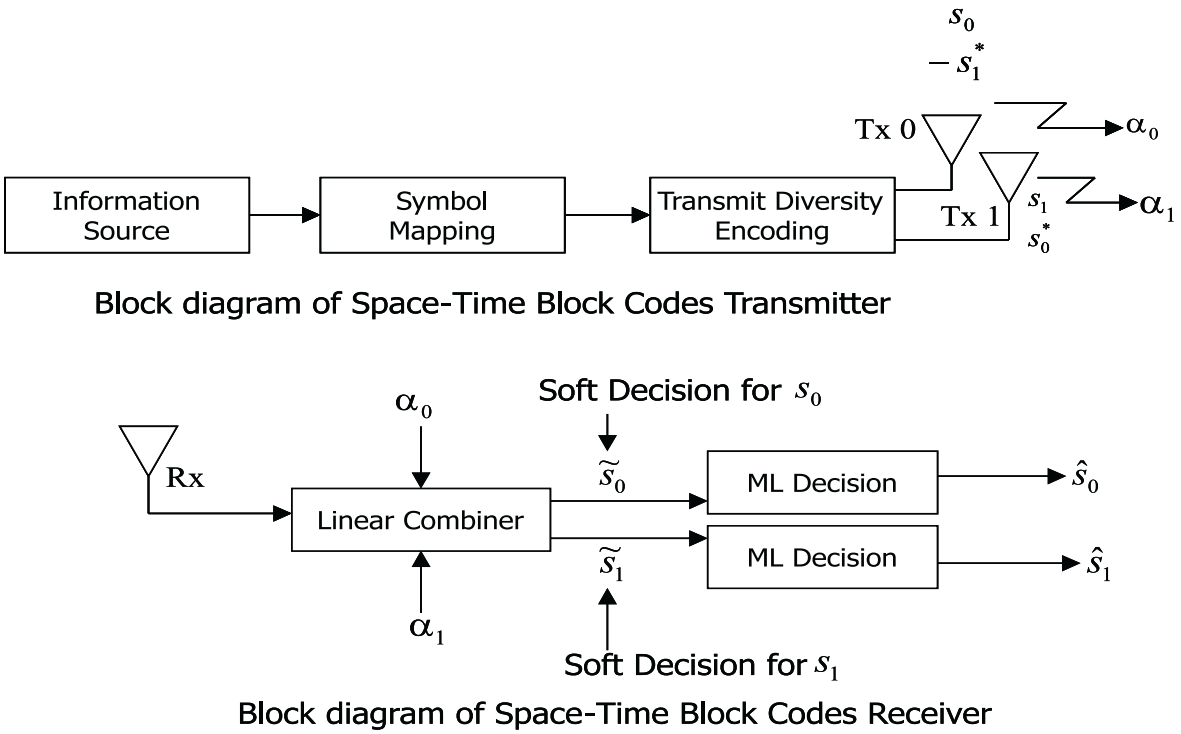

Figure 2.4: Block diagram of transmit diversity transmitter and receiver.

diversity.

2.2.1 Transmit Diversity Review

The transmit diversity (it is also called 'Alamouti Scheme') is the scheme that STBC is designed in complex orthogonal method using two transmit antennas to achieve full transmission rate and full diversity.

Figure 2.4 shows the block diagram of a transmit diversity scheme with two transmitters and one receiver. Channel path gains between transmitters and the receiver are denoted as α_0 and α_1. Assuming that the fading channel is constant across two consecutive symbols, the received signal at time t and $t + \tau$ is denoted as r_0 and r_1 at the receiver

end, where τ represents one symbol period.

$$\begin{aligned} r_0 &= \alpha_0 s_0 + \alpha_1 s_1 + \eta_0, \\ r_1 &= -\alpha_0 s_1^* + \alpha_1 s_0^* + \eta_1, \end{aligned} \tag{2.13}$$

where η_0 and η_1 represent zero mean complex AWGN. Two symbol signals passed through QPSK symbol mapping are simultaneously transmitted from two transmitters at a given symbol period. Once s_0 and s_1 are denoted as symbols transmitted from transmitter 0 and transmitter 1, respectively, then -s_1^* and s_0^* are transmitted from transmitter 0 and 1 over the next symbol period.

Two outputs of *Linear Combiner* at the receiver are denoted as $\tilde{s}_0$ and $\tilde{s}_1$ as follows,

$$\begin{aligned} \tilde{s}_0 &= \alpha_0^* r_0 + \alpha_1 r_1^*, \\ \tilde{s}_1 &= \alpha_1^* r_0 - \alpha_0 r_1^*. \end{aligned} \tag{2.14}$$

For two receivers case, we can define the received signal at time t and $t+\tau$ to be $r_{0,0}$ and $r_{1,0}$ at receiver 0, and $r_{0,1}$ and $r_{1,1}$ at receiver 1. Channel path gains between the nth transmitter and the mth receiver also can be denoted as $\alpha_{n,m}$. Then the received signals are

$$\begin{aligned} r_{0,0} &= \alpha_{0,0} s_0 + \alpha_{1,0} s_1 + \eta_{0,0}, \\ r_{1,0} &= -\alpha_{0,0} s_1^* + \alpha_{1,0} s_0^* + \eta_{1,0}, \\ r_{0,1} &= \alpha_{0,1} s_0 + \alpha_{1,1} s_1 + \eta_{0,1}, \\ r_{1,1} &= -\alpha_{0,1} s_1^* + \alpha_{1,1} s_0^* + \eta_{1,1}, \end{aligned} \tag{2.15}$$

where $\eta_{0,0}$ and $\eta_{1,0}$ represent zero mean complex AWGN at time t and $t+\tau$ for receiver 0, and $\eta_{0,1}$ and $\eta_{1,1}$ for receiver 1. Hence, two outputs $\tilde{s}_0$ and $\tilde{s}_1$ are given as [21]

$$\begin{aligned} \tilde{s}_0 &= \alpha_{0,0}^* r_{0,0} + \alpha_{1,0} r_{1,0}^* + \alpha_{0,1}^* r_{0,1} + \alpha_{1,1} r_{1,1}^*, \\ \tilde{s}_1 &= \alpha_{1,0}^* r_{0,0} - \alpha_{0,0} r_{1,0}^* + \alpha_{1,1}^* r_{0,1} - \alpha_{0,1} r_{1,1}^*. \end{aligned} \tag{2.16}$$

For PSK signals, the decision rule may be simplified to choose $\mathbf{s_i}$ iff

$$d^2(\tilde{\mathbf{s}}_\mathbf{0}, \mathbf{s_i}) \leq d^2(\tilde{\mathbf{s}}_\mathbf{0}, \mathbf{s_k}) \tag{2.17}$$

, for all $\mathbf{i} \neq \mathbf{k}$.

Figure 2.5 shows the BER performance comparison of coherent QPSK with MRRC (Maximal Ratio Receiver Combining: Combining the received signals transmitted from

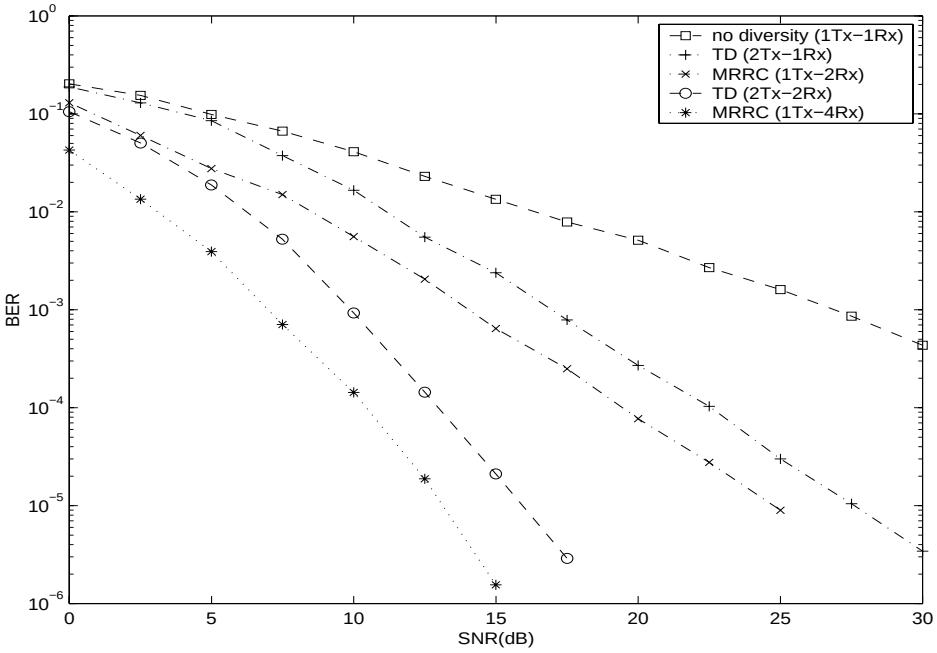

Figure 2.5: BER performance comparison of coherent QPSK between MRRC and transmit diversity in Rayleigh fading.

Table 2.1: QPSK Symbol Mapping I

Index s_t	Bits u_0u_1	Modulation $I_t = I(s_t)$
0	0 0	$\frac{1}{\sqrt{2}} + j\frac{1}{\sqrt{2}}$
1	1 0	$-\frac{1}{\sqrt{2}} + j\frac{1}{\sqrt{2}}$
2	1 1	$-\frac{1}{\sqrt{2}} - j\frac{1}{\sqrt{2}}$
3	0 1	$\frac{1}{\sqrt{2}} - j\frac{1}{\sqrt{2}}$

one transmitter,at the multiple receiver antennas using the linear combination), with the no-diversity system, and with the transmit diversity in Rayleigh fading channel environment. Although the transmit diversity is supposed to show the same diversity gain as MRRC, it is observed that there is about 3dB penalty for using transmit diversity opposed to using MRRC. That is because the total transmitted power is equally split among those two transmitter antennas, resulting in 3 dB reduced SNR.

We did not take the Doppler frequency effect into account for Rayleigh fading channel for this simulation. Since the statistics for the envelope of channel impulse response is a Rayleigh distribution where the channel impulse response is a complex Gaussian random process, we generate zero mean complex Gaussian random numbers with variance 0.5 for the channel information, $\alpha_{n,m}$. Since we perform a baseband simulation, QPSK modulation symbol mapping is done as in Table 2.1. From Table 2.1, the energy per symbol E_s is obtained as

$$E_s = \frac{1}{2}|I_n|^2 = \frac{1}{2}.$$

For no ISI continuous time channel with unit energy square root Nyquist pulses and a matched filter receiver, the symbol pulse energy E_s is $\frac{1}{2}$ and the noise variance (Equivalent baseband representation of white noise) at the output of the matched filter is

$$\sigma_\eta^2 = N_0 = \frac{E_s}{E_s/N_0} = \frac{1}{2E_s/N_0},$$

where $\frac{N_0}{2}$ is two sided spectral density of white noise. Hence, the noise variance σ_η^2 is $1/(2SNR)$. For N transmitters, the variance becomes $N/(2SNR)$. This fact makes the 3 dB difference in performance between MRRC and transmit diversity.

We also need to explain how we obtained the MRRC results in Figure 2.5. When we denote the channel between the transmitter and the ith receiver to be α_i, and the received signal at the ith receiver to be r_i, then the baseband received signal is

$$r_i = \alpha_i s_0 + \eta_i, \tag{2.18}$$

where η_i is AWGN at the ith receiver. Hence, the receiver combining scheme for total M receivers is as follows:

$$\tilde{s}_0 = \alpha_0^* r_0 + \alpha_1^* r_1 + ... + \alpha_M^* r_M. \tag{2.19}$$

Therefore, the decision rule for PSK signals is to choose s_i iff

$$d^2(\tilde{s}_0, s_i) \leq d^2(\tilde{s}_0, s_k) \tag{2.20}$$

, for all $i \neq k$.

2.2.2 STBC Designed in Orthogonal Method

A Space-Time Block Code (STBC) can be generally represented by a T x N transmission matrix G, where T is the number of time slots needed for transmitting symbols processed repeatedly together and N is the number of transmit antennas [8][20][22]. The rate R of G is defined as K/T, where K represents the number of constellation symbols in G. R is the relative concept to the maximum possible rate of a full-diversity code which is less than or equal to one ($R \leq 1$) [7][22].

We consider a wireless communication system with N transmission antennas and M receiver antennas. The channel is assumed to be quasi-static so that the path gains, $\alpha_{n,m}$ from n^{th} transmit antenna to m^{th} receiver antenna, are constant over a time frame

of length T and vary from one frame to another. The channel is also assumed to be flat fading. The received signal $r_{t,m}$ at the receiver antenna m and at the receiving time t is given by

$$r_{t,m} = \sum_{n=0}^{N-1} \alpha_{n,m} C_{t,n} + \eta_{t,m}. \tag{2.21}$$

The real and imaginary part of $\eta_{t,m}$ have equal variance $N/(2SNR)$, assuming the energy of each symbol is $1/2$ in baseband.

We consider that a maximum-likelihood receiver decides erroneously in favor of a signal, $e_{t,n}$, assuming that signals $C_{t,n}$, $n = 0, 2, ..., N-1$ and $t = 0, 1, ..., l-1$ are transmitted simultaneously from the nth transmit antennas at each time slot, t [7][20]. Then, for a block of data of length l, we define the NxN error matrix A as

$$A(C, e) = \sum_{l=0}^{l-1} (C_l - e_l)(C_l - e_l)^* \tag{2.22}$$

where $(.)^*$ denotes the conjugate operation for scalars and the conjugate transpose for matrices and vectors [5]. References [7] and [20] introduce the following diversity criterion that the matrix, A must be full rank for any pair of distinct codewords C and e in order to achieve the maximum diversity MN. If $A(C, e)$ has minimum rank r over those pairs of distinct codewords, then a diversity of rM is achieved.

For the STBC designed in orthogonal methods where the columns of transmission matrices are orthogonal, we describe the encoding and decoding algorithm in detail.

A. Encoding Algorithm T x N, a Space-Time Block Code matrix, G is composed of linear combinations of constellation symbols $s_0, s_1, ..., s_{K-1}$ and their conjugates. Each symbol is formed by log_2^{MPSK} bits, where $MPSK$ represents the number of symbol constellations according to the modulation method. Encoding only requires linear processing, because elements of G are linear combinations of constellation symbols and their conjugates. It is required that

$$G^H G = \left(|x_1|^2 + ... + |x_K|^2 \right) I,$$

where G^H is the Hermitian of G and I is the NxN identity matrix.

At the first time frame, the first row of G is transmitted through all transmitters at the same time, where each column of G represents each transmitter. The number of rows, T, represents the total number of time slots transmitting all K symbols. For instance, two transmitter codes achieving full rate and full diversity are represented in G_2 and the rate 1/2 codes using three transmitters achieving full diversity can be given in G_3 as follows,

$$G_2 = \begin{bmatrix} s_0 & s_1 \\ -s_1^* & s_0^* \end{bmatrix}, \quad G_3 = \begin{bmatrix} s_0 & s_1 & s_2 \\ -s_1 & s_0 & -s_3 \\ -s_2 & s_3 & s_0 \\ -s_3 & -s_2 & s_1 \\ s_0^* & s_1^* & s_2^* \\ -s_1^* & s_0^* & -s_3^* \\ -s_2^* & s_3^* & s_0^* \\ -s_3^* & -s_2^* & s_1^* \end{bmatrix}. \tag{2.23}$$

As we see from Equation (2.23), G_2 is the same scheme as transmit diversity described in section 2.2.1.

B. Decoding Algorithm For a known channel state information, the decision metric at the receiver is given by,

$$\arg\min_{s_x} \sum_{m=0}^{M-1} \sum_{t=0}^{T-1} \left| r_{t,m} - \sum_{n=0}^{N-1} \alpha_{n,m} C_{t,n} \right|^2 \tag{2.24}$$

over all possible s_x. This maximum likelihood decoding is achieved only using linear processing at the receiver, which makes the decoder simple in complexity. Let us illustrate the decoding process by an STBC designed in the complex orthogonal method with two transmitters, G_2 of Equation (2.23) [8][26].

The maximum likelihood decision of metric (2.24) for G_2 is expanded as

$$\sum_{m=0}^{M-1} \left[|r_{0,m}|^2 - 2A_1 + A_2 + |r_{1,m}|^2 - 2B_1 + B_2 \right], \tag{2.25}$$

where

$$\begin{aligned} A_1 &= r^*_{0,m} \sum_{n=0}^{1} \alpha_{n,m} C_{0,n} + r_{0,m} \left(\sum_{n=0}^{1} \alpha_{n,m} C_{0,n} \right)^*, \\ A_2 &= \left| \sum_{n=0}^{1} \alpha_{n,m} C_{0,n} \right|^2, \\ B_1 &= r^*_{1,m} \sum_{n=0}^{1} \alpha_{n,m} C_{1,n} + r_{1,m} \left(\sum_{n=0}^{1} \alpha_{n,m} C_{1,n} \right)^*, \\ B_2 &= \left| \sum_{n=0}^{1} \alpha_{n,m} C_{1,n} \right|^2. \end{aligned} \tag{2.26}$$

Using the following properties of complex numbers

$$\begin{aligned} |xy| &= |x||y|, \\ |x-y|^2 &= |x|^2 - 2(x^*y + xy^*) + |y|^2, \\ (x+y)^* &= (x^* + y^*), \end{aligned} \tag{2.27}$$

deleting the terms ($|r_{0,m}|^2$ and $|r_{1,m}|^2$) that are independent of codewords, and using the following relation

$$A_2 + B_2 = 2(|s_0|^2 + |s_1|^2) \sum_{n=0}^{1} |\alpha_{n,m}|^2, \tag{2.28}$$

we can get the decision metric as

$$\sum_{m=0}^{M-1} \left[-(AA + BB) + (|s_0|^2 + |s_1|^2) \sum_{n=0}^{1} |\alpha_{n,m}|^2 \right], \tag{2.29}$$

where

$$\begin{aligned} AA &= r_{0,m} \alpha^*_{0,m} s^*_0 + r^*_{0,m} \alpha_{0,m} s_0 + r_{1,m} \alpha^*_{1,m} s_0 + r^*_{1,m} \alpha_{1,m} s^*_0, \\ BB &= r_{0,m} \alpha^*_{1,m} s^*_1 + r^*_{0,m} \alpha_{1,m} s_1 - r_{1,m} \alpha^*_{0,m} s_1 - r^*_{1,m} \alpha_{0,m} s^*_1. \end{aligned} \tag{2.30}$$

The metric (2.29) decomposes into two parts, one of which

$$\sum_{m=0}^{M-1} \left[-AA + |s_0|^2 \sum_{n=0}^{1} |\alpha_{n,m}|^2 \right] \tag{2.31}$$

is only a function of s_0, and the other one

$$\sum_{m=0}^{M-1} \left[-BB + |s_1|^2 \sum_{n=0}^{1} |\alpha_{n,m}|^2 \right] \tag{2.32}$$

is only a function of s_1.

Adding terms, $|r_{0,m}\alpha^*_{0,m} + r^*_{1,m}\alpha_{1,m}|^2$ that are independent of codewords and mul-

tiplying an integer, 2 to the decision metric (2.31) do not affect the overall performance. Thus, the metric (2.31) becomes

$$\begin{array}{l}\sum_{m=0}^{M-1}[|r_{0,m}\alpha_{0,m}^{*}+r_{1,m}^{*}\alpha_{1,m}|^{2}-2\{r_{0,m}\alpha_{0,m}^{*}s_{0}^{*}+r_{0,m}^{*}\alpha_{0,m}s_{0}+r_{1,m}\alpha_{1,m}^{*}s_{0}+r_{1,m}^{*}\alpha_{1,m}s_{0}^{*}\} \\ +|s_{0}|^{2}-|s_{0}|^{2}+|s_{0}|^{2}\sum_{n=0}^{1}|\alpha_{n,m}|^{2}] \\ =\sum_{m=0}^{M-1}[|\{r_{0,m}\alpha_{0,m}^{*}+r_{1,m}^{*}\alpha_{1,m}\}-s_{0}|^{2}+(-1+\sum_{n=0}^{1}|\alpha_{n,m}|^{2})|s_{0}|^{2}].\end{array} \tag{2.33}$$

In the same way, the metric (2.32) is obtained as

$$\sum_{m=0}^{M-1}[|\{r_{0,m}\alpha_{1,m}^{*}-r_{1,m}^{*}\alpha_{0,m}\}-s_{1}|^{2}+(-1+\sum_{n=0}^{1}|\alpha_{n,m}|^{2})|s_{1}|^{2}]. \tag{2.34}$$

For PSK systems, the second terms in Equation (2.33) and (2.34) are constant for all symbols case. Thus, the outputs of linear combiner at the receiver end of a STBC system are computed as

$$\begin{array}{rcl}\tilde{s}_{0} & = & \sum_{m=0}^{M-1}\left\{r_{0,m}\alpha_{0,m}^{*}+r_{1,m}^{*}\alpha_{1,m}\right\}, \\ \tilde{s}_{1} & = & \sum_{m=0}^{M-1}\left\{r_{0,m}\alpha_{1,m}^{*}-r_{1,m}^{*}\alpha_{0,m}\right\}.\end{array} \tag{2.35}$$

It is no wonder that Equation (2.35) is observed to be equal to Equations (2.14) and (2.16), since G_2 scheme is the matrix form of transmit diversity.

Hence, the decision rule for *Maximum Likelihood Decoder* may be simplified to choose $\mathbf{s_i}$ for PSK systems,

$$iff \quad d^{2}(\tilde{\mathbf{s}}_{\mathbf{x}},\mathbf{s_i})\leq d^{2}(\tilde{\mathbf{s}}_{\mathbf{x}},\mathbf{s_k}), \tag{2.36}$$

for all $\mathbf{i}\neq\mathbf{k}$. $\tilde{s}_x$ represents either $\tilde{s}_0$ or $\tilde{s}_1$. Since the output of STBC decoder, $\tilde{s}_x$ is in the form of soft information, this is passed to the turbo decoder for coding gain improvement, when STBC is concatenated by turbo codes [5][25][56].

The soft output, $\tilde{s}$ for G_3 also can be obtained in the same way as for G_2 scheme. Hence, for PSK systems, $\tilde{s}$ for G_3 is acquired as

$$\begin{array}{l}\tilde{s}_{0}=\sum_{m=0}^{M-1}(r_{0,m}\alpha_{0,m}^{*}+r_{1,m}\alpha_{1,m}^{*}+r_{2,m}\alpha_{2,m}^{*}+r_{4,m}^{*}\alpha_{0,m}+r_{5,m}^{*}\alpha_{1,m}+r_{6,m}^{*}\alpha_{2,m}), \\ \tilde{s}_{1}=\sum_{m=0}^{M-1}(r_{0,m}\alpha_{1,m}^{*}-r_{1,m}\alpha_{0,m}^{*}+r_{3,m}\alpha_{2,m}^{*}+r_{4,m}^{*}\alpha_{1,m}-r_{5,m}^{*}\alpha_{0,m}+r_{7,m}^{*}\alpha_{2,m}), \\ \tilde{s}_{2}=\sum_{m=0}^{M-1}(r_{0,m}\alpha_{2,m}^{*}-r_{2,m}\alpha_{0,m}^{*}-r_{3,m}\alpha_{1,m}^{*}+r_{4,m}^{*}\alpha_{2,m}-r_{6,m}^{*}\alpha_{0,m}-r_{7,m}^{*}\alpha_{1,m}), \\ \tilde{s}_{3}=\sum_{m=0}^{M-1}(-r_{1,m}\alpha_{2,m}^{*}+r_{2,m}\alpha_{1,m}^{*}-r_{3,m}\alpha_{0,m}^{*}-r_{5,m}^{*}\alpha_{2,m}+r_{6,m}^{*}\alpha_{1,m}-r_{7,m}^{*}\alpha_{0,m}).\end{array} \tag{2.37}$$

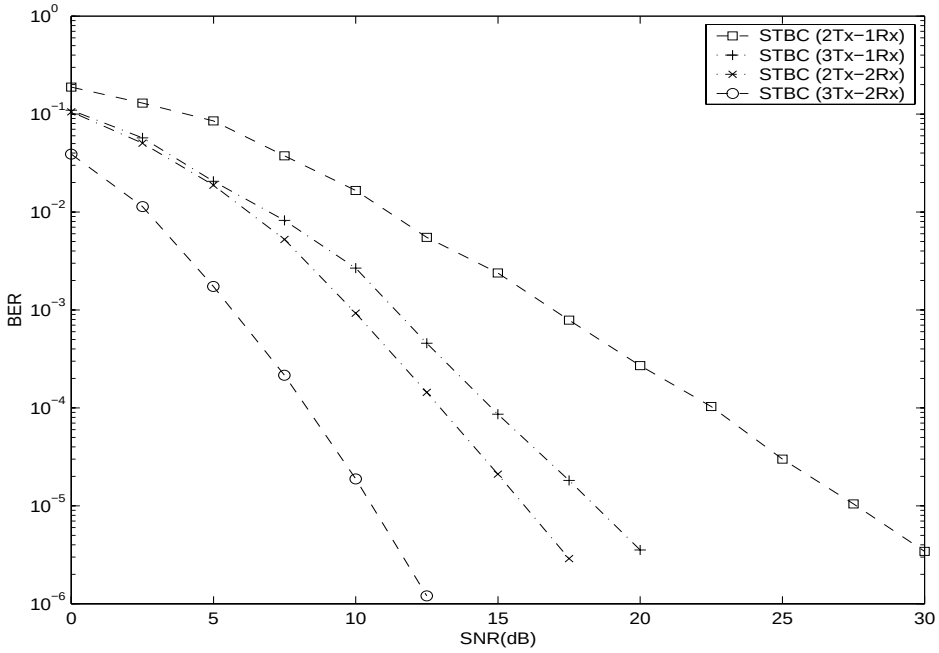

Figure 2.6: BER performance comparison of coherent QPSK between STBC, G_2 scheme and G_3 scheme in Rayleigh fading.

Figure 2.6 shows the BER performance comparison of coherent QPSK with STBC, G_2 scheme and with G_3 scheme in Rayleigh fading channel environment. Since both G_2 and G_3 schemes are designed to achieve full diversity, the diversity gain for both schemes is MN, where M and N represent the number of receivers and the number of transmitters. That is, the diversity for the G_2 scheme with one and two receivers are 2 and 4, respectively. In the same way, the diversity advantage for the G_3 scheme with one and two receivers are 3 and 6. As we observe from Figure 2.6, the performance gets better in the order of diversity gain.

For this simulation, we generate zero mean complex Gaussian random numbers with variance 0.5 for the channel information, $\alpha_{n,m}$.

2.2.3 STBC Designed in Quasi Orthogonal Method

Transmission matrices designed in quasi orthogonal method are not orthogonal in columns but in groups.

A. Encoding Algorithm Whereas the codes designed in orthogonal methods use the orthogonal property of the codes, [22] proposed structures that are not orthogonal but rather divided into groups. The columns within each group are not orthogonal to each other, but different groups are orthogonal among each other. This structure is called a quasi-orthogonal design [22]. We can take the following STBC for N=T=K=4 achieving full rate with a diversity of $2M$ as an example designed in the quasi-orthogonal method,

$$G_4 = \begin{bmatrix} s_0 & s_1 & s_2 & s_3 \\ -s_1^* & s_0^* & -s_3^* & s_2^* \\ -s_2^* & -s_3^* & s_0^* & s_1^* \\ s_3 & -s_2 & -s_1 & s_0 \end{bmatrix}. \tag{2.38}$$

It has been proved from [20] that the full diversity of $4M$ for a rate one code is impossible for the matrix, G_4. Thus, STBC designed in quasi orthogonal method achieves the full transmission rate at the cost of diversity gains.

B. Decoding Algorithm From the fact that the first and the second, the first and the third, the second and the fourth, and the third and the fourth columns are orthogonal each other, respectively, the minimization of equation (2.24) is equivalent to minimizing $f_{03}(s_0, s_3)$ and $f_{12}(s_1, s_2)$ defined below [22].

$$f_{03}(s_0, s_3) = \sum_{m=0}^{M-1} \left(\left(\sum_{n=0}^{3} |\alpha_{n,m}|^2 \right) \left(|s_0|^2 + |s_3|^2 \right) + 2Re\left\{ K_1 + K_2 + K_3 \right\} \right) \tag{2.39}$$

$$f_{12}(s_1, s_2) = \sum_{m=0}^{M-1} \left(\left(\sum_{n=0}^{3} |\alpha_{n,m}|^2 \right) \left(|s_1|^2 + |s_2|^2 \right) + 2Re\left\{ K_4 + K_5 + K_6 \right\} \right) \tag{2.40}$$

where

$$K_1 = \left(-\alpha_{0,m} r_{0,m}^* - \alpha_{1,m}^* r_{1,m} - \alpha_{2,m}^* r_{2,m} - \alpha_{3,m} r_{3,m}^* \right) s_0$$

$$K_2 = \left(-\alpha_{3,m} r^*_{0,m} + \alpha^*_{2,m} r_{1,m} + \alpha^*_{1,m} r_{2,m} - \alpha_{0,m} r^*_{3,m}\right) s_3$$

$$K_3 = \left(\alpha_{0,m} \alpha^*_{3,m} - \alpha^*_{1,m} \alpha_{2,m} - \alpha_{1,m} \alpha^*_{2,m} + \alpha^*_{0,m} \alpha_{3,m}\right) s_0 s^*_3$$

$$K_4 = \left(-\alpha_{1,m} r^*_{0,m} + \alpha^*_{0,m} r_{1,m} - \alpha^*_{3,m} r_{2,m} + \alpha_{2,m} r^*_{3,m}\right) s_1$$

$$K_5 = \left(-\alpha_{2,m} r^*_{0,m} - \alpha^*_{3,m} r_{1,m} + \alpha^*_{0,m} r_{2,m} + \alpha^*_{1,m} r^*_{3,m}\right) s_2$$

$$K_6 = \left(\alpha_{1,m} \alpha^*_{2,m} - \alpha^*_{0,m} \alpha_{3,m} - \alpha_{0,m} \alpha^*_{3,m} + \alpha^*_{1,m} \alpha_{2,m}\right) s_1 s^*_2$$

The decision metric (2.24) can be computed as the sum of two equations (2.39) and (2.40), where (2.39) is independent of s_1 and s_2, and (2.40) is independent of s_0 and s_3. Therefore, the minimization of (2.24) is equal to minimizing these two equations independently. That is, the decoder finds the symbol pair (s_0, s_3) that minimizes the equation (2.39) among all possible (s_0, s_3) pairs. Then, or in parallel, the decoder selects the pair (s_1, s_2) which minimizes the equation (2.40). Using equations (2.39) and (2.40) instead of equation (2.24) reduces the complexity of decoding without sacrificing the performance [22].

It is very important to obtain soft outputs of STBC decoder, when it is concatenated with turbo codes which require soft outputs to process. Soft outputs of STBC decoder designed in quasi orthogonal method will be derived in chapter 4.

Figure 2.7 shows the BER performance comparison of coherent QPSK with STBC, G_2 scheme and with G_4 scheme in Rayleigh fading channel environment. Since G_2 schemes are designed to achieve full diversity, the diversity gain for G_2 scheme is $2M$, where the number of receivers M, times the number of transmitters, 2. On the contrary, G_4 scheme is designed to fulfill the full transmission rate at the cost of diversity, its diversity is obtained as $2M$, where M is the number of receivers. Therefore, the diversity advantages for both schemes G_2 and G_4 are equal, although Figure 2.7 shows the slight better performance for G_4 scheme. Since G_4 scheme achieves the full transmission rate and about equal diversity over G_2 scheme and it is easier to implement multiple antennas in a base station for a down link communication, G_4 scheme is recommended for the low

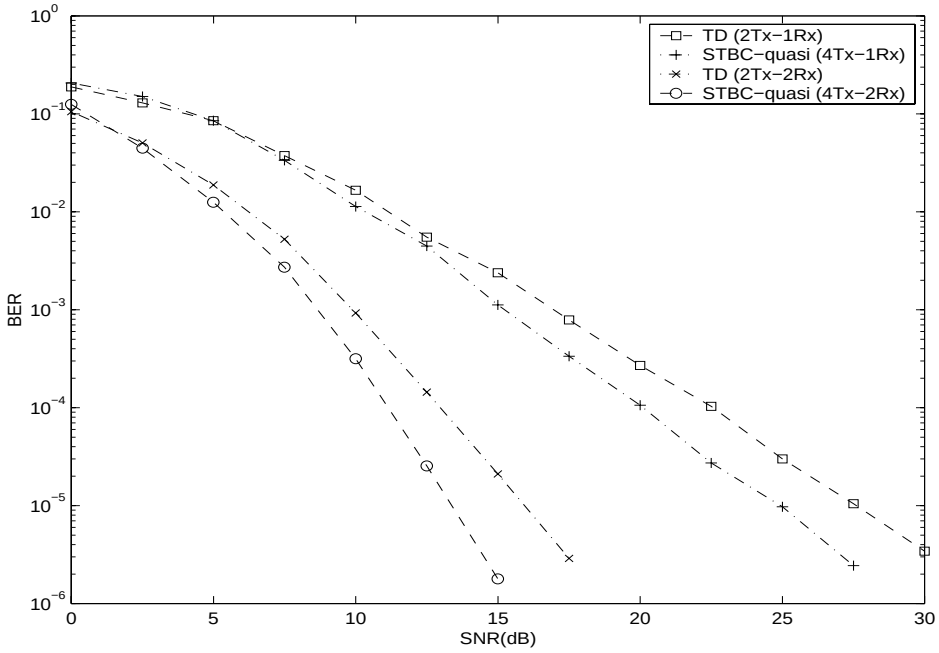

Figure 2.7: BER performance comparison of coherent QPSK between STBC, G_2 scheme and G_4 scheme in Rayleigh fading.

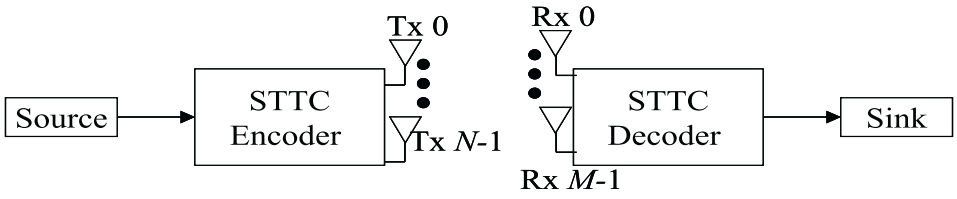

Figure 2.8: Block diagram of a STTC system.

SNR and high BER situation.

For this simulation, we generate zero mean complex Gaussian random numbers with variance 0.5 for the channel information, $\alpha_{n,m}$.

2.3 Space-Time Trellis Codes

A block diagram for a simple STTC system is given in Figure 2.8. The STTC system operates with N transmitters and M receivers. Source data are encoded by the corresponding trellis diagram for each STTC system. Input data bits will be mapped into symbols, which will be transmitted through the partial numbers of transmitters. Delayed redundant data symbols are transmitted through the rest of transmitters. It explains why it is called the *Space* and *Time* coding.

For a flat fading channel, the received signal at time t and at the receiver m, can be represented in the same way as Equation (6.1). If we repeat it here,

$$r_{t,m} = \sum_{n=0}^{N-1} \alpha_{n,m} C_{t,n} + \eta_{t,m}, \tag{2.41}$$

where the real and imaginary part of AWGN $\eta_{t,m}$ have equal variance $\sqrt{2}/(2SNR)$, assuming the energy of each symbol is $\sqrt{2}/2$ in baseband. The $C_{t,n}$ and $\alpha_{n,m}$ represent the codeword transmitted from the nth transmitter and the channel path gain between the nth transmitter and the mth receiver, respectively. The decoder is performed by maximum likelihood decision, which is obtained by computing the lowest accumulated

squared Euclidean distance to extract the most likely transmitted symbols [7][13]. The branch metric of STTC decoder is obtained by this squared Euclidean distance computation between the received symbol and each possible candidate set of transmitted codewords, which is given by,

$$\arg\min_{s_x} \sum_{m=0}^{M-1} \left| r_{t,m} - \sum_{n=0}^{N-1} \alpha_{n,m} C_{t,n} \right|^2, \tag{2.42}$$

where s_x represents the element of codewords, C.

Assuming the decoder decides erroneously in favor of code sequences e, then, for a block of data of length l, we define the NxN error matrix A as

$$A(C,e) = \sum_{l=0}^{l-1} (C_l - e_l)(C_l - e_l)^* \tag{2.43}$$

where $(.)^*$ denotes the conjugate operation for scalars and the conjugate transpose for matrices and vectors [5]. Denoting r to be the rank of matrix A, the kernel of A has dimension N-r and exactly N-r eigenvalues of A are zero. If we consider the nonzero eigenvalues of A are λ_0,λ_1,...,λ_{r-1}, then the probability of transmitting C as in the matrix of equation (2.43) and deciding in favor of e at the decoder is given by [5][7][15]

$$P(e|C) \leq \left(\prod_{i=0}^{r-1} \lambda_i \right)^{-M} (E_s/4N_0)^{-rM} \tag{2.44}$$

where $N_0/2$ is the noise variance and M is the number of receiver. The first term, $\left(\prod_{i=0}^{r-1} \lambda_i\right)^{-M}$ in equation (2.44) represents the coding gain achieved by the STTC and the second term, $(E_s/4N_0)^{-rM}$ represents a diversity gain of rM.

As an example of evaluating STTC design criteria, we show a STTC scheme with 4-state, QPSK symbol mapping, and 2 transmitters proposed in [7]. The trellis of STTC in Figure 2.9 starts from state 0 at symbol period t=0. Two data bits are grouped into a symbol 0, 1, 2, or 3 for the QPSK system, and those are eventually mapped into 1+j, 1-j, -1+j, and -1-j as in Table 2.2. These symbols are transmitted from both transmitters. We denote the first transmitter as Tx0 and the second one as Tx1. At t=0, Tx0

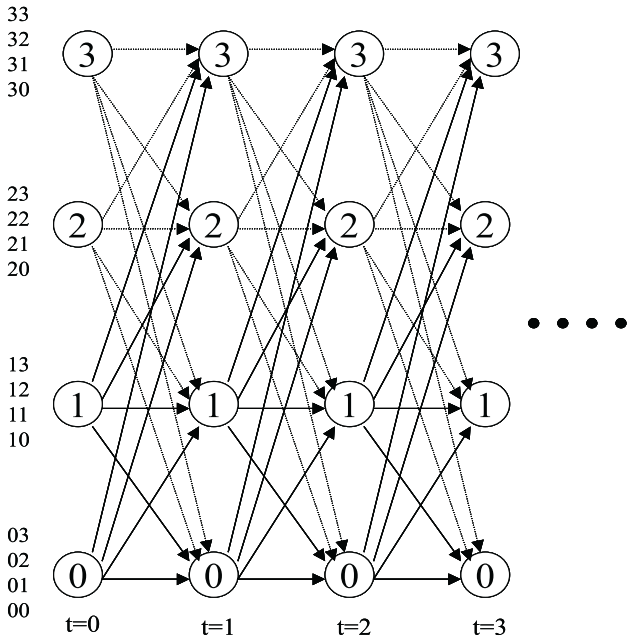

Figure 2.9: An STTC trellis in 2-STC, QPSK, 4 states.

Table 2.2: QPSK Symbol Mapping II

Index s_t	Bits u_0u_1	Modulation $I(s_t) + jQ(s_t)$
0	1 1	$1 + j$
1	1 0	$1 - j$
2	0 1	$-1 + j$
3	0 0	$-1 - j$

transmits symbol zero $(1+j)$, because the trellis starts at state zero. At the same time, Tx1 transmits the first input symbol. At t=1, Tx0 transmits the symbol transmitted at t=0 from Tx1, and Tx1 transmits the next input symbol. This process will continue until all the symbols of data block whose size is equal to the trellis length, are transmitted. The first digit on the numeral column of Figure 2.9 represents the symbol transmitted through 'Tx0' and the second digit represents the symbol transmitted through 'Tx1'.
We apply a Viterbi decoding algorithm for decoding the STTC scheme. The branch metric for the viterbi algorithm (VA) is obtained by computing the metric (2.42). The channel state information $\alpha_{n,m}$ is assumed to be known at the decoder to compute the branch metric. The back-trace VA can be applied to any trellis. For the specific trellis in Figure 2.9, among all the incoming branch metric to each state at a trellis time, we choose the minimum sum of the branch metric and the node metric of previous node the branch departs from. The input symbol making the trellis-transition for the minimum sum of branch metric with the node metric at the previous trellis time, are saved in the back-trace array. Once the trellis reaches the last trellis time, we trace back from the ending state retrieving the input symbol saved in the back-trace array. Detail description of VA is provided in Section 3.2.3.

The frame error rate (FER) performance comparison with the frame size 100 bits between STTC and STBC with two transmitters is shown in Figure 2.10. Two transmitters, 4-state trellis, and QPSK symbols are used for our STTC simulation, and the STBC is designed in Alamouti scheme. Both STTC and STBC schemes operate under Rayleigh fading channel environment with normalized Doppler frequency $(f_d T_s)$, 0.01 with one or two receivers. The performance of STTC with one receiver shows little improvement over STBC, but the STTC scheme with two receivers achieves about 1.5 dB improvement over the STBC at the FER of 10^{-1}.
The following example illustrates another STTC scheme with 8-state trellis, QPSK, and 2 transmitters. Just as the STTC with 4-state trellis, the first digit on the numeral

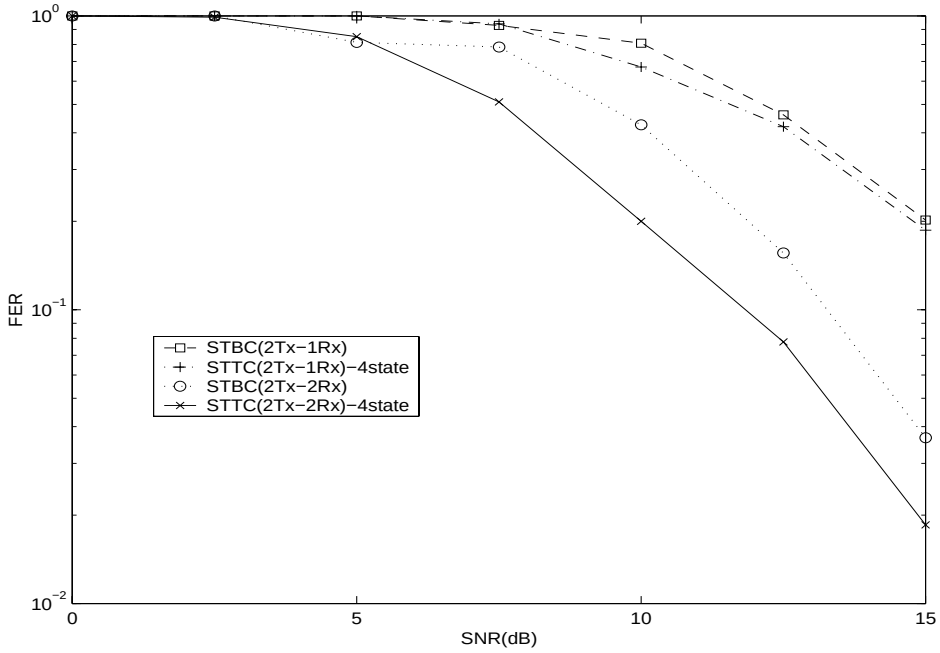

Figure 2.10: FER performance comparison of coherent QPSK between STBC and STTC with 4-state trellis under Rayleigh fading environment with $f_d T_s$, 0.01.

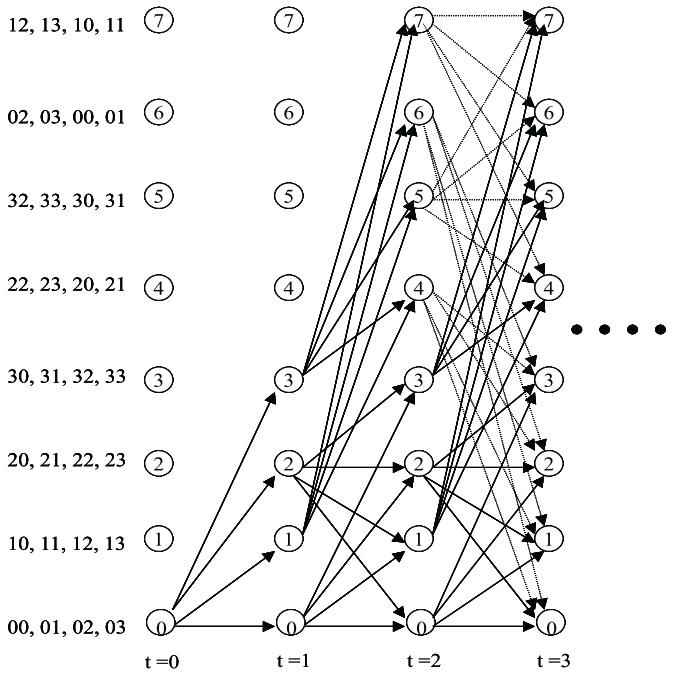

Figure 2.11: An STTC scheme in 2-STC, QPSK, 8 state-trellis.

column of Figure 2.11 represents the symbol transmitted through 'Tx0' and the second digit represents the symbol transmitted through 'Tx1'. Input data determine the symbol which will be transmitted through 'Tx1', but the symbol transmitted through 'Tx0' is whatever the current state is, for state 3 or less. That is, if the current state is 3, then the symbol 3, -1-j according to the QPSK mapping in Table 2.2, is transmitted through 'Tx0'. The next state which the current state will make a transition to will be the same number state as the input symbol for the even numbered current state, and will become the number state that the input symbol is added by 4 for the odd numbered current state. These explanation is obvious from Figure 2.11. For the case that the current state number is 4 or above, the symbol transmitted through 'Tx0' is different by whether the current state number is even or odd. For the even numbered state, the symbol is the current state number added by two and divided by the modular 4 operator. And the

next state it makes a transition to is determined by the current input symbol added by 2 and divided by the modular 4 operator. For the odd numbered case, the symbol transmitted through 'Tx0' is computed in the same way as the even numbered case, but the next state it makes a transition to is determined by the current input symbol. If the current input symbol is greater than 1 among the symbols from 0 to 3, the next state number is the current input symbol added by 2 or, if the current input symbol is not greater than 1, then the next state number becomes the current input symbol added by 6. This process is repeated until all the block of data whose size is equal to the trellis length, are transmitted. The STTC decoder employs the same kind of Viterbi algorithm as was used for the STTC with 4-state trellis. Of course, the channel state information $\alpha_{n,m}$ is assumed to be known at the decoder to compute the branch metric.

Figure 2.12 shows the frame error rate (FER) performance comparison with the frame size 100 bits between STTC in 4-state trellis and STTC in 8-state trellis with two transmitters. Both schemes in Figure 2.12 operate under Rayleigh fading channel environment with normalized Doppler frequency ($f_d T_s$), 0.01 with one or two receivers. The performance of STTC with 8-state trellis shows about 2 dB gain at the FER of 10^{-1} over the STTC with 4-state trellis, regardless of number of receivers. We can confirm through the results that the performance reproduced from our research agrees with the results in [7]. These basic results from various STBC and STTC schemes will be used toward our proposed work in the following Sections.

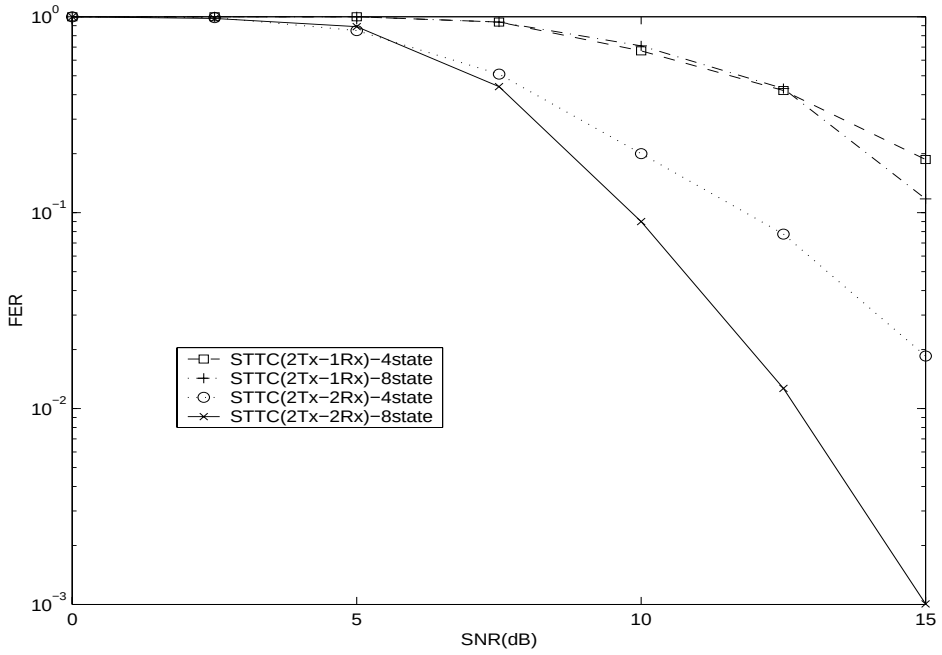

Figure 2.12: FER performance comparison of coherent QPSK between STTC with 4-state trellis and STTC with 8-state trellis under Rayleigh fading environment with $f_d T_s$, 0.01.

Chapter 3

Overview of Turbo Codes

Coding theorists have traditionally explored the issue of designing good codes with a lot of structure, which is a bit contradictory to the coding theory that codes chosen at random should perform well if the block size is large enough. Until recently, the challenge to find practical decoders for 'almost' random large codes has not been seriously considered [11][57][58]. However, in 1993, perhaps the most exciting and potentially important development in coding history was proposed by French researchers, Berrou et al., which is the dramatic announcement of 'turbo codes'. It has been known to perform near the Shannon limit in AWGN (Additive White Gaussian Noise) channel environment. The performance was so good in [45] that the initial reaction was big skepticism. But, now many researchers in the world reproduce the performance and improve. Turbo code chip is already implemented for the third generation wireless communications.

Since turbo code is an error correction code to improve energy efficiency, it is proper to review the development of channel coding schemes before we go over the details of turbo codes. Encoding and decoding schemes for block codes based upon 'hamming codes' will be described. Convolutional encoding schemes, 'MAP', and 'Viterbi' decoding algorithms will be explained in detail. Turbo code design scheme, performance, and its mathematic analysis will be shown in this Chapter.

3.1 Block Codes

Around the same time Shannon was developing the theoretical basis on coding, Hamming introduced the first practical block-code-type of error correction coding [32]. Block codes add n-k parity check symbols to produce an n symbol code word. Following the 'hamming' codes, other linear block codes, 'cyclic' codes were introduced. Cyclic codes use the fact that any cyclic shift of a code word is also a code word. One benefit of cyclic codes is that they can be represented by a 'generator polynomial' of degree n-k. The 'BCH' codes show a class of cyclic code polynomials that provide a large selection of block lengths, code rates, alphabet sizes, and error correcting capability. One specific subclass of BCH codes that BCH codes were extended to the non binary case is called 'Reed Solomon' (RS) codes [36]. RS codes began to find many practical applications, since Berlekamp proposed an efficient decoding algorithm in [40].

Encoding of block codes consists of decomposing the information into k-tuples $\mathbf{u}$ called messages, and taking a one-to-one mapping of $\mathbf{u}$ into an n-tuple $\mathbf{v}$ called a codeword. A linear block codes can be represented by

$$\mathbf{v} = \mathbf{uG}, \tag{3.1}$$

where $\mathbf{G}$ is the kxn generator matrix and the matrix is over the field $GF(2)$. Linear codes have the property that the sum over $GF(2)$ of two codewords is also a codeword, and thus all linear block codes must contain the all-zeros codeword [59]. Let us take a $(7, 4)$ hamming code as an example to illustrate it.

3.1.1 Hamming Code Example

The generator matrix $\mathbf{G}$ used for the hamming code is as follows,

$$\mathbf{G} = \begin{bmatrix} 1\,1\,1\,0\,0\,0\,0 \\ 0\,1\,1\,1\,1\,0\,0 \\ 0\,0\,1\,1\,0\,0\,1 \\ 1\,0\,1\,1\,0\,1\,0 \end{bmatrix}$$

and the transpose of parity check matrix $\mathbf{H^T}$ is given as

$$\mathbf{H^T} = \begin{bmatrix} 1\ 0\ 0 \\ 0\ 1\ 0 \\ 0\ 0\ 1 \\ 0\ 1\ 1 \\ 1\ 0\ 1 \\ 1\ 1\ 0 \\ 1\ 1\ 1 \end{bmatrix}.$$

When message vectors are defined to be $\mathbf{u}$=[m_0 m_1 m_2 m_3], the codewords $\mathbf{v}$ is $\mathbf{uG}$. Thus, $\mathbf{v}$=[$(m_1 + m_2 + m_3)$ $(m_0 + m_2 + m_3)$ $(m_0 + m_1 + m_3)$ (m_0) (m_1) (m_2) (m_3)]. Assuming that one bit error is correctable, the error patterns are set as follows,

$$\mathbf{e} = \begin{bmatrix} 0\ 0\ 0\ 0\ 0\ 0\ 0 \\ 0\ 0\ 0\ 0\ 0\ 0\ 1 \\ 0\ 0\ 0\ 0\ 0\ 1\ 0 \\ 0\ 0\ 0\ 0\ 1\ 0\ 0 \\ 0\ 0\ 0\ 1\ 0\ 0\ 0 \\ 0\ 0\ 1\ 0\ 0\ 0\ 0 \\ 0\ 1\ 0\ 0\ 0\ 0\ 0 \\ 1\ 0\ 0\ 0\ 0\ 0\ 0 \end{bmatrix}.$$

The syndrome $\mathbf{S}$ for error correction decoding is $\mathbf{rH^T} = \mathbf{eH^T}$, because the received messages $\mathbf{r} = \mathbf{u} + \mathbf{e}$. Thus, the syndrome $\mathbf{S}$ is

$$\mathbf{S} = \begin{bmatrix} S_0\ S_1\ S_2 \\ 0\ 0\ 0 \\ 1\ 1\ 1 \\ 1\ 1\ 0 \\ 1\ 0\ 1 \\ 0\ 1\ 1 \\ 0\ 0\ 1 \\ 0\ 1\ 0 \\ 1\ 0\ 0 \end{bmatrix}. \tag{3.2}$$

The syndrome is simply computed for the simulation purpose as follows,

$$\begin{aligned} S_0 &= r_0 + r_4 + r_5 + r_6 \\ S_1 &= r_1 + r_3 + r_5 + r_6 \\ S_2 &= r_2 + r_3 + r_4 + r_6. \end{aligned}$$

Once a syndrome computed above falls into one of the pattern in Equation (3.2), the corresponding bit is corrected. Out of these corrected received bits, the last four bits become the actual decoded information bits.

When we define the 'hamming distance' $d(\mathbf{v_i}, \mathbf{v_j})$ to be the number of bit positions that two codewords differ, the 'minimum distance' d_{min} of a code is the smallest hamming distance between any two codewords

$$d_{min} = \min_{i \neq j} d(\mathbf{v_i}, \mathbf{v_j}). \tag{3.3}$$

A code with d_{min} can correct all codewords with t or fewer errors,

$$t = \left\lfloor \frac{d_{min} - 1}{2} \right\rfloor, \tag{3.4}$$

where $\lfloor \cdot \rfloor$ denotes the largest integer no greater than the expression inside.

3.2 Convolutional Codes

Convolutional codes provide the continuous encoding of input streams, different from the block codes with a fixed block size for the message and codeword. The encoder of convolutional codes contains memory m, and the n encoder outputs at any given time unit do not depend only on the k inputs at that time unit, but also on m previous input blocks. An (n,k,m) convolutional code can be implemented with a k-input, n-output linear sequential circuit with input memory m. Typically, n and k are small integers with $k < n$, but the memory order m should be made large to achieve low error probabilities. In the important special case when $k = 1$, the information sequence is not divided into blocks and can be processed continuously [59].

Convolutional codes were first published by Elias [42] in 1955 as an alternative to block codes. Several decoding algorithms are introduced thereafter, Wozencraft [60] proposed sequential decodings, and experimental studies soon began to follow. Massey proposed a less efficient but simpler-to-implement called threshold decoding in 1963 [61]. Then

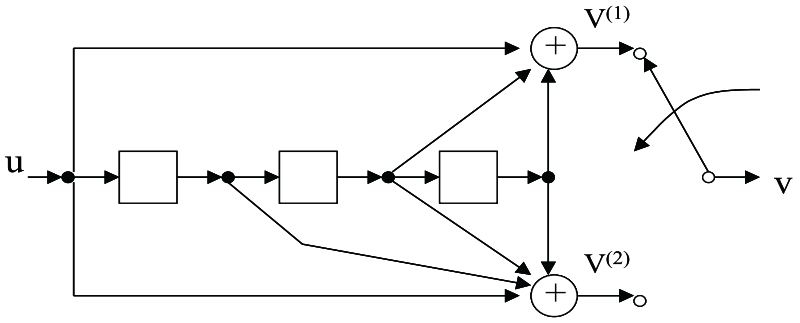

Figure 3.1: A (2,1,3) binary convolutional encoder.

in 1967, the famous Viterbi Algorithm (VA) was proposed by Viterbi in [43]. This scheme is a maximum likelihood decoding scheme that was relatively easy to implement for codes with small memory orders. The VA, together with sequential decoding led to the many applications of convolutional codes, especially to deep-space and satellite communication in the early 1970s. The convolutional codes serially concatenated with 'Reed-Solomon' codes are the standard error correction codes of the second generation wireless communication, PCS. The detail encoding and decoding procedures will be covered in this Section.

3.2.1 Encoding of Convolutional Codes

A convolutional code can be represented by *generator polynomials*, *encoder diagram*, *state diagram*, *trellis diagram*, and/or *forward* and *backward transition function*.
As an examplbacke, for the encoder diagram in Figure 3.1, the forward state transition function is

$$S_i = 2(S_{i-1}\%4) + u_i \tag{3.5}$$

where S_{i-1} and S_i are the previous state and current state respectively and u_i is the input for the branch at the time of transition, i. The '%4' represents the modular 4

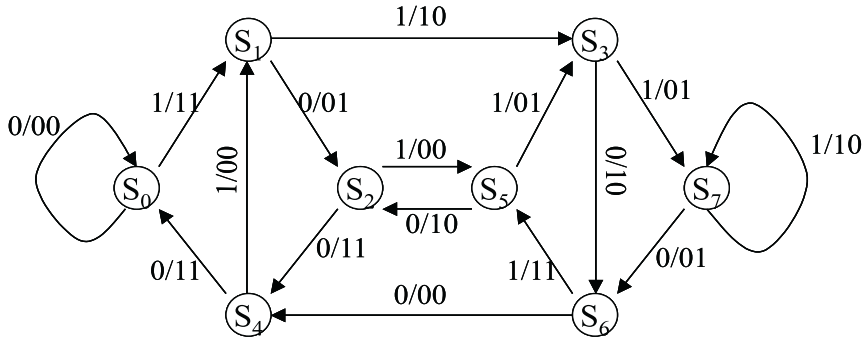

Figure 3.2: State diagram for the encoder in Figure 3.1.

operation. The backward state transition function is

$$S_{i-1} = (S_i/2) + 4 * u_x \tag{3.6}$$

where u_x represents the input of the transition branch, that is, 0 when the arrow is coming from upper branch to S_i and 1 when coming from lower branch to S_i. Figure 3.2 shows the state diagram for the encoder in Figure 3.1. The generator sequences for the state diagram in Figure 3.2 is obtained by inputting the impulse, $(1, 0, 0, ...)$ into the system and they are

$$\begin{aligned} \mathbf{g^{(1)}} &= (1, 0, 1, 1) \\ \mathbf{g^{(2)}} &= (1, 1, 1, 1). \end{aligned}$$

From [59], encoding equations can now be written as

$$\begin{aligned} \mathbf{v^{(1)}} &= \mathbf{u} * \mathbf{g^{(1)}} \\ \mathbf{v^{(2)}} &= \mathbf{u} * \mathbf{g^{(2)}}, \end{aligned}$$

where '*' denotes discrete convolution and all operations are modulo-2. The convolution operation implies that, for all $l \geq 0$,

$$v_l^{(j)} = \sum_{i=0}^{m} u_{l-i} g_i^{(j)} = u_l g_0^{(j)} + u_{l-1} g_1^{(j)} + ... + u_{l-m} g_m^{(j)}, \quad j = 1, 2$$

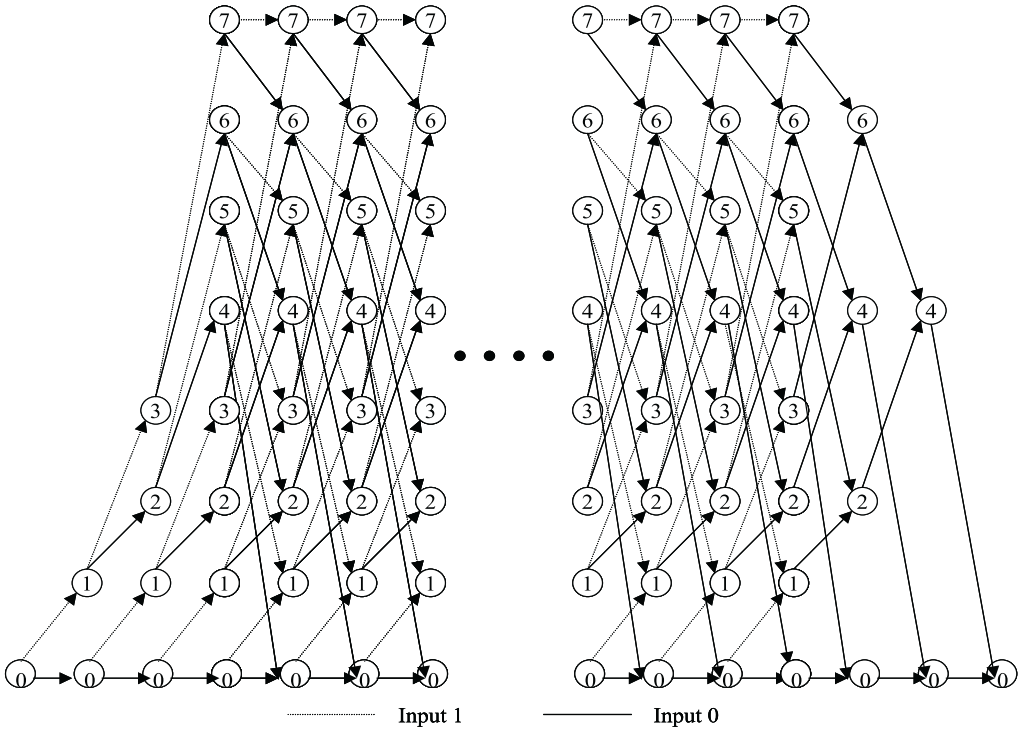

Figure 3.3: Trellis diagram for the encoder in Figure 3.1.

where $u_{l-i} = 0$ for all $l < i$.

Figure 3.3 shows the trellis diagram for the encoder of Figure 3.1. There are two branches coming out of a state whose transition is determined by the input. The branch label, that is, the output of the encoder is determined by the input value and the previous state.

3.2.2 Recursive Systematic Convolutional Codes

As block codes can be made systematic without changing the minimum distance, so can convolutional codes be made systematic without changing the minimum free distance. Turbo decoders in passing the extrinsic information between two constituent decoders, require systematic codes. Since the parity output of convolutional codes can be produced

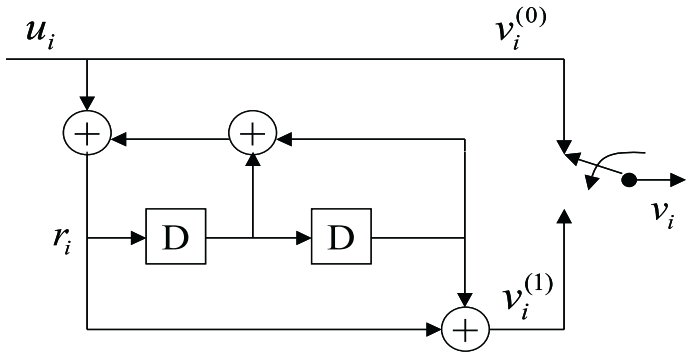

Figure 3.4: A rate 1/2, RSC encoder.

by computing the feedback variable in the recursive matter, it is called the recursive systematic convolutional codes (RSC) [11]. For an example, a rate 1/2 RSC encoder diagram is shown in Figure 3.4. The feedback polynomial $g^{(0)}$ and the feed-forward polynomial $g^{(1)}$ for the encoder scheme in Figure 3.4 are [1 1 1] and [1 0 1], respectively. RSC encoding performs by first obtaining the feedback variable (r_i),

$$r_i = u_i + \sum_{j=1}^{K_c} r_{i-j} g_j^{(0)}, \tag{3.7}$$

and then by getting the parity output ($v_i^{(1)}$)

$$v_i^{(1)} = \sum_{j=0}^{K_c} r_{i-j} g_j^{(1)}, \tag{3.8}$$

where $r_0 = u_0$ and K_c is the constraint length of encoder, which is 3 for the encoder in Figure 3.4. The systematic output $v_i^{(0)}$ is just the message bit, u_i. The state diagram and the trellis diagram of the encoder in Figure 3.4 are shown in Figure 3.5 and 3.6, respectively.

The forward and the backward state transition functions for the RSC encoder of Figure 3.4 are

$$S_i = (S_{i-1}\%3) == 0?2(s_{i-1}\%2) + u_i : 2(s_{i-1}\%2) + (1 - u_i), \tag{3.9}$$

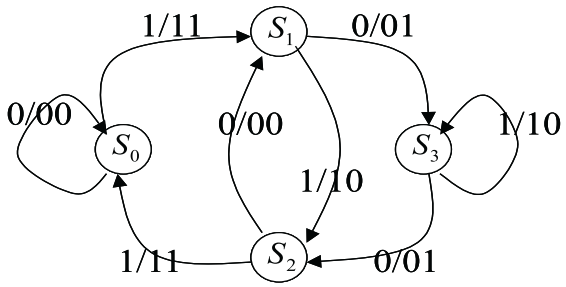

Figure 3.5: State diagram for the RSC encoder in Figure 3.4.

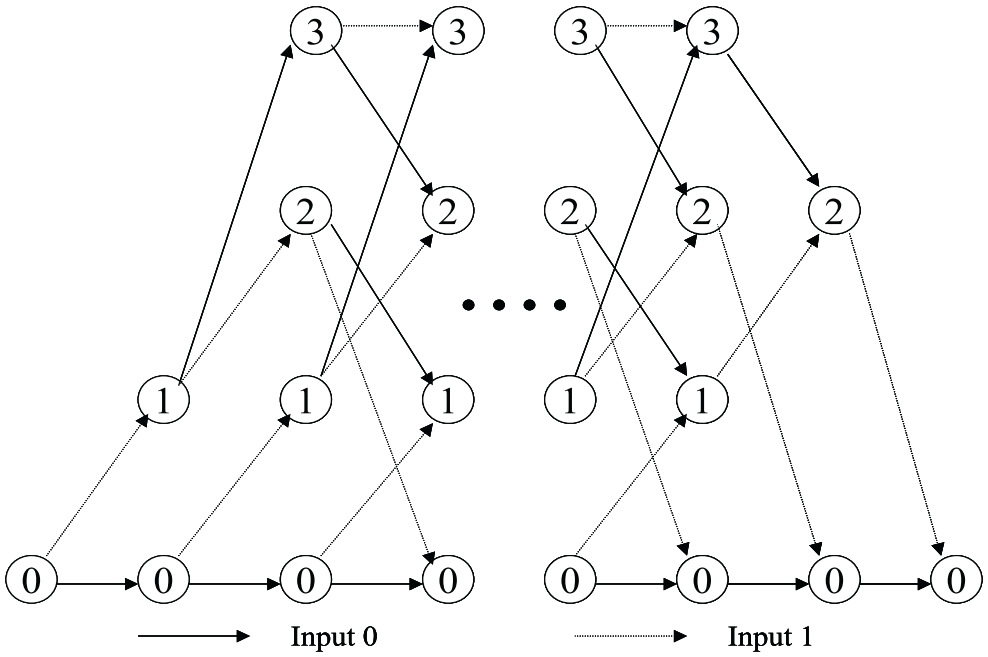

Figure 3.6: Trellis diagram for the RSC encoder in Figure 3.4.

$$S_{i-1} = (S_i\%3) == 0?(s_i\%2) + 2u_i : (s_i + 1)\%2 + 2(1 - u_i), \tag{3.10}$$

respectively. The operator '?' represents a ternary operator of C-programming language, which has the following form, *(condition) ? Expression 1 : Expression 2*. If the *(condition)* is satisfied, the *Expression 1* is performed, and otherwise the *Expression 2* is executed. The '%2' operator returns the remainder '0', or '1' of 'division 2' operation, and in the same way, the '%3' operator returns the remainder '0', '1', or '2' of 'division 3' operation.

In order to decode RSC, especially using *MAP* decoder, trellis needs to be terminated at state '0' at the last trellis time. Different from the general convolutional encoder, RSC cannot terminate the trellis by just adding the redundant all zero bits at the end of data bits. There are many ways to accomplish the termination. We terminate the trellis by running a *for* loop or a *while* loop of the forward state transition function in Equation (3.9) over the whole trellis length to find out the last state ending, and then adding the redundant bits. These redundant bits are not all zero bits, but determined by the last state ended. For an example of Figure 3.6, state '0' and '2' transit to state '0' at the next trellis time by input bits 0 and 1, respectively. State '1' and '3' can be moved to the next state '2' by input bits 1 and 0, then state '2' can always transit to state '0' by input bit 1. Hence, any state can reach state '0' within two trellis time.

3.2.3 Viterbi Algorithm

The VA can be implemented in two ways, which are 'survivor path algorithm' and 'back trace algorithm'. The 'Back trace algorithm' is much more concise in both complexity and the concept. The reference [62] describes 'survivor path algorithm' in detail. The presentation of VA in this Section is based upon 'back trace algorithm'. The VA in 'back trace algorithm' is composed of three major computations, 'Branch Metric Computation', 'Node Metric Computation' and 'Back-trace Metric Computation'. The sequence of VA is summarized as follows,

1. **Initialization of states at the first trellis time** Set the state '0' to be zero and all other states to be very big number at the trellis time 0.

2. **Node Metric Computation** Compute the node metric by figuring out the branch metric for all states at each trellis. Compare the node metric for two branches coming into the node and save the minimum node metric to the back trace array for all states at each trellis time. Repeat this job for all trellis time. The branch metric is obtained by adding the previous node metric connecting to the current node metric with the hamming distance (for hard decision case) or with the Euclidean distance (for soft decision case) between the original convolutional encoder outputs and the received codewords.

3. **Getting the minimum node metric at the last trellis time** Find out the state that has the minimum node metric at the last trellis time.

4. **Tracing back the trellis** Start tracing back from the state obtained at the previous sequence, 3. Find out the input for each branch determined, which will be the decoded information bits. Use the backward tracing transition function from Equation (3.6) when tracing back.

3.2.4 MAP Algorithm

Another important decoding algorithm for convolutional codes is the *Maximum A Posteriori* (*MAP*) decoding algorithm. The MAP algorithm was first introduced in [44], which is better known as *BCJR* algorithm. The computational complexity of MAP algorithm is so much higher than VA that MAP algorithm was almost forgotten until turbo codes were proposed. The fact of exchanging the extrinsic information between constituent decoders in turbo codes requires the MAP type of decoding algorithm.

From the Figure 3.7, *a priori* probability, $p(\underline{u})$, is defined as $\prod_{k=1}^{N} p_k(u_k)$ for $\underline{u} = \{u_1, u_2, ..., u_N\}$, which is 2^{-N} here, and *a posteriori* probability, $\hat{p}_k(u)$ is defined as $p(\underline{u}|\underline{y})$.

Figure 3.7: Block diagram of MAP decoder.

By the Bayes' rule and the total probability theory,

$$\begin{aligned} p(\underline{u} = u_k|\underline{y}) &= \frac{\sum_{\underline{u}:u_k=a} p(\underline{y}|\underline{u})p(\underline{u})}{p(\underline{y})} \\ &= \frac{\sum_{\underline{u}:u_k=a} p(\underline{y}|\underline{u})p(\underline{u})}{\sum_{\underline{u'}:u_k=a'} p(\underline{y}|\underline{u'})p(\underline{u'})} \end{aligned} \tag{3.11}$$

where u_k and a are either 0 or 1 respectively, and a' is both 1 and 0. $\underline{u'}$ represents the total information space. The MAP decoding algorithm handles the property of Equation (3.11) in the way maximizing it.

From Figure 3.7, the input to the encoder at bit time t is the bit $u(t)$ where $u(t)$ is 0 or 1. The encoder output, $x(u(t))$ at bit time t is corrupted by the channel, creating the MAP decoder input $y(t)$. Denoting the state at time $t-1$ to be $S_{t-1} = m'$, the probability that the state at t, S_t becomes m is expressed as

$$P(m|m') = P(S_t = m|S_{t-1} = m'). \tag{3.12}$$

The equation (3.12) will take on the value, 1/2 for two specific values of m and zero for all other values of m, that is, any state can transition to only two specific other states, which is equally likely. The state transition from m' to m results from a particular input bit $u(t)$. The likelihood ratio for each bit time is the ratio between the *a posteriori* probability for input bit one and for input bit zero. The log likelihood ratio is

$$\Lambda(u(t)) = log(P(u(t) = 1|Y)) - log(P(u(t) = 0|Y)) \tag{3.13}$$

where Y represents the received sequence of symbols. Equation (3.13) outputs one when the equation (3.13) is positive and the equation (3.13) becomes zero when it is negative. Here we can think of the probability that the state at time $t-1$ is m' and the state at

time t is m given the received sequence of symbols, Y.

$$P(S_t = m, S_{t-1} = m'|Y). \tag{3.14}$$

Summing the equation (3.14) over all the sets of states m' and m corresponding to the input one is equal to the probability that the input bit at time t is one. That is,

$$P(u(t) = 1|Y) = \sum_{m,m':u(t)=1} P(S_t = m, S_{t-1} = m'|Y).$$

Then the log likelihood ratio becomes

$$\Lambda(u(t)) = log(\sum_{m,m':u(t)=1} P(S_t = m, S_{t-1} = m'|Y)) - log(\sum_{m,m':u(t)=0} P(S_t = m, S_{t-1} = m'|Y)). \tag{3.15}$$

By multiplying both numerator and denominator of likelihood ratio (before taking a *log* operation) with $P(Y)$ after applying the Bayes' rule, the equation (3.15) becomes

$$\Lambda(u(t)) = log(\sum_{m,m':u(t)=1} P(S_t = m, S_{t-1} = m', Y)) - log(\sum_{m,m':u(t)=0} P(S_t = m, S_{t-1} = m', Y)). \tag{3.16}$$

The original paper, [44] that published $BCJR$ algorithm breaks the sequence Y into three segments; the set of channel symbols that comes before time t, the set of channel symbols that occur at bit time t and the set of channel symbols that occur after bit time t. Using this property and the Bayes' rule, the following equation can be defined

$$\begin{aligned} \sigma_t(m, m') &= P(S_t = m, S_{t-1} = m', Y) \\ &= P(S_{t-1} = m', Y_0^{t-1}) P(Y_{t+1}^{N-1}|S_{t-1} = m', Y_0^{t-1}, S_t, Y_t) \\ &\cdot \quad P(S_t = m, Y_t|S_{t-1} = m', Y_0^{t-1}). \end{aligned}$$

Referring to [44] is recommended for detail derivation of equations above. Since any value of the state at the previous bit time prior to time t or the received symbols prior to t can not affect the probability, $\sigma_t(m, m')$ is reduced to

$$\sigma_t(m, m') = P(S_{t-1} = m', Y_0^{t-1}) P(Y_{t+1}^{N-1}|S_t = m) P(S_t = m, Y_t|S_{t-1} = m'). \tag{3.17}$$

Now we make the following definitions according to [44]:

$$\begin{aligned} \alpha_t(m) &= P(S_t = m, Y_0^t) \\ \gamma_t(m', m) &= P(S_t = m, Y_t | S_{t-1} = m') \\ \beta_t(m) &= P(Y_{t+1}^{N-1} | S_t = m). \end{aligned}$$

$\gamma_t(m', m)$ is analogous to a branch metric in the Viterbi algorithm (VA), while $\alpha_t(m)$ is analogous to the node metric in the VA. By substituting these α, β and γ into the equation (3.17), $\sigma_t(m, m')$ can be represented as

$$\sigma_t(m, m') = \alpha_{t-1}(m') \cdot \gamma_t(m', m) \cdot \beta_t(m). \tag{3.18}$$

The equation (3.16) is rewritten by inserting the equation (3.18) as follows

$$\begin{aligned} \Lambda(u(t)) = \; & log(\textstyle\sum_{m,m':u(t)=1} \alpha_{t-1}(m') \cdot \gamma_t(m', m) \cdot \beta_t(m)) - \\ & log(\textstyle\sum_{m,m':u(t)=0} \alpha_{t-1}(m') \cdot \gamma_t(m', m) \cdot \beta_t(m)). \end{aligned} \tag{3.19}$$

Next thing to do is to compute α, β and γ.

$$\gamma_t(m', m) = P(S_t = m, Y_t | S_{t-1} = m'). \tag{3.20}$$

By the Bayes' rule, the equation (3.20) becomes

$$P(Y_t | S_t = m, S_{t-1} = m') P(S_t = m | S_{t-1} = m'). \tag{3.21}$$

Applying the total probability over the entire X space, the equation (3.21) can be expressed as

$$\sum_X P(Y_t, X_t = X | S_t = m, S_{t-1} = m') P(S_t = m | S_{t-1} = m') \tag{3.22}$$

, if we use the Bayes' rule again here, the equation (3.22) is

$$\sum_X P(X_t = X | S_t = m, S_{t-1} = m') P(S_t = m | S_{t-1} = m') P(Y_t | X_t = X). \tag{3.23}$$

For a AWGN channel, $P(Y_t|X_t = X)$ is

$$\prod_{k=0}^{k=K-1} \frac{1}{\sqrt{2\pi}\sigma} exp\left(-\frac{1}{2\sigma^2}(y_t^k - x_t^k)^2\right). \tag{3.24}$$

The equation (3.24) can be expressed as follow in the summation form.

$$\left(\frac{1}{\sqrt{2\pi}\sigma}\right)^K exp\left(-\frac{1}{2\sigma^2}\sum_{k=0}^{k=K-1}(y_t^k - x_t^k)^2\right). \tag{3.25}$$

Since X is the encoder output, K in equation (3.25) represents the number of bits composing a symbol. σ^2 is the noise variance. $\sum_X P(X_t = X|S_t = m, S_{t-1} = m')$ is either 1 or 0, since X is deterministic. And $P(S_t = m|S_{t-1} = m')$ is zero or 1/2, since each state m' can transition to only two other states with equal probability. Taking all these into account, we express the equation (3.23) as follows

$$A\left(\frac{1}{\sqrt{2\pi}\sigma}\right)^K exp\left(-\frac{1}{2\sigma^2}\sum_{k=0}^{k=K-1}(y_t^k - x_t^k)^2\right) \tag{3.26}$$

where A implies a constant taking care of the first two probability of equation (3.23) and results in no different consequence over the likelihood ratio computation. Actually, all the constants in equation (3.25) does not affect on the result of likelihood ratio computation. Thus, implementing only $\sum_{k=0}^{k=K-1}(y_t^k - x_t^k)^2$ in the simulation program ends up resulting in no difference on the final performance, and $\sum_{k=0}^{k=K-1}(y_t^k - x_t^k)^2$ is nothing but the squared Euclidean distance. It is also true that x^k values can be $+1$ or -1 instead of $+1$ or 0, after the symbol mapping at the encoding process.

As for α and β, these are obtained using recursion as below,

$$\begin{aligned}
\alpha_t(m) &= P(S_t = m, Y_0^t) \\
&= \textstyle\sum_{m'} P(S_t = m, S_{t-1} = m', Y_0^{t-1}, Y_t) \\
&= \textstyle\sum_{m'} P(S_{t-1} = m', Y_0^{t-1}) P(S_t = m, Y_t|S_{t-1} = m', Y_0^{t-1}) \\
&= \textstyle\sum_{m'} \alpha_{t-1}(m') P(S_t = m, Y_t|S_{t-1} = m') \\
&= \textstyle\sum_{m'} \alpha_{t-1}(m') \cdot \gamma_t(m', m).
\end{aligned} \tag{3.27}$$

Since the recursion for β requires whole block of symbols to be received before computation, it begins at the end of the block in trellis and computes backward.

$$\begin{aligned}
\beta_t(m) &= P(Y_{t+1}^{N-1}|S_t = m) \\
&= \textstyle\sum_{m'} P(S_{t+1} = m', Y_{t+1}^{N-1}|S_t = m) \\
&= \textstyle\sum_{m'} P(S_{t+1} = m', Y_{t+1}, Y_{t+2}^{N-1}|S_t = m) \\
&= \textstyle\sum_{m'} P(S_{t+1} = m', Y_{t+1}|S_t = m)P(Y_{t+2}^{N-1}|S_t = m, S_{t+1} = m', Y_{t+1}) \\
&= \textstyle\sum_{m'} \gamma_{t+1}(m, m')P(Y_{t+2}^{N-1}|S_{t+1} = m') \\
&= \textstyle\sum_{m'} \gamma_{t+1}(m, m') \cdot \beta_{t+1}(m').
\end{aligned} \tag{3.28}$$

In summary, the steps to implement BCJR Algorithm are

1. Initialize the α and β arrays as follows,

$$\begin{aligned}
\alpha_{t=0}(m = 0) &= 1 \\
\alpha_{t=0}(m \neq 0) &= 0 \\
\beta_{t=N-1}(m = 0) &= 1 \\
\beta_{t=N-1}(m \neq 0) &= 0
\end{aligned}$$

where N is the length of block.

2. Compute the gammas according to the equation (3.26).

3. Compute the alphas according to the equation (3.27).

4. When the last stage of the trellis block is reached, start processing backward through the trellis computing the betas according to the equation (3.28).

5. The log likelihood ratio can be computed using these α, β, and γ obtained above according to the equation (3.19).

3.2.5 Log-MAP Algorithm

Since the MAP algorithm is processed by the multiplication of exponentials, it requires large computer resources. But taking a logarithm over MAP algorithm converts these

multiplication into an addition process and ends up reducing the computational complexity. Following conversion process explains how to replace MAP into Log-MAP [63]. If we denote following equations,

$$\begin{array}{rcl} \Gamma_t(m,m') & = & log(\gamma_t(m,m')) \\ A_t(m) & = & log(\alpha_t(m)) \\ B_t(m) & = & log(\beta_t(m)) \\ L(u(t)) & = & log(\Lambda(u(t))) \end{array} \tag{3.29}$$

where $\Lambda(u(t))$ is

$$\Lambda(u(t)) = \frac{\sum_{m,m':u(t)=1} \alpha_{t-1}(m')\gamma_t(m',m)\beta_t(m)}{\sum_{m,m':u(t)=0} \alpha_{t-1}(m')\gamma_t(m',m)\beta_t(m)} \tag{3.30}$$

instead of equation (3.19),

equations (3.27), (3.28) and (3.30) are redefined as follows

$$\begin{array}{rcl} \Gamma_t(m,m') & = & log(\gamma_t(m,m')) \\ A_t(m) & = & log\left(\sum_{m'} exp(A_{t-1}(m') + \Gamma_t(m,m'))\right) \\ B_t(m) & = & log\left(\sum_{m'} exp(\Gamma_{t+1}(m,m') + B_{t+1}(m'))\right) \\ L(u(t)) & = & log\left(\sum_{m,m':u(t)=1} exp(A_{t-1}(m') + B_t(m) + \Gamma_t(m',m))\right) \\ & - & log\left(\sum_{m,m':u(t)=1} exp(A_{t-1}(m') + B_t(m) + \Gamma_t(m',m))\right) \end{array} \tag{3.31}$$

with the following initializations:

$$\begin{cases} A_{t=0}(m=0) & = & 0 \\ A_{t=0}(m\neq 0) & = & -\infty \end{cases} \tag{3.32}$$

3.2.6 Max-Log-MAP Algorithm

Though MAP algorithm calculates the likelihood ratio at each bit time precisely, it suffers from a couple of practical problems [11]. First of all, the MAP algorithm requires 6 x 2^{M_c} multiplications per estimated bit and an equal number of additions. Second, it is sensitive to the round-off errors occuring from numerical values with limited precision [11]. In order to solve these computational problems, Log-MAP algorithm was proposed in the subsection B processing the entire algorithm in the *log*-domain, rather than taking the logarithm of the likelihood ratio only at the last step. However, Log-MAP

algorithm still requires the exponential computation still causing the same problems as MAP algorithm, though it alleviates those problems.

Denoting,

$$A_M = \max_i A_i,$$

following relation is obtained [63].

$$log\left[\sum_i exp(A_i)\right] = A_M + log\left(1 + \sum_{A_i \neq A_M} exp(A_i - A_M)\right). \tag{3.33}$$

The second term of equation (3.33) can be neglected in case $A_M \gg A_i$, though it is true that the second term can be approximated into simple numerical value to minimize errors from the true value. [11] and [63] are good references for detail approximation information. About 0.2dB degradation is said to be observed from neglecting the second term [63]. Since it does not cause severe degradation in coding gain to neglect the second term of equation (3.33), the most simple MAP algorithm, Max-Log-MAP will be employed for the project in this report. Since we have the following relation,

$$log\left[\sum_i exp(A_i)\right] = A_M, \tag{3.34}$$

following new equations are obtained.

$$\begin{array}{rcl} \Gamma_t(m,m') & = & log(\gamma_t(m,m')) \\ A_t(m) & = & \max_{m'}\left(A_{t-1}(m') + \Gamma_t(m,m')\right) \\ B_t(m) & = & \max_{m'}\left(B_{t+1}(m') + \Gamma_{t+1}(m,m')\right) \\ L(u(t)) & = & \max_{(m,m':u(t)=1)}\left(A_{t-1}(m') + B_t(m) + \Gamma_t(m',m)\right) \\ & - & \max_{(m,m':u(t)=0)}\left(A_{t-1}(m') + B_t(m) + \Gamma_t(m',m)\right) \end{array} \tag{3.35}$$

Figure 3.8 shows the BER performance comparison of coherent QPSK system between hamming decoder, Viterbi decoder, and Max-Log-Map decoder concatenated with transmit diversity (2Tx-1Rx) in Rayleigh fading channel. Rayleigh fading channel parameters are generated by zero mean complex Gaussian random numbers with variance 0.5. Channel codes take care of coding gains and the transmit diversity handles the diversity gains. Since we concatenated the same transmit diversity scheme to different channel coding

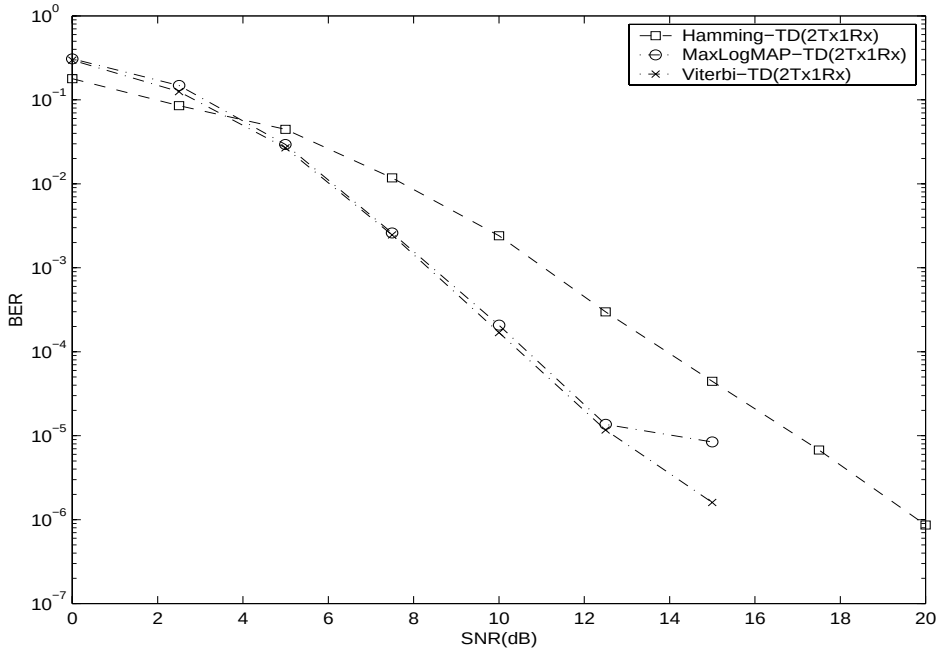

Figure 3.8: BER performance comparison of coherent QPSK between hamming decoder, Viterbi decoder, and Max-Log-Map decoder concatenated with transmit diversity (2Tx-1Rx) in Rayleigh fading channel.

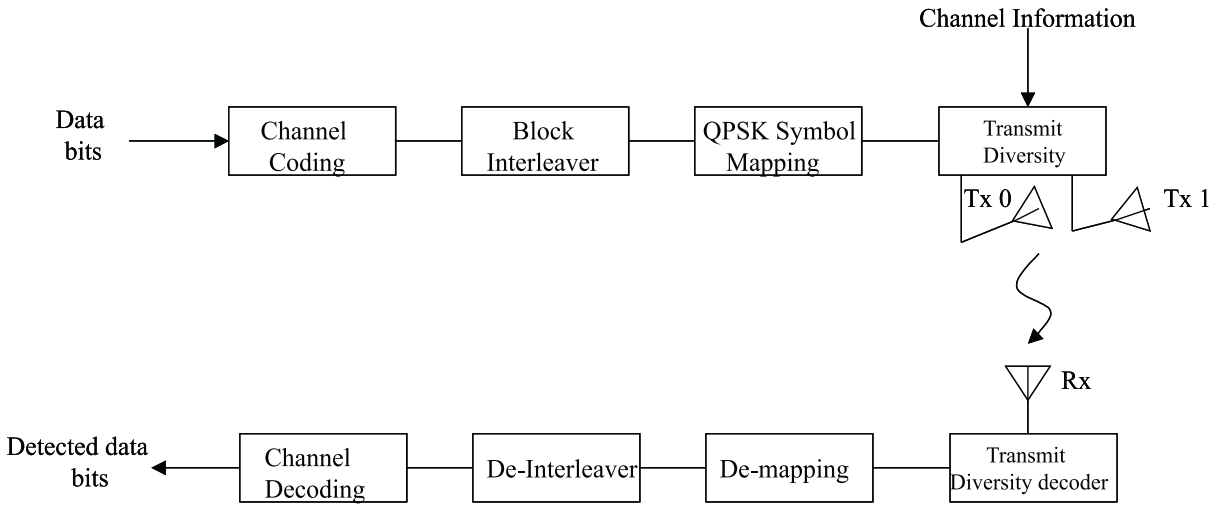

Figure 3.9: Block diagram of transmit diversity (2Tx-1Rx) concatenated with different channel coding schemes.

schemes as in Figure 3.9, the performance difference is mostly influenced by the different channel codes. Hamming codes shows about 3 dB degradation against the Viterbi decoders, when it is measured around BER, 10^{-4} area. Considering about 0.2 dB degradation by using Max-Log-MAP instead of Log-MAP algorithm, Viterbi decoder shows almost equal performance with Max-Log-MAP algorithm. The error floor of Max-Log-MAP decoder formed over the high SNR area can be lowered by increasing the block size of the trellis.

3.3 Turbo Codes

Turbo decoding algorithm consists of two constituent decoders that compute *MAP* for noise added information on two separate channels and then these two decoders iteratively feed their results into each other, updating the *a posteriori* probability by passing the updated *a priori* probability as the algorithm repeats the iteration.

3.3.1 Turbo Code Design

Turbo decoder consists of two constituent MAP decoders with parallel concatenation, working iteratively. As for the turbo decoder, the assumption that the *a priori* probability stays equal over the whole process of MAP algorithm is no longer true. The output of one decoder in turbo decoder is passed out as an input to the other decoder. Since the information passed between two decoders should be precise and detail, the data passing should be soft information. Turbo encoder transmits block-interleaved two replica of information over the channel. Thus, the turbo-encoded information should be composed of systematic and parity bits, that is, the turbo encoder generates systematic codes.

1. **Turbo Encoder** Turbo encoder needs to implement a systematic convolutional encoder than a regular convolutional encoder. While conventional convolutional encoders are finite impulse response filters, systematic encoders are infinite impulse response filter [11]. Since it is recursively implemented, it is also called the recursive systematic codes (RSC). Section 3.2.2 well explains about RSC.

2. **Trellis Termination** Since it is impossible to force the trellis to converge to zero state by simply adding redundant all zero input at the end of block of data, more sophisticated algorithm is required to have the trellis converge to zero. One way of doing it, employed in our project, is to add an extra algorithm to find the last state ending, according to the encoder scheme and the input data for one MAP decoder and to leave the other MAP decoder open. Section 3.2.2 describes our trellis termination scheme in detail.

3. **Turbo Decoder** From the equation (3.23), the second probability carries the *a priori* information which was ignored for MAP algorithm case, but it should be taken into account for turbo codes. Since the first probability in equation (3.23)

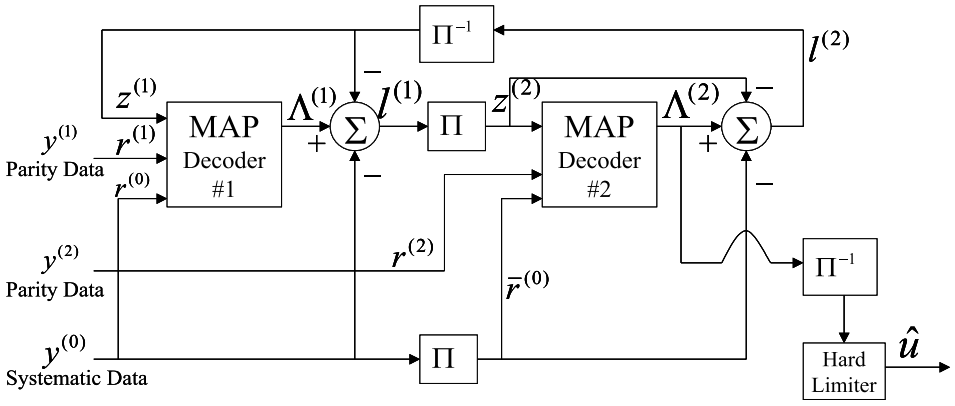

Figure 3.10: Block diagram of Turbo decoder.

is constant, we will express the branch metric, γ with the second and third probability in equation (3.23). Taking the logarithm on this, it is

$$\gamma_t(m', m) = logP(Y_t|X_t) + logP(u(t)).$$

$P(u(t))$ is derived from the *a priori* input, z_t as in Figure 3.10 as follows [11]:

$$P(u(t)) = \begin{cases} \frac{exp(z_t)}{1+exp(z_t)} & \text{for } u(t) = 1 \\ \frac{1}{1+exp(z_t)} & \text{for } u(t) = 0 \end{cases} \tag{3.36}$$

and

$$logP(u(t)) = z_t u(t) - log(1 + exp(z_t)). \tag{3.37}$$

$log(1 + exp(z_t)) = log(exp(0) + exp(z_t))$ can be approximated as $max(0, z_t)$ by the relation in equation (3.34). This approximation reduces the possibility of computational overflow by avoiding the exponential calculation. The likelihood ratio ($\Lambda(u(t))$), the output of each MAP decoder at a trellis time t has the relation with other parameters in Figure 3.10 as follows

$$\Lambda(u(t)) = y_t + z_t + l_t, \tag{3.38}$$

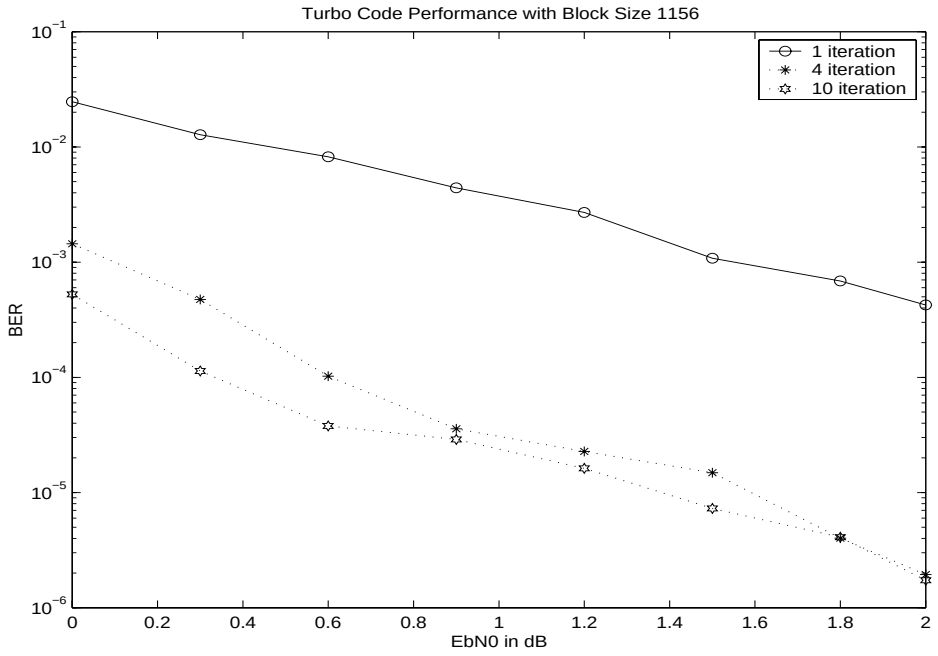

Figure 3.11: BER performance of Turbo codes with block size 1156 over AWGN.

where y=$a(2x-1)+n$. a and n here, correspond to the α and η of equation (6.1) respectively. The role of '$2x$-1' is symbol mapping from bits 0 or 1 to -1 or 1. The one thing to note in implementing Max-Log-MAP algorithm for a turbo code is to normalize α and β at each trellis time by the maximum α and β value to avoid the possible overflow.

Turbo codes with Max-Log-MAP as its decoding algorithm has been reviewed so far. Its BER performance over AWGN is shown in Figure 3.11. The received signal y in Equation (3.38) for AWGN environment can be expressed as y=$(2x-1)+n$. The following section shows performance results of a turbo code whose constituent encoder is designed in the RSC of Figure 3.4.

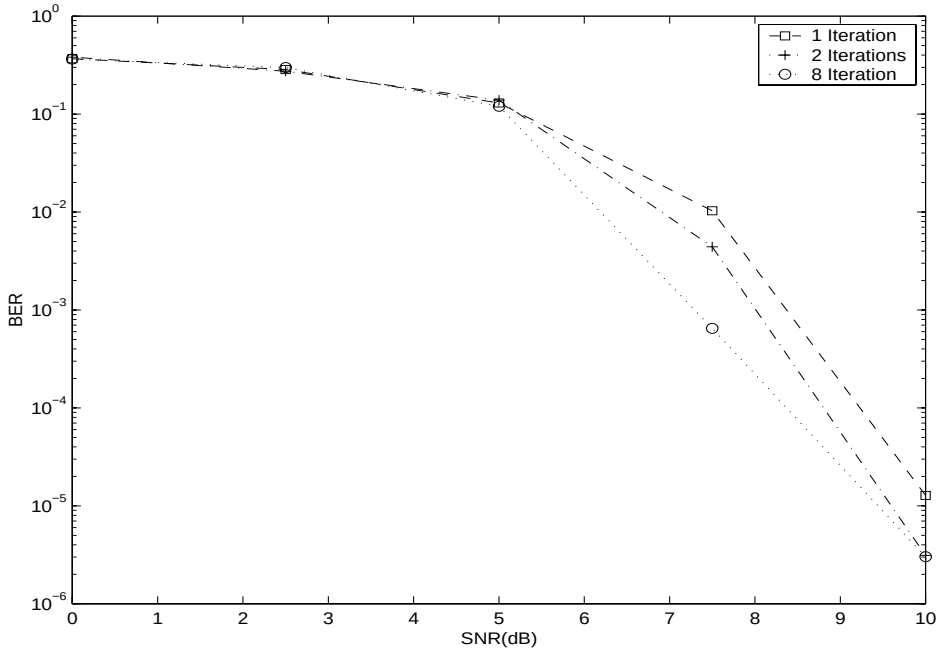

Figure 3.12: BER performance of Turbo codes with block size 1156 over Rayleigh fading channel with f_dT_s 0.01.

3.3.2 Performance Results

The trellis length of the turbo codes in Figure 3.11 is 1156 bits. The turbo codes of Figure 3.11 achieve the BER of 10^{-4} with 4 iterations even at 0.6 dB. It is verified from the Figure that the near-Shannon-limit performance is achieved at the very low SNR over the AWGN environment. The performance of the same turbo codes over Rayleigh fading channel with f_dT_s 0.01 is shown in Figure 3.12. The BER 10^{-3} is achieved at SNR 8.8 dB with 2 iterations. Since the error floor which is a natural property of turbo codes starts getting formed around $2\text{x}10^{-6}$, the performance between 2 and 8 iterations gets closer above SNR 7 dB. The error floor can be lowered to some extent by increasing the block size. The turbo codes shown in this Section have the block size 1156 bits for both Figure 3.11 and 3.12.

Chapter 4

Serial Concatenation of Turbo Codes with Space-Time Block Codes

Concatenated codes provide the desired error performance with a relatively lower overall system complexity than what should be demanded by a single code. It is the main goal of this research to observe the contribution of turbo codes in improving the coding gain, when concatenated with STBC.

The serial concatenation of turbo codes with the various STBC schemes does not only provide the coding gain but also mitigates the channel correlation factors caused from the Doppler frequency. The interleaver implemented in turbo codes plays a role of diminishing the channel correlation [64].

Several STBC schemes designed in an orthogonal method or an quasi-orthogonal method were presented in Section 2.2.2. Detail design procedures of encoders and decoders for these schemes were also shown in Section 2.2.2. Since the soft decoded information should be passed from the STBC decoder to the turbo decoder, when they are serially concatenated, it is important to get soft decoded outputs out of STBC decoder. Section 2.2.2 describes how to obtain the soft information from the STBC decoder outputs, especially for the STBC scheme designed in orthogonal method.

This Chapter illustrates analytical procedures to obtain the soft outputs from the STBC

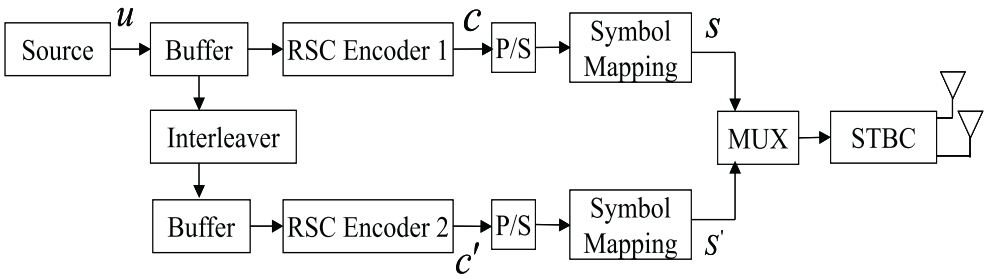

Figure 4.1: Transmitter block diagram for STBC concatenated with turbo codes.

designed in quasi-orthogonal method. In addition to the mathematic analysis of STBC decoders, the performance results and design details about the STBC serially concatenated with turbo codes will be shown in this Chapter.

4.1 Space-Time Block Codes Concatenated with Turbo Codes

Turbo codes will be concatenated as an outer code with Space-Time Block Codes as an inner code in order to improve coding gains. The transmitter block diagram for STBC concatenated with turbo codes is shown in Figure 4.1. Since the rate 1/2, RSC encoder is used for a constituent turbo encoder, two bit codeword C will be fed to the QPSK symbol mapping to generate symbols S. The parallel to serial converter is required for turbo codes and STBC to be performed in a block of data and in iterations of four symbols, respectively. The parallel to serial converter turns the block of data, outputs of RSC Encoders in Figure 4.1 into four symbol long data, respectively per each RSC Encoder to reduce memory consumption. RSC Encoders include the algorithm to find the last state of trellis and to terminate the trellis by adding a couple of redundant bits according to the last state found. The trellis termination procedure is described in Section 3.2.2 in detail.

Since the QPSK modulation is used, the data bit out of systematic codes becomes the real part of symbol and the parity bit is used for the imaginary part of symbol. Each bit is turned into 1 or -1 through the turbo encoder, hence, the energy of a baseband symbol is $\sqrt{2}/2$.

The output of STBC decoder, $\tilde{s}$ is passed to the turbo decoder for the error correction [5][26][56][65][66]. It was illustrated how to get $\tilde{s}$ for G_2 of Equation (2.23) in Section 2.2.2. $\tilde{s}$ for G_3 also can be obtained in the same way as described in the Decoding Algorithm of Section 2.2.2 and was given in Equation (2.37). The complete procedure to obtain soft outputs, $\tilde{s}$ for G_4 will be illustrated in this Section. Applying the properties of complex numbers and deleting the terms that are independent of codewords, the decision metric of (2.24) can be expanded as

$$\sum_{m=0}^{M-1}[-2V + V_1 - 2W + W_1 - 2X + X_1 - 2Y + Y_1], \tag{4.1}$$

where

$$\begin{aligned}
V &= \left\{r_{0,m}^* \left(\textstyle\sum_{n=0}^{3} \alpha_{n,m} C_{0,n}\right) + r_{0,m} \left(\textstyle\sum_{n=0}^{3} \alpha_{n,m} C_{0,n}\right)^*\right\},\\
W &= \left\{r_{1,m}^* \left(\textstyle\sum_{n=0}^{3} \alpha_{n,m} C_{1,n}\right) + r_{1,m} \left(\textstyle\sum_{n=0}^{3} \alpha_{n,m} C_{1,n}\right)^*\right\},\\
X &= \left\{r_{2,m}^* \left(\textstyle\sum_{n=0}^{3} \alpha_{n,m} C_{2,n}\right) + r_{2,m} \left(\textstyle\sum_{n=0}^{3} \alpha_{n,m} C_{2,n}\right)^*\right\},\\
Y &= \left\{r_{3,m}^* \left(\textstyle\sum_{n=0}^{3} \alpha_{n,m} C_{3,n}\right) + r_{3,m} \left(\textstyle\sum_{n=0}^{3} \alpha_{n,m} C_{3,n}\right)^*\right\},\\
V_1 &= \left|\textstyle\sum_{n=0}^{3} \alpha_{n,m} C_{0,n}\right|^2,\ W_1 = \left|\textstyle\sum_{n=0}^{3} \alpha_{n,m} C_{1,n}\right|^2,\\
X_1 &= \left|\textstyle\sum_{n=0}^{3} \alpha_{n,m} C_{2,n}\right|^2,\ Y_1 = \left|\textstyle\sum_{n=0}^{3} \alpha_{n,m} C_{3,n}\right|^2,
\end{aligned}$$

respectively. V_1 through Y_1 can be expanded again as

$$\begin{aligned}
V_1 &= |\alpha_{0,m} s_0 + \alpha_{1,m} s_1|^2 + 2V_a + |\alpha_{2,m} s_2 + \alpha_{3,m} s_3|^2,\\
W_1 &= |-\alpha_{0,m} s_1^* + \alpha_{1,m} s_0^*|^2 + 2W_a + |-\alpha_{2,m} s_3^* + \alpha_{3,m} s_2^*|^2,\\
X_1 &= |-\alpha_{0,m} s_2^* - \alpha_{1,m} s_3^*|^2 + 2X_a + |\alpha_{2,m} s_0^* + \alpha_{3,m} s_1^*|^2,\\
Y_1 &= |\alpha_{0,m} s_3 - \alpha_{1,m} s_2|^2 + 2Y_a + |-\alpha_{2,m} s_1 + \alpha_{3,m} s_0|^2,
\end{aligned} \tag{4.2}$$

where

$$\begin{aligned}
V_a &= (\alpha_{0,m} s_0 + \alpha_{1,m} s_1)^* (\alpha_{2,m} s_2 + \alpha_{3,m} s_3) + (\alpha_{0,m} s_0 + \alpha_{1,m} s_1)(\alpha_{2,m} s_2 + \alpha_{3,m} s_3)^*,\\
W_a &= (-\alpha_{0,m} s_1^* + \alpha_{1,m} s_0^*)^* (-\alpha_{2,m} s_3^* + \alpha_{3,m} s_2^*) + (-\alpha_{0,m} s_1^* + \alpha_{1,m} s_0^*)(-\alpha_{2,m} s_3^* + \alpha_{3,m} s_2^*)^*,\\
X_a &= (-\alpha_{0,m} s_2^* - \alpha_{1,m} s_3^*)^* (\alpha_{2,m} s_0^* + \alpha_{3,m} s_1^*) + (-\alpha_{0,m} s_2^* - \alpha_{1,m} s_3^*)(\alpha_{2,m} s_0^* + \alpha_{3,m} s_1^*)^*, \text{ and}\\
Y_a &= (\alpha_{0,m} s_3 - \alpha_{1,m} s_2)^* (-\alpha_{2,m} s_1 + \alpha_{3,m} s_0) + (\alpha_{0,m} s_3 - \alpha_{1,m} s_2)(-\alpha_{2,m} s_1 + \alpha_{3,m} s_0)^*.
\end{aligned}$$

Then, $(V_1 + W_1 + X_1 + Y_1)$ becomes

$$\left(|s_0|^2 + |s_1|^2 + |s_2|^2 + |s_3|^2\right) \sum_{n=0}^{3} |\alpha_{n,m}|^2 + 2(V_a + W_a + X_a + Y_a). \tag{4.3}$$

Since s_0=1+j, s_1=1-j, s_2=-1+j, and s_3=-1-j for QPSK, $(V_a + W_a + X_a + Y_a)$ becomes zero.

Hence, the decision metric of (2.24) becomes

$$\begin{array}{l} \sum_{m=0}^{M-1} \left[-2V + |s_0|^2 \sum_{n=0}^{3} |\alpha_{n,m}|^2\right] + \sum_{m=0}^{M-1} \left[-2W + |s_1|^2 \sum_{n=0}^{3} |\alpha_{n,m}|^2\right] + \\ \sum_{m=0}^{M-1} \left[-2X + |s_2|^2 \sum_{n=0}^{3} |\alpha_{n,m}|^2\right] + \sum_{m=0}^{M-1} \left[-2Y + |s_3|^2 \sum_{n=0}^{3} |\alpha_{n,m}|^2\right]. \end{array} \tag{4.4}$$

It does not make a difference in the overall decision of (4.4) to add the term independent of codewords. Hence, we add $\left|r_{0,m}\alpha_{0,m}^* + r_{1,m}^*\alpha_{1,m} + r_{2,m}^*\alpha_{2,m} + r_{3,m}\alpha_{3,m}^*\right|^2$ to the first term of (4.4), to make -2V a perfect square form. Thus, the first term of (4.4) becomes

$$\sum_{m=0}^{M-1} [|(r_{0,m}\alpha_{0,m}^* + r_{1,m}^*\alpha_{1,m} + r_{2,m}^*\alpha_{2,m} + r_{3,m}\alpha_{3,m}^*) - s_0|^2 + (-1 + \sum_{n=0}^{3} |\alpha_{n,m}|^2)|s_0|^2]. \tag{4.5}$$

In the same way, the second, the third, and the fourth terms of (4.4) can be obtained as,

$$\sum_{m=0}^{M-1} [|(r_{0,m}\alpha_{1,m}^* - r_{1,m}^*\alpha_{0,m} + r_{2,m}^*\alpha_{3,m} - r_{3,m}\alpha_{2,m}^*) - s_1|^2 + (-1 + \sum_{n=0}^{3} |\alpha_{n,m}|^2)|s_1|^2], \tag{4.6}$$

$$\sum_{m=0}^{M-1} [|(r_{0,m}\alpha_{2,m}^* + r_{1,m}^*\alpha_{3,m} - r_{2,m}^*\alpha_{0,m} - r_{3,m}\alpha_{1,m}^*) - s_2|^2 + (-1 + \sum_{n=0}^{3} |\alpha_{n,m}|^2)|s_2|^2], \tag{4.7}$$

$$\sum_{m=0}^{M-1} [|(r_{0,m}\alpha_{3,m}^* - r_{1,m}^*\alpha_{2,m} - r_{2,m}^*\alpha_{1,m} + r_{3,m}\alpha_{0,m}^*) - s_3|^2 + (-1 + \sum_{n=0}^{3} |\alpha_{n,m}|^2)|s_3|^2]. \tag{4.8}$$

For PSK systems, the second terms in the expressions, (4.5), (4.6), (4.7), and (4.8) are constant for all symbols cases. Therefore, soft outputs of STBC decoder for G_4 are obtained as

$$\begin{array}{l} \tilde{s}_0 = \sum_{m=0}^{M-1}(r_{0,m}\alpha_{0,m}^* + r_{1,m}^*\alpha_{1,m} + r_{2,m}^*\alpha_{2,m} + r_{3,m}\alpha_{3,m}^*), \\ \tilde{s}_1 = \sum_{m=0}^{M-1}(r_{0,m}\alpha_{1,m}^* - r_{1,m}^*\alpha_{0,m} + r_{2,m}^*\alpha_{3,m} - r_{3,m}\alpha_{2,m}^*), \\ \tilde{s}_2 = \sum_{m=0}^{M-1}(r_{0,m}\alpha_{2,m}^* + r_{1,m}^*\alpha_{3,m} - r_{2,m}^*\alpha_{0,m} - r_{3,m}\alpha_{1,m}^*), \\ \tilde{s}_3 = \sum_{m=0}^{M-1}(r_{0,m}\alpha_{3,m}^* - r_{1,m}^*\alpha_{2,m} - r_{2,m}^*\alpha_{1,m} + r_{3,m}\alpha_{0,m}^*). \end{array} \tag{4.9}$$

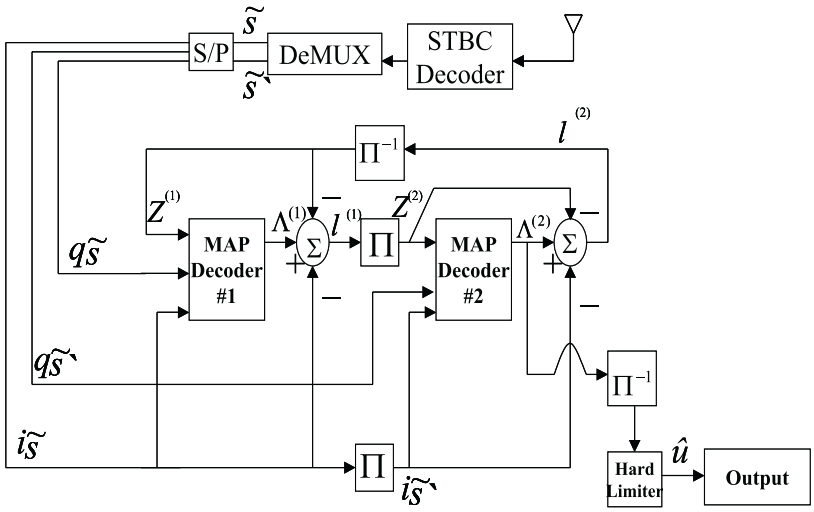

Figure 4.2: Receiver block diagram for STBC concatenated with turbo codes.

These soft outputs of STBC decoders are passed to the turbo decoder. Figure 4.2 shows the receiver block diagram for STBC concatenated with turbo codes. The serial to parallel converter in Figure 4.2 stores these soft outputs of STBC decoder until the whole block of data arrive, because turbo codes are performed over a block of data. The in-phase and quadrature-phase components of $\tilde{S}$ and the *a priori* information $Z^{(1)}$ which is initialized to be zero are inputs to the first MAP decoder. The likelihood ratio output of the first decoder, $\Lambda^{(1)}$ is passed, together with interleaved components, to the second MAP decoder. These procedures are repeated over a certain number of iterations between two constituent decoders as seen in Figure 4.2. Once the iterations are completed, the final likelihood ratio outputs of the second MAP decoder result in the decoded data bits after going through the deinterleaver and the hard limiter. The following Section shows the BER performance of STBC concatenated with turbo codes.

4.2 Performance Results for STBC Concatenated with Turbo Codes

Three STBC schemes are serially concatenated with turbo codes according to the procedures in Section 4.1. The encoding schemes for those three schemes are presented in Section 2.2. The G_2 and G_3 schemes are designed in an orthogonal method, given in Equation (2.23), on the other hand, the G_4 scheme is designed in a quasi-orthogonal method, and given in Equation (2.38). The specific differences and properties of these STBC schemes were described in Section 2.2. These G_2, G_3, and G_4 schemes are concatenated with the turbo code scheme which was given in Section 3.3.1, and their BER performances are shown via simulation in this Section. The simulation results in this Section are obtained over the same channel environment, Rayleigh fading channel with the normalized Doppler frequency parameter ($f_d T_s$), 0.01.

The BER performance for the turbo concatenation to G_2 scheme is shown in Figure 4.3. The *SNR* in the result is controlled by the variance of AWGN. Since the energy of a baseband symbol is $\sqrt{2}/2$, the baseband noise variance is $(N\sqrt{2})/(2SNR)$, where N is the number of transmitter. The trellis length for the turbo code is 1024 trellis times, and the block interleaver of the same length is used for this scheme. Since the exponential computation in the MAP decoding algorithm causes the round-off errors occuring from numerical values with limited precision, the Max-Log-MAP algorithm which turns the exponential computation into a simple selection algorithm is used for our simulation.

About 5.5 dB gain between 2 receivers and 1 receiver was observed for G_2 scheme before the concatenation in Section 2.2 and approximately the same gain is achieved after the concatenation in Figure 4.3. The coding gain contributed by the turbo concatenation is easily observed, when we compare the performance of STBC concatenated to turbo codes with the performance of STBC alone. The diversity gain which differs by each STBC scheme makes the difference in each performance result. The large performance

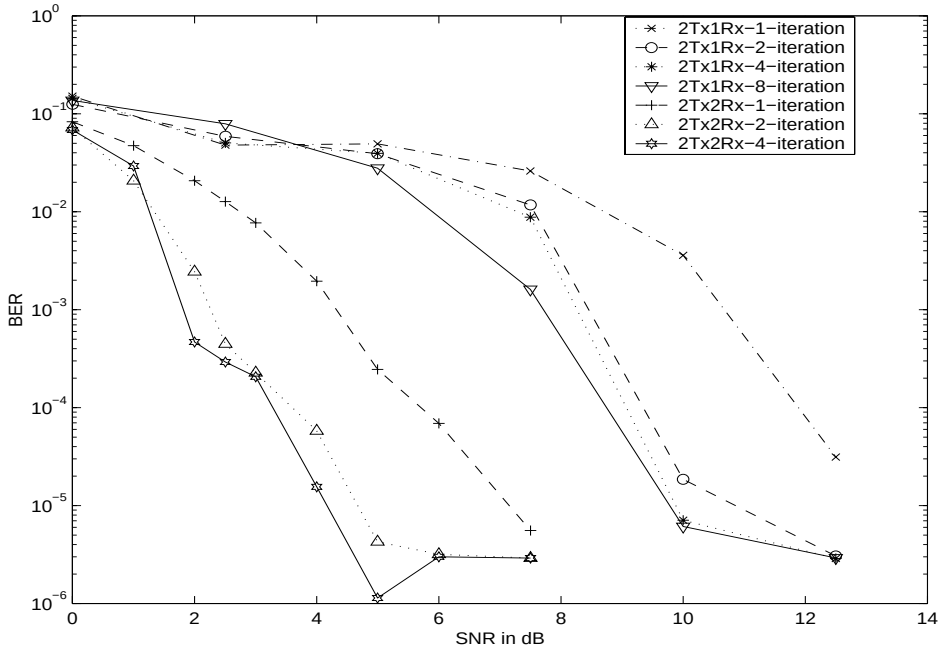

Figure 4.3: BER performance for STBC (G_2) concatenated with turbo codes over Rayleigh fading channel with $f_d T_s$, 0.01.

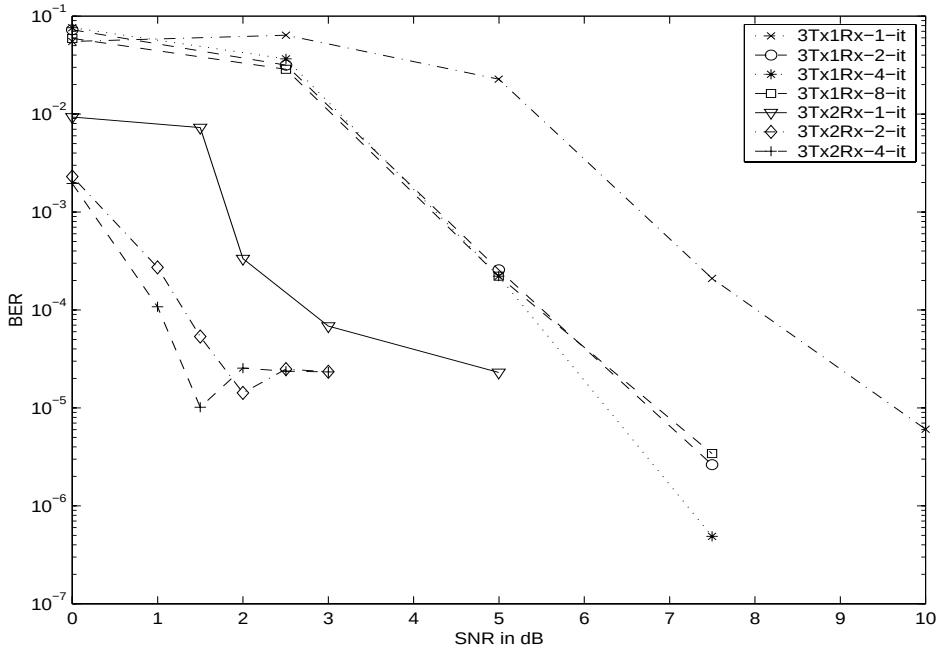

Figure 4.4: BER performance for STBC (G_3) concatenated with turbo codes over Rayleigh fading channel with $f_d T_s$, 0.01.

gap between one iteration and two iterations for ISTTC reflects the typical performance of iterative decoding.

At least two iterations in decoding of turbo codes are required for the considerable improvement in BER performance for all three concatenation cases. The BER performances of turbo concatenation with G_3 and G_4 schemes are shown in Figure 4.4 and 4.5, respectively. Whereas G_2 and G_3 schemes achieve full diversity whose diversity gain is calculated by the number of transmitters times the number of receiver (NM), the G_4 scheme has diversity gain of $2M$, which shows an inferior performance for one receiver case to G_2 or G_3 schemes concatenated with turbo codes. But as Figure 4.5 shows, it compensates for the lower diversity gain easily by increasing the number of receivers. Full transmission rate is more important for very low SNR and high BER, however, full diversity is the right choice for high SNR and low BER [22]. But the concatenation of

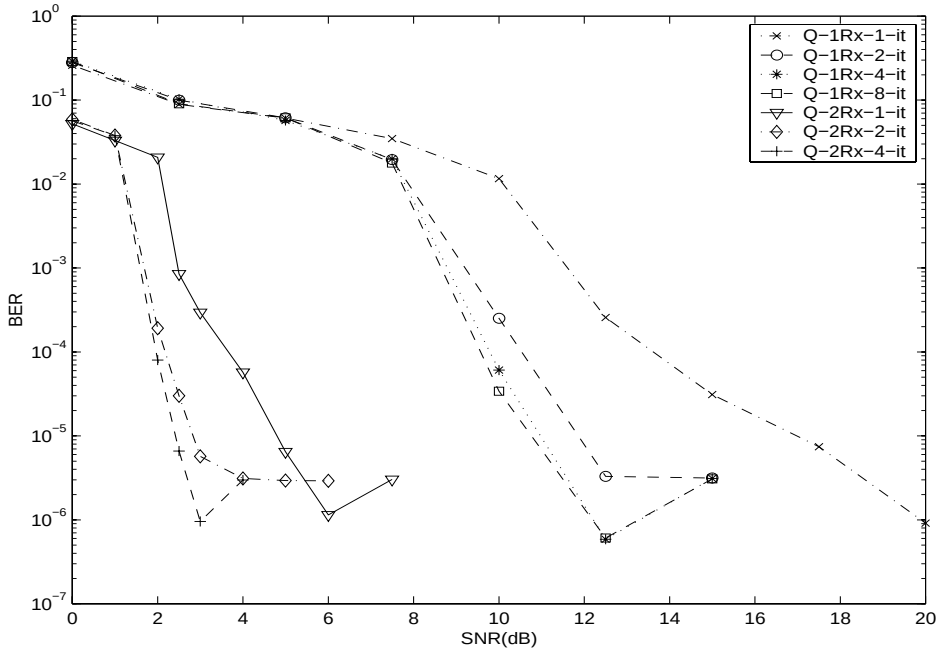

Figure 4.5: BER performance for STBC (Quasi-Orthogonal) concatenated with turbo codes over Rayleigh fading channel with $f_d T_s$, 0.01.

turbo code to G_4 with two receivers achieves almost an equal performance to other two cases as well as the higher transmission rate.

There is a considerable performance gain by concatenating turbo codes with STBC, as seen from the results. It is achieved by a relatively simple design procedure. Full transmission rate as well as the diversity gain can be accomplished even with the higher number of transmitters by concatenating turbo codes to STBC designed in quasi-orthogonal method and increasing the number of receivers. The fact that the interleaver of turbo codes are known to mitigate the channel correlation effect caused from the fading channel [64], which eventually contributes to the performance improvement, is another advantage we can reap by turbo concatenation.

Chapter 5

Serial Concatenation of Turbo Codes with Space-Time Block Codes in No Channel Estimation

Although STBC provides fairly good diversity gain over the Rayleigh fading channel using only linear processing at the receiver, it requires the channel state estimation for decoding at the receiver end. Sending extra symbols for initial estimates of the time varying channel increases the complexity of the system and decreases the transmission rate as well. It has been considered difficult to estimate the time varying channel, thus, the transmit diversity with no channel estimation (TDNC) where neither the transmitter nor the receiver requires channel state estimation was proposed in [23]. The TDNC was concatenated with turbo codes and it showed conspicuous improvement in BER performance [25]. Serial concatenation of turbo codes to the STBC with no channel estimation (STBCNC) was also proposed in [24]. TDNC is a special case of STBCNC, that is, STBC having higher number of transmitters than TDNC also can be performed without channel estimation. Design procedures for TDNC and STBCNC are described in this Chapter. The TDNC scheme as well as the STBCNC is performed recursively and differentially using the received symbols in the previous time frame, thus, the hard

decision information needs to be passed recursively back to the next symbol detection. On the other hand, turbo codes need the soft information for the iterative decoding. Hence, it is necessary to implement two different decoding routines (one for the hard decision and the other for the soft decision) for the concatenation of turbo codes to the TDNC or STBCNC.

The restriction on f_dT_s which was imposed for the proper operation of TDNC or STBCNC can be loosened from the serial concatenation of turbo codes. Mathematic analysis on this fact will be illustrated and the BER performances for these schemes will be shown in this Chapter.

5.1 Space-Time Block Codes with No Channel Estimation

Some previous researches, [23][25] introduced the transmit diversity without channel estimation to reduce the overall system complexity. Their results were restricted to two transmitters. However, space-time codes with no channel estimation can be implemented for any number of transmitters in [24]. Design procedures for these STBCNC schemes, and their restrictions for proper operation will be illustrated in this Section.

5.1.1 Transmit Diversity with No Channel Estimation

The TDNC description in this Section is based upon the references, [23][25]. About 3 dB degradation of SNR at BER 10^{-3} is observed for TDNC, when it is compared with TD proposed by Alamouti under the restriction of $f_dT_s \leq 10^{-3}$. Since the TD (Alamouti Scheme) requires the complete channel estimation, extra symbols for initial estimates of the time varying channel need to be sent, which results in higher complexity to the system and decreases the transmission rate as well. The TDNC lowers the system complexity at the cost of 3 dB performance penalty.

A. Method A TDNC does not require the channel state information. However, the transmission of two known symbols at the start of an information block is necessary to compute the next symbols at the receiver.

The channel is assumed to be constant from t to $t+3\tau$ for four consecutive transmission symbol periods, where τ is one symbol period. The receiver computes the next symbols, s_2 and s_3 from the known s_0, s_1, $r_{0,m}$, $r_{1,m}$, $r_{2,m}$ and $r_{3,m}$ and proceeds to obtain further symbols recursively.

The received symbols for four consecutive transmission periods, $r_{0,m}$, $r_{1,m}$, $r_{2,m}$ and $r_{3,m}$ can be written as,

$$\begin{array}{rcccl} r_{0,m} & = & r(t) & = & \alpha_{0,m}s_0 + \alpha_{1,m}s_1 + \eta_{0,m}, \\ r_{1,m} & = & r(t+\tau) & = & -\alpha_{0,m}s_1^* + \alpha_{1,m}s_0^* + \eta_{1,m}, \\ r_{2,m} & = & r(t+2\tau) & = & \alpha_{0,m}s_2 + \alpha_{1,m}s_3 + \eta_{2,m}, \\ r_{3,m} & = & r(t+3\tau) & = & -\alpha_{0,m}s_3^* + \alpha_{1,m}s_2^* + \eta_{3,m}, \end{array} \tag{5.1}$$

where $\alpha_{i,m}$ and $\eta_{t,m}$ are channel path gains and AWGN respectively.

The receiver builds intermediate values A and B from the received symbols,

$$\begin{array}{rcl} A & = & \sum_{m=0}^{M-1} \{r_{0,m} \cdot (r_{3,m})^* - r_{2,m} \cdot (r_{1,m})^*\}, \\ B & = & \sum_{m=0}^{M-1} \{r_{2,m} \cdot (r_{0,m})^* + r_{1,m} \cdot (r_{3,m})^*\}. \end{array} \tag{5.2}$$

The next step is to build estimates of s_2 and s_3 as follows,

$$\begin{array}{rcl} \tilde{s_2} & = & As_1^* + Bs_0, \\ \tilde{s_3} & = & -As_0^* + Bs_1. \end{array} \tag{5.3}$$

The receiver now decodes s_2 and s_3 by computing the closest symbol constellation to $\tilde{s_2}$ and $\tilde{s_3}$. Once s_2 and s_3 are obtained, s_0, s_1, s_2, and s_3 in Equation (5.1) are replaced by s_2, s_3, s_4, and s_5. Those terms, r_0, r_1, r_2, and r_3 are replaced by r_2, r_3, r_4, and r_5, as well. This process is recursively continued to compute all following symbols.

B. Method B The symbol transmitted from antenna 0 is s_0, and s_1 from antenna 1. The symbol transmitted from antenna 0 is ($-s_1^*$) and the symbol transmitted from antenna 1 is s_0^* over the next symbol period, where $*$ is the complex conjugate

Table 5.1: Transmitted and received sequences over channel path gains α_0 and α_1 for the scheme, G_2

Receiver	Transmitter 0	Transmitter 1
r_0 at time $\mathbf{t_0}$	s_0	s_1
r_1 at time $\mathbf{t_0}+\mathbf{T}$	-s_1^*	s_0^*
Channel path gains –>	$\tilde{\alpha}_0$	$\tilde{\alpha}_1$

operation.

As seen from the Table 5.1, α_0 is obtained by multiplying two received symbols with the complex conjugates of symbols in Transmitter 0 column and dividing by the energy of tranmitted symbols in that column. The α_1 is calculated in the same way. That is, the channel path gain is computed as

$$\tilde{\alpha}_{0,m} = \frac{r_{0,m}s_0^* - r_{1,m}s_1}{|s_0|^2 + |s_1|^2}, \quad \tilde{\alpha}_{1,m} = \frac{r_{0,m}s_1^* + r_{1,m}s_0}{|s_0|^2 + |s_1|^2}. \tag{5.4}$$

Once these channel path gains are obtained, we can apply the obtained channel information to Equation (2.35) to get $\tilde{s}$. The receiver decodes s_0 or s_1 by computing the closest symbol constellation to $\tilde{s_0}$ or $\tilde{s_1}$. After these s_0 and s_1 are decoded, they are fed back to the TD decoder to compute the next set of two symbols.

The performance of both 'Method A' and 'Method B' is exactly identical. The BER performance of TD and TDNC is compared in Figure 5.1. We can observe the TDNC is 3 dB degraded from the performance of TD at the BER of 10^{-3}. The TD system in the Figure is designed over the Rayleigh fading channel with f_dT_s, 10^{-2} and the TDNC is performed over the Rayleigh fading channel with f_dT_s, 10^{-4}, because TDNC is optimally performed when $f_dT_s \leq 10^{-4}$. The restriction on f_dT_s will be described in the following Section 5.1.3 in detail.

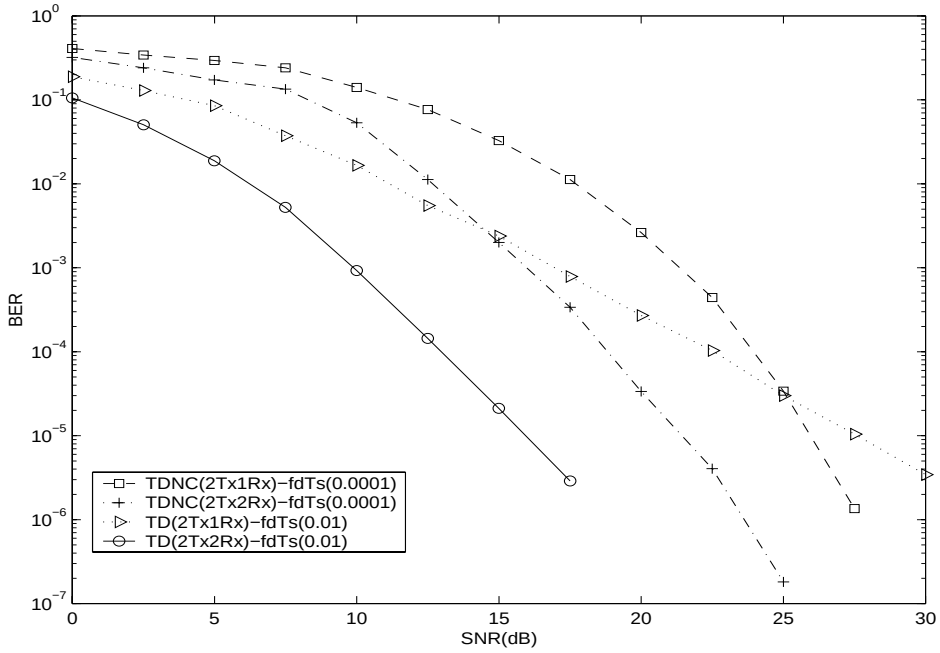

Figure 5.1: BER performance comparison between TD and TDNC transmitted over Rayleigh fading channel.

5.1.2 Space-Time Block Codes with No Channel Estimation

The 'Method B' of TDNC design can be generalized for any number of transmitter case, which is the STBC design with no channel estimation. Although the channel state information is not needed for STBCNC, the transmission of K known symbols at the start of an information block is necessary to compute the next symbols at the receiver. K is the number of constellation symbols transmitted over T time slots. The channel is assumed to be constant over $2T$ periods. The receiver computes the next K symbols from the known previous K symbols and the received symbols and proceeds to obtain further symbols recursively. The channel path gain, $\alpha_{n,m}$ represents the channel state information between the nth transmitter and the mth receiver.

In general, since an STBC is represented by a T x N transmission matrix G, the elements in the nth column of G are symbols transmitted over T symbol periods at the nth transmitter and denoted as X_{0n}, X_{1n}, ..., $X_{(T-1)n}$. Then, the channel path gain is computed as

$$\tilde{\alpha}_{n,m} = \frac{r_{0,m}X^*_{0n} + r_{1,m}X^*_{1n} + ... + r_{(T-1),m}X^*_{(T-1)n}}{|X_{0n}|^2 + |X_{1n}|^2 + ... + |X_{(T-1)n}|^2}, \tag{5.5}$$

where $r_{t,m}$ is the received symbol at time t at the mth receiver.

The calculated channel path gain, $\tilde{\alpha}_{n,m}$ is used for decoding the next K symbols, and this process is recursively continued to compute all following symbols.

For example, the channel path gain for G_3 in Equation (2.23) is calculated as

$$\begin{array}{l} \tilde{\alpha}_{0,m} = \frac{A}{2(|s_0|^2+|s_1|^2+|s_2|^2+|s_3|^2)}, \\ \tilde{\alpha}_{1,m} = \frac{B}{2(|s_0|^2+|s_1|^2+|s_2|^2+|s_3|^2)}, \\ \tilde{\alpha}_{2,m} = \frac{C}{2(|s_0|^2+|s_1|^2+|s_2|^2+|s_3|^2)}, \end{array} \tag{5.6}$$

where A, B, and C are

$$\begin{array}{rcl} A & = & r_{0,m}s^*_0 - r_{1,m}s^*_1 - r_{2,m}s^*_2 - r_{3,m}s^*_3 + r_{4,m}s_0 \\ & & -r_{5,m}s_1 - r_{6,m}s_2 - r_{7,m}s_3, \\ B & = & r_{0,m}s^*_1 + r_{1,m}s^*_0 + r_{2,m}s^*_3 - r_{3,m}s^*_2 + r_{4,m}s_1 \\ & & +r_{5,m}s_0 + r_{6,m}s_3 - r_{7,m}s_2, \\ C & = & r_{0,m}s^*_2 - r_{1,m}s^*_3 + r_{2,m}s^*_0 + r_{3,m}s^*_1 + r_{4,m}s_2 \\ & & -r_{5,m}s_3 + r_{6,m}s_0 + r_{7,m}s_1. \end{array} \tag{5.7}$$

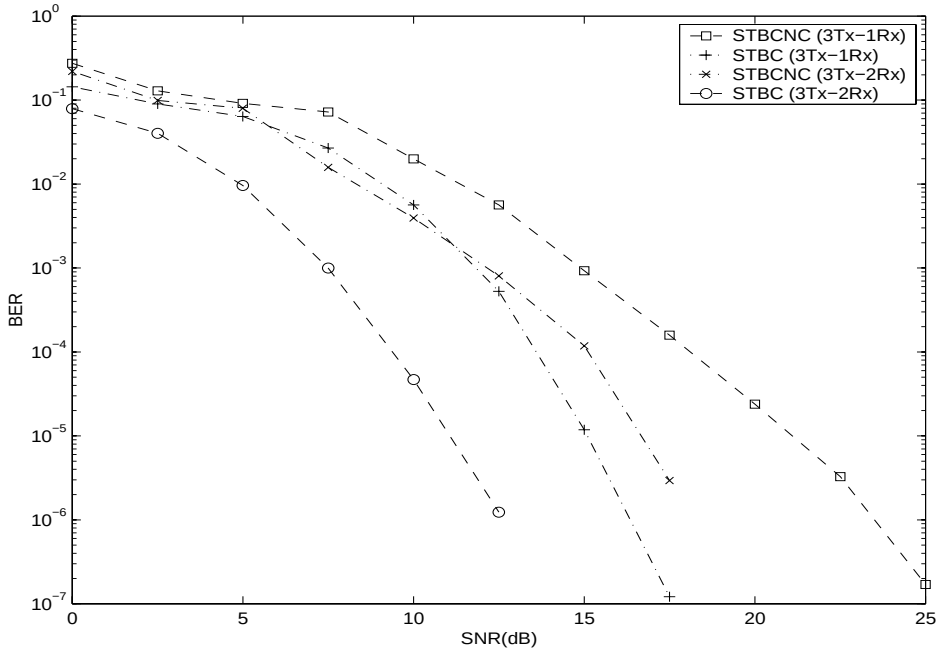

Figure 5.2: BER performance comparison between STBC (G_3) and STBCNC transmitted over Rayleigh fading channel.

Once these channel path gains are obtained, we can apply the obtained channel information to Equation (2.37) to get $\tilde{s}$ according to each STBC scheme. The receiver decodes s_x where x is 0 through K-1 by computing the closest symbol constellation to $\tilde{s_x}$. After these s_x are decoded, they are fed back to the STBC decoder to compute the next set of K symbols.

The BER performance of STBC designed in G_3 and STBCNC is compared in Figure 5.2. The STBCNC is observed to be 3.5 dB degraded from the performance of STBC at the BER of 10^{-3} in case of one receiver. The performance degradation for STBCNC with two receiver case is deepened to 5 dB. The STBC system in the Figure is designed over the Rayleigh fading channel with f_dT_s, 10^{-2} and the STBCNC is performed over the Rayleigh fading channel with f_dT_s, 10^{-4}. This is because STBCNC is optimally performed when $f_dT_s \leq 10^{-4}$.

5.1.3 Channel Restriction for the Optimal Performance of ST-BCNC

For the proper operation of STBCNC, the channel is assumed to be constant for $2T$ periods. Thus, we need to illustrate the restriction on f_dT_s for the optimal operation of STBCNC.

The level crossing rate and average fade duration of a Rayleigh fading signal are two important factors which are useful to relate the time variance of the received signal to the signal level and velocity of the mobile. The number of level crossings per second (N_R) is defined as

$$N_R = \sqrt{2\pi} f_d \rho e^{-\rho^2}, \tag{5.8}$$

where f_d is the maximum Doppler frequency and $\rho = R/R_{rms}$ is a specified signal level R normalized to the rms value of Rayleigh fading envelope [51]. The average fade duration is defined as the average period of time for which the received signal is below a specified level R [51]. For a Rayleigh fading channel, this is given as $\bar{\tau} = \frac{1}{N_R} P[r \leq R]$, where $P[r \leq R]$ is the probability that the received signal r is less than R.

$$P[r \leq R] = \int_0^R p(r)dr = 1 - exp\left(-\frac{R^2}{2\sigma^2}\right), \tag{5.9}$$

where $p(r)$ is the probability density function of Rayleigh distribution. Since R_{rms} is the square root of the mean square, that is, $\sqrt{2}\sigma$, the Equation (5.9) becomes $1 - exp(-\rho^2)$. Thus, combining the Equation (5.8) and (5.9), the average fade duration ($\bar{\tau}$) as a function of the fading depth normalized to the symbol duration is obtained as,

$$\bar{\tau} = \frac{e^{\rho^2} - 1}{\rho f_d T_s \sqrt{2\pi}}. \tag{5.10}$$

The unit of the average fade duration ($\bar{\tau}$) is the number of symbols, because $\bar{\tau}$ represents a certain length of symbol period. When we set the ρ to be 0.01, $\bar{\tau}$ gets $1/(100\sqrt{2\pi} f_d T_s)$ and $\bar{\tau}$ becomes $1/(10\sqrt{2\pi} f_d T_s)$ for the ρ, 0.1. Since the channel is assumed to be constant for at least four consecutive symbols for the right performance of TDNC system, the

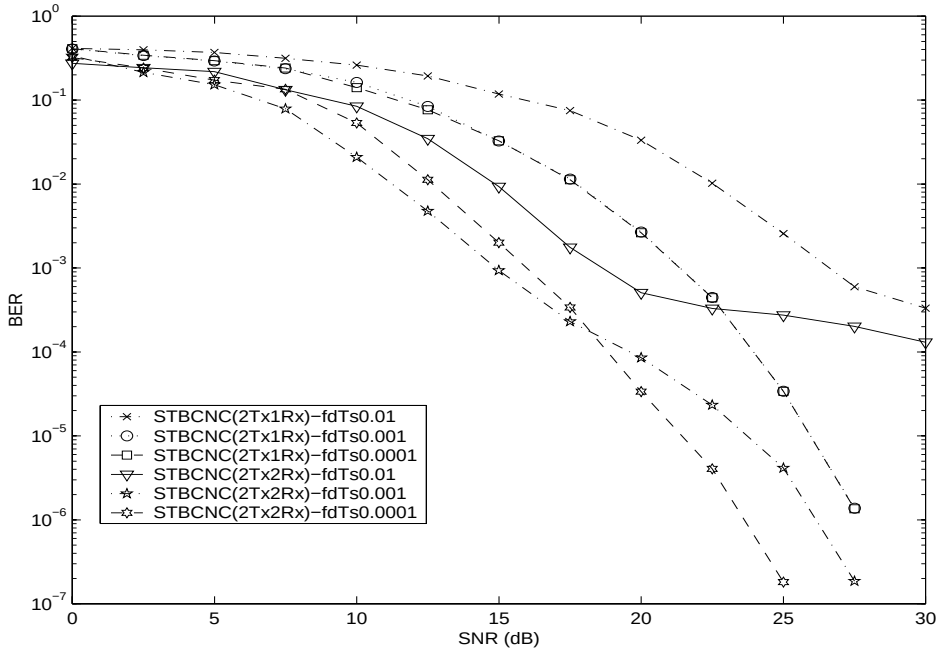

Figure 5.3: BER performance for TDNC over Rayleigh fading channel with various f_dT_s.

f_dT_s should be less than 9 x 10^{-4} for the ρ, 0.01 and it should be less than 10^{-2} for the ρ, 0.1.

Figure 5.3 shows the BER performance of TDNC designed both with two transmitters and two receivers and with two transmitters and one receiver, transmitted over Rayleigh fading channel with f_dT_s, from 10^{-2} to 10^{-4}. As seen from the figure, TDNC does not perform properly on high SNR area when f_dT_s is 0.01, though the performance for f_dT_s, 10^{-3} is not much distorted from f_dT_s, 10^{-4}.

We can observe the similar results for STBCNC in G_3 scheme in Figure 5.4. Since the channel is assumed to be constant for at least 16 consecutive symbol periods for G_3, the f_dT_s should be much less than 9 x 10^{-4}. However, we can see that STBCNC using G_3 performs well around f_dT_s, 10^{-4} from Figure 5.4, and 5.5. It is simply deduced that the G_3 scheme also raises the diversity gain as well as the number of time slots T, which helps

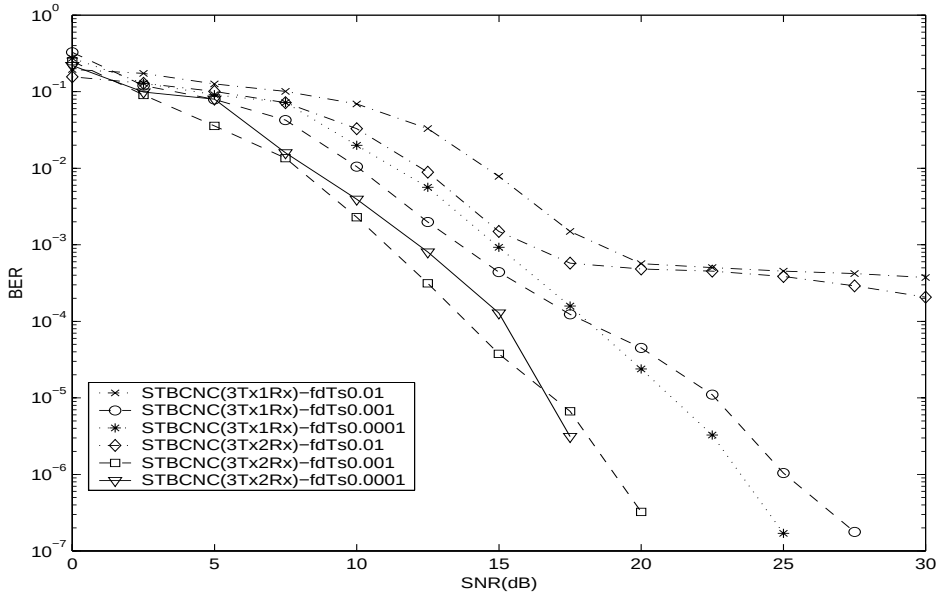

Figure 5.4: BER performance of STBCNC over Rayleigh fading channel with various $f_d T_s$.

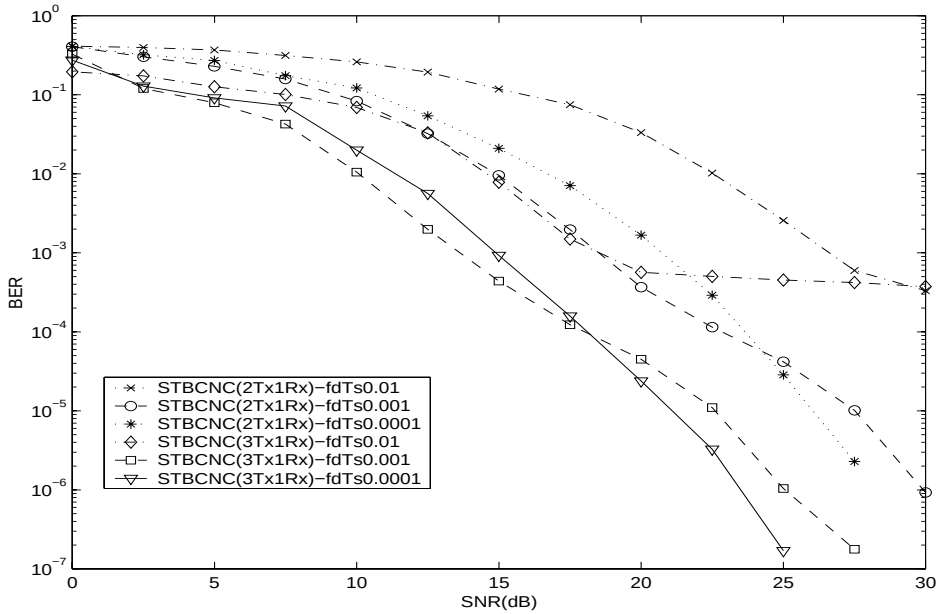

Figure 5.5: BER performance comparison between STBCNC (3Tx-1Rx) and TDNC (2Tx-1Rx) over Rayleigh fading channel with various $f_d T_s$.

STBCNC using G_3 to perform as optimally as TDNC around f_dT_s, 10^{-4}. Figure 5.5 shows the BER performance comparison between STBCNC with 3 transmitters and TDNC. We can confirm the optimal performance of STBCNC, as long as f_dT_s is less than 10^{-4}.

5.2 Serial Concatenation of Turbo Codes with STBCNC

Since STBCNC is performed recursively and differentially using the received symbols in the previous time frame, the hard decision information need to be passed recursively back to the next symbol detection. On the other hand, turbo codes need the soft decision information for the iterative decoding. Hence, it is necessary to implement two different decoding routines, one for the hard decision and the other for the soft decision, for the concatenation of turbo codes with STBCNC. Figure 5.6 shows the receiver block diagram for STBCNC concatenated with turbo codes. The block diagram of the transmitter part for STBCNC concatenated with turbo codes is identical to Figure 4.1.

The initial two symbols among the transmitted block of data from each constituent RSC encoder should be known at the decoder to implement STBCNC. It depends on the interleaver design to have the first two symbols transmitted from RSC encoder 2 in Figure 4.1 known at the decoder. In order to make turbo codes as simple as possible, $\sqrt{BS}$ x $\sqrt{BS}$ block interleaver is used, where BS is the block size of turbo codes set in the way to make $\sqrt{BS}$ be an integer. For a rate 1/2 of each constituent RSC encoder, two input bits create four outputs and thus, two symbols according to the QPSK symbol mapping. Hence, we can set the first and the $\sqrt{BS}$th bit for RSC encoder 2 as well as the first and the second bit for RSC encoder 1 to be known at the decoder. The output of STBCNC decoder, $\tilde{s}$ is soft information which is passed to the turbo decoder for the error correction and is also passed to *Decision* to be turned into hard decision symbols

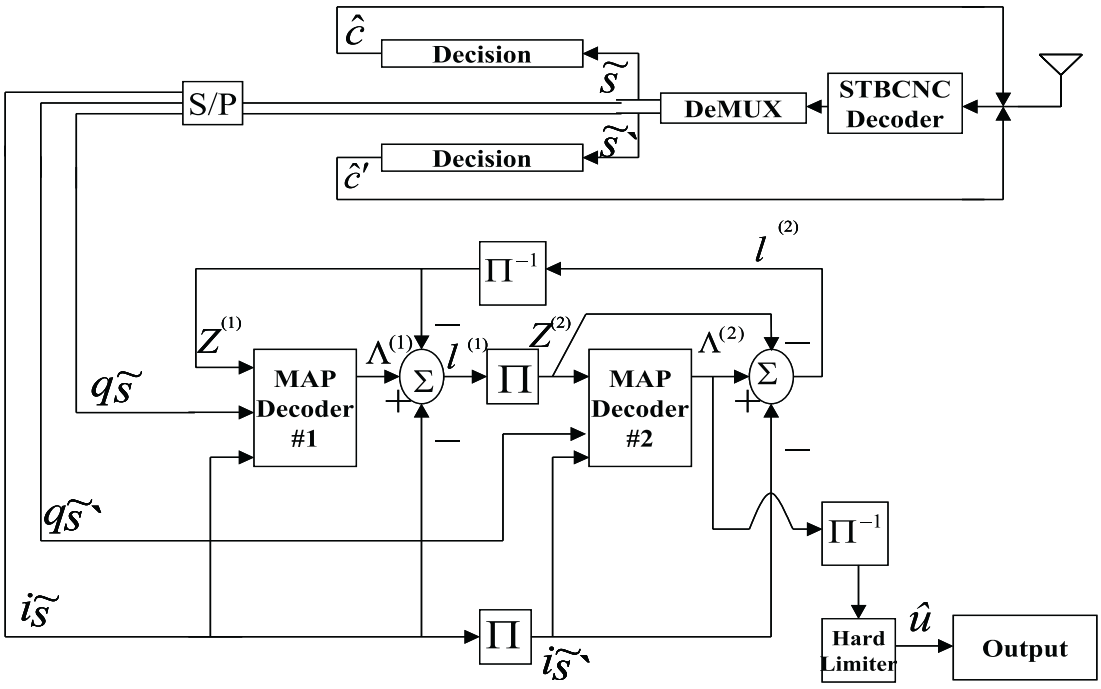

Figure 5.6: Receiver block diagram for STBCNC concatenated with turbo codes.

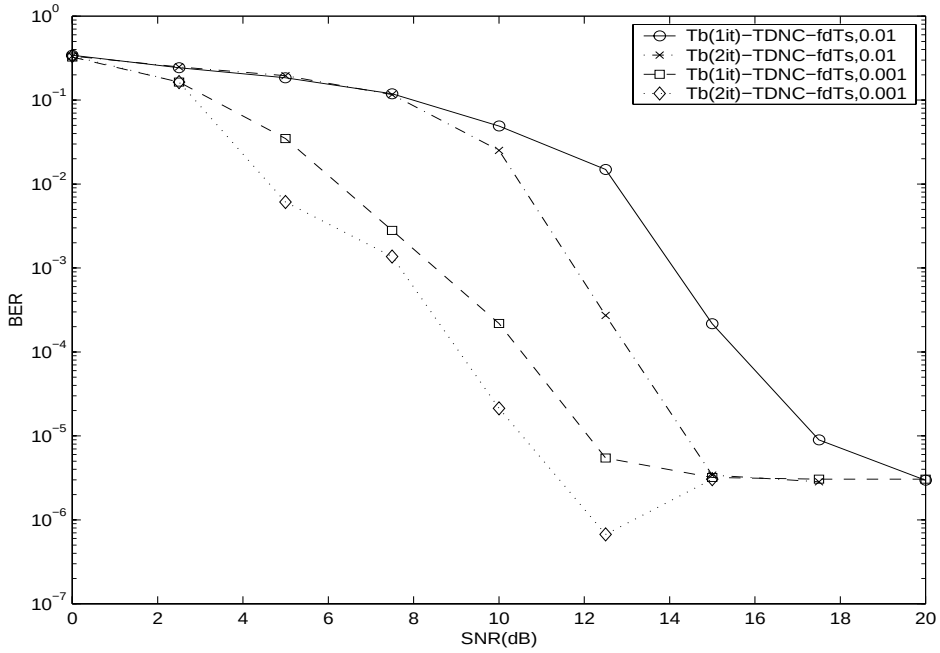

Figure 5.7: BER performance for STBCNC (2Tx-1Rx) concatenated with turbo codes over Rayleigh fading channel with f_dT_s, 0.01 and 0.001.

and recursively fed back to the STBCNC decoder.

Performance results for these STBC systems concatenated with turbo codes are shown at the following section. The SNR in the result is controlled by the variance of AWGN. Since the energy of a baseband symbol is $\sqrt{2}/2$, the baseband noise variance is $(N\sqrt{2})/(2SNR)$, where N is the number of transmitter.

5.3 Performances for Serial Concatenation of Turbo Codes with STBCNC

The optimal performance of STBCNC is achieved on condition that f_dT_s is less than 10^{-4}. However, the restriction on f_dT_s can be loosened when STBCNC is concatenated with turbo codes. As seen from Figure 5.7 and 5.8, STBCNC (2Tx-1Rx) concatenated

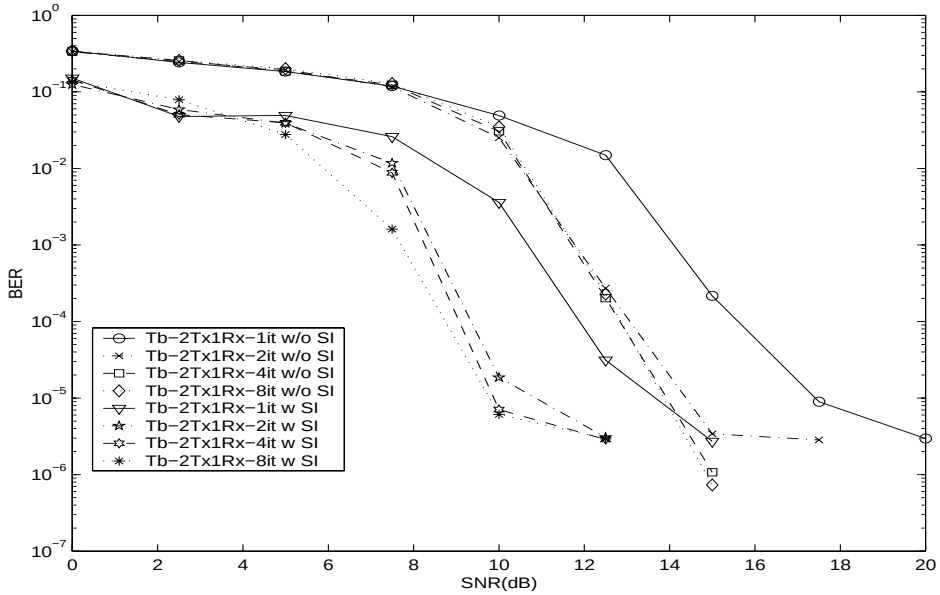

Figure 5.8: BER performance of transmit diversity (2Tx-1Rx) concatenated with turbo codes with or without channel estimation (or SI-channel side info.) over Rayleigh fading channel with f_dT_s, 0.01.

with turbo codes does perform optimally even for f_dT_s, 0.01. For BER 10^{-3}, 4 dB performance difference is observed between STBCNC concatenated with turbo codes over Rayleigh fading channel with f_dT_s, 10^{-2} and with f_dT_s, 10^{-3}. For the STBC schemes in two transmitters with or without channel estimation concatenated with turbo codes in Figure 5.8, SNR 3.2 dB difference is observed in BER scope from 10^{-3} to 10^{-4} over Rayleigh fading channel with f_dT_s, 0.01. Most results in this article are obtained by iterating turbo decoders in 1, 2, 4, or 8 times. In Figure 5.9, the STBCNC with 2 transmitters and 2 receivers performs 6 dB better than the STBCNC with 2 transmitters and 1 receiver at BER 10^{-3}, when they are concatenated with turbo codes.

The trellis length for turbo codes is 1024 bits, and the block interleaver of the same length is used for this scheme. Since the exponential computation in the MAP decoding algorithm causes the round-off errors occuring from numerical values with limited

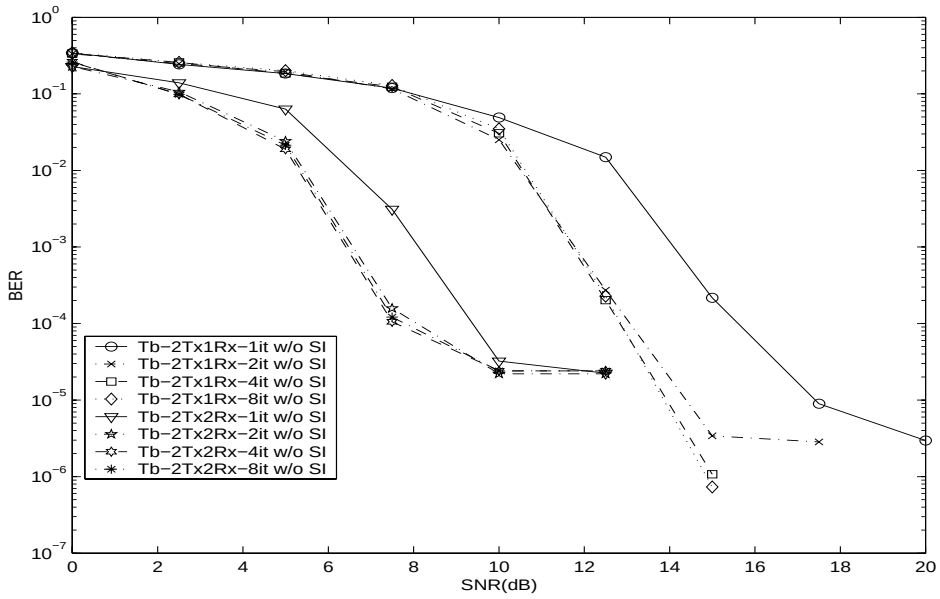

Figure 5.9: BER performance comparison between STBCNC (2Tx-2Rx) and STBCNC (2Tx-1Rx), concatenated with turbo codes over Rayleigh fading channel with f_dT_s, 0.01.

precision, the Max-Log-MAP algorithm which turns the exponential computation into a simple selection algorithm is used for our simulation of turbo codes.

The BER performance comparison among the STBCNC schemes with 3 transmitters are shown in Figure 5.10. There is about 5 dB advantage for 3 transmitters and 2 receivers case at the BER of 10^{-3}. In Figure 5.11, the STBCNC with 3 transmitters and 1 receiver shows 2 dB degradation from the STBC with the same condition over the BER range between 10^{-3} and 10^{-4}, when they are concatenated with turbo codes. Two iterations of turbo decoders are enough for the optimal performance of both STBCNC and STBC concatenated with turbo codes. The large performance gap between one iteration and two iterations reflects the natural performance property of turbo codes. The performance results under the Rayleigh fading channel environment with different f_dT_s are shown in Figure 5.12. The STBCNC scheme with f_dT_s 0.01 is 3 dB inferior to the same scheme with f_dT_s 0.001, when they are concatenated with turbo codes.

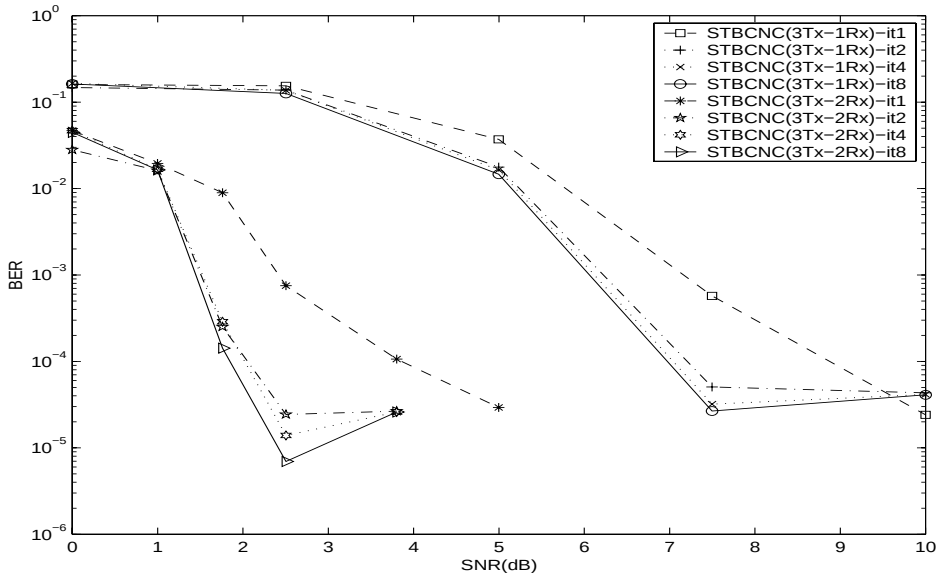

Figure 5.10: BER performance for STBCNC (3Tx-1Rx and 3Tx-2Rx) concatenated with turbo codes in 1, 2, 4, and 8 iterations over Rayleigh fading channel with f_dT_s, 0.01.

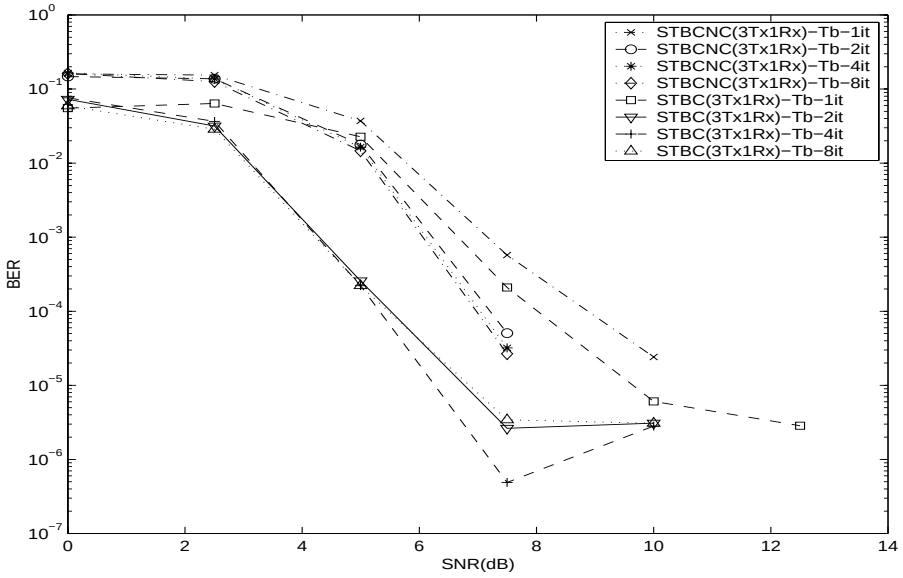

Figure 5.11: BER performance comparison between STBCNC (3Tx-1Rx) and STBC (3Tx-1Rx) concatenated with turbo codes in 1, 2, 4, and 8 iterations over Rayleigh fading channel with f_dT_s, 0.01.

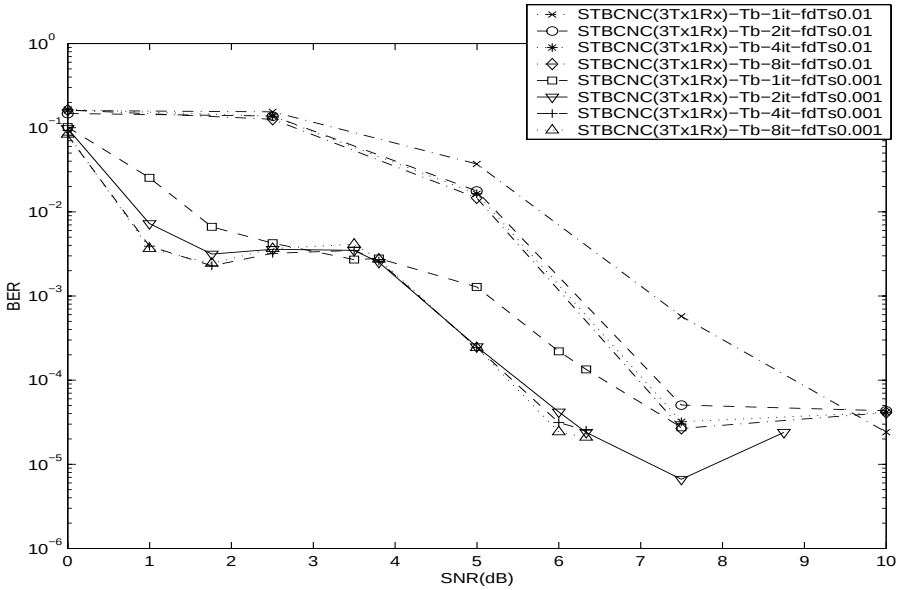

Figure 5.12: BER performance for STBCNC (3Tx-1Rx) concatenated with turbo codes in 1, 2, 4, and 8 iterations over Rayleigh fading channel with f_dT_s, 0.01 and 0.001.

We introduced various design schemes of STBC without channel estimation, and their concatenation with turbo codes. Reliable communication is achieved, in a relatively simple design procedure even without channel estimation, and by the diversity created by STBC. The concatenation of turbo codes with the STBCNC systems improves coding gains and results in the improvement of energy efficiency.

We also analytically showed the relationship between the performance improvement of STBCNC and f_dT_s in Section 5.1.3. Our simulation results verified our findings. For STBCNC, hard decision outputs from the STBCNC decoder are required to be fed back to the STBCNC decoder, itself for the next symbol detection, whereas soft decision outputs are needed for outer turbo decoders. This implementation detail is shown via the block diagram of Figure 5.6.

Finally, we showed that the concatenation of turbo codes with STBCNC loosened the restriction on f_dT_s. As was shown in Figure 5.3 and 5.4, distortions for fast fading chan-

nels occured in the high SNR region. The turbo-concatenation brings the performance region of our interest down to the low SNR region in which the STBCNC schemes are less susceptible to f_dT_s. Another reason that the restriction on f_dT_s is loosened by concatenating turbo codes with STBCNC is that the channel correlation factor caused from f_dT_s is mitigated by interleavers inside turbo coding system [64].

Chapter 6

Iteratively Decoded Space-Time Trellis Codes

We propose an iteratively decoded space-time trellis code (ISTTC) scheme in this Chapter. That is, a space-time trellis code (STTC) is used as a constituent code of turbo codes. The details about computing the extrinsic information shared between two constituent STTC decoders are described. Our simulation shows that ISTTC outperforms the space-time block codes (STBC) achieving the same data rate.

The performance upper bound for ISTTC is analyzed in addition to the simulation results. We provide mathematic analyses for an iteratively decoded space-time trellis code (ISTTC) scheme according to the transfer function bound principle illustrated in [68]. The transfer function for the proposed ISTTC scheme is obtained and used toward computing the performance bound. The analytical results will be compared with simulation results.

6.1 Implementation of ISTTC

The STTC system in this Section consists of two transmitters and one or two receivers. The channel is assumed to be Doppler-shifted flat fading. The received signal $r_{t,m}$ at

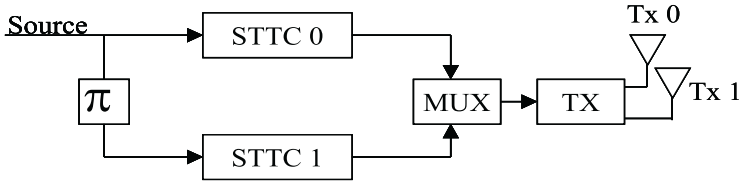

Figure 6.1: ISTTC encoder block diagram I.

the receiver m and time t is given by

$$r_{t,m} = \sum_{n=0}^{1} \alpha_{n,m} S_{t,n} + \eta_{t,m}, \tag{6.1}$$

where the parameter $\eta_{t,m}$ represents the AWGN. The symbol, $S_{t,n}$ is transmitted at time t from transmitter n. At a certain symbol period t, two symbols in both transmitters are sent out at the same time. The channel path gain $\alpha_{n,m}$ between the n^{th} transmitter and the m^{th} receiver is assumed to be independent of different paths.

Figure 6.1 shows the encoder block diagram of our ISTTC scheme. For the constituent STTC with 4-state trellis and the throughput of 2 bits/sec/Hz given in [7], the symbols transmitted from 'Tx 1' of Figure 6.1 make a decision on the trellis-transition, thus only those symbols making a trellis-transition are interleaved for the constituent encoder 'STTC 1' in Figure 6.1.

The source data and the interleaved data are encoded through each constituent STTC encoder. Two symbols together out of each constituent code are alternately transmitted through the multiplexer, and two transmitters. That is, two symbols from 'STTC 0' are transmitted at one symbol period, and two symbols from 'STTC 1' are transmitted at the next symbol period. The received signal $r_{t,m}$ and its interleaved version $r'_{t,m}$ is shown in the decoder block diagram, Figure 6.2. The serial-to-parallel ('S/P') converter stores all the incoming data, $r_{t,m}$ and $r'_{t,m}$ over whole trellis, which are denoted as $\bar{r}$ and $\bar{r'}$. The parameters $i\bar{r}$, $q\bar{r}$, $i\bar{r'}$, and $q\bar{r'}$ in Figure 6.2 represent the in-phase or quadrature-phase components of $\bar{r}$ and $\bar{r'}$. These are fed to the MAP decoder 0, or 1 in Figure 6.2.

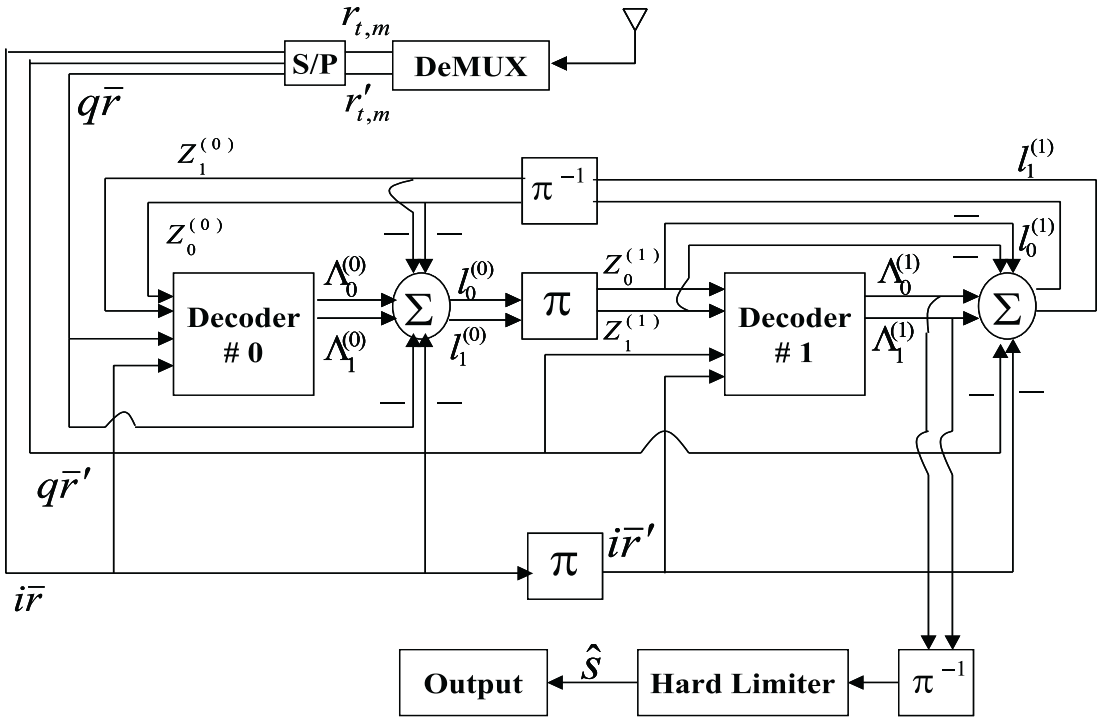

Figure 6.2: ISTTC decoder block diagram.

Since one QPSK symbol consists of two bits, which decide a trellis-transition, the *a priori* probability information which will be passed between two constituent decoders is composed of two independent information, Z_0 and Z_1 as in Figure 6.2. That is, when m_0 and m_1 are denoted as those two bits mapped into one symbol, the *a priori* probability for a symbol is

$$\begin{aligned} P(S_t) &= P(m_0 \cap m_1) \\ &= P(m_0)P(m_1), \end{aligned} \tag{6.2}$$

for independent m_0 and m_1. Thus, the branch metric known as γ for a *Log-MAP* algorithm is given as $logP(r_t|S_t)+logP(m_0)+logP(m_1)$. The probability $P(m_0)$ is derived from the *a priori* input, Z_0 as follows :

$$logP(m_0) = Z_0 m_0 - log(1 + exp(Z_0)). \tag{6.3}$$

Table 6.1: QPSK Symbol Mapping III

Index S_t	Bits $m_0 m_1$	Modulation $I(S_t) + Q(S_t)$
0	1 1	$1 + j$
1	1 0	$1 - j$
2	0 1	$-1 + j$
3	0 0	$-1 - j$

$P(m_1)$ is obtained from the *a priori* input, Z_1 in the same way as $P(m_0)$.

Two likelihood ratios need to be computed for m_0 and m_1, respectively. If we denote the total sum of the forward recursion α, the branch metric, γ, and the backward recursion, β for each symbol S_0, S_1, S_2, and S_3 as λ_0, λ_1, λ_2, and λ_3, respectively, then the log-likelihood ratio for m_0 is

$$\Lambda_0 = (\lambda_0 + \lambda_1) - (\lambda_2 + \lambda_3), \tag{6.4}$$

and the log-likelihood ratio for m_1 is

$$\Lambda_1 = (\lambda_0 + \lambda_2) - (\lambda_1 + \lambda_3). \tag{6.5}$$

From Table 6.1, both λ_0 and λ_1 are computed when m_0 is 1 and both λ_2 and λ_3 are obtained when m_0 is 0. Thus, Λ_0 is obtained as in (6.4). Similarly, both λ_0 and λ_2 are computed when m_1 is 1, and when m_1 is 0, both λ_1 and λ_3 are obtained. Hence, Λ_1 is obtained as (6.5).

The log-likelihood ratios Λ_0 and Λ_1 have the following relation with extrinsic information, l_0 and l_1 in Figure 6.2,

$$\begin{aligned} \Lambda_0 &= i\bar{r} + Z_0 + l_0, \\ \Lambda_1 &= q\bar{r} + Z_1 + l_1. \end{aligned} \tag{6.6}$$

After a certain set of iterations, the final log-likelihood ratios of the second constituent decoder are passed through the deinterleaver and the decisions for m_0 and m_1 at each trellis time are made.

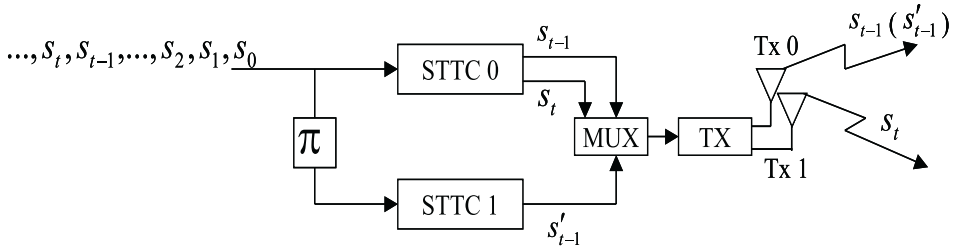

Figure 6.3: ISTTC encoder block diagram II.

6.2 Performance Bounds on Iteratively Decoded Space-Time Trellis Codes

The analogy between ISTTC and turbo codes spawns the idea that the transfer function bound principle illustrated in [68] can be also applied toward obtaining the performance bound for ISTTC. The transfer function bound technique employs a recursion equation to compute the necessary transfer function coefficients efficiently for large block length. The performance bound is obtained using the result of transfer function coefficients. This bound will be compared with simulation results.

6.2.1 Derivation of Transfer Function

We analyze an STTC scheme with a 4-state trellis and throughput of 2 bits/sec/Hz. Figure 2.9 shows the 4-state trellis diagram for an STTC scheme where symbols are mapped in QPSK modulation. The trellis implies the encoding scheme is processed in a systematic way, because the input symbols are transmitted from 'Tx 1' in Figure 6.3, whereas 'Tx 0' transmits the same symbols transmitted from 'Tx 1' at the previous symbol period. The first digit shown in the numeral column of Figure 2.9 represents the symbols transmitted from 'Tx 0' and the second digit represents the symbols transmitted from 'Tx 1'. Thus, the symbols from 'Tx 0' are redundant and all the transmitted

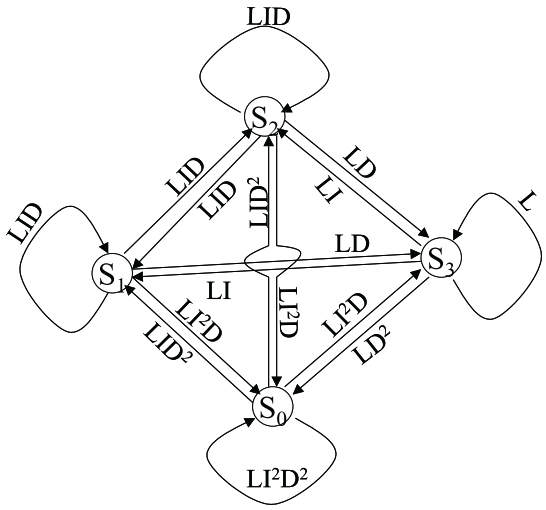

Figure 6.4: State diagram for an STTC scheme in 2-STC, QPSK, 4 states.

symbols from 'Tx 1' are information symbols.

The trellis scheme of Figure 2.9 can be converted to state diagram as in Figure 6.4. A label of the state diagram is expressed with a monomial $L^l I^i D^d$, where l is always equal to 1, and i and d are either 0, 1, or 2, depending on whether the corresponding input and output symbol indexes are 0 through 3 as in Table 6.1. Since the labels represent input and output symbols, the corresponding hamming weight in bits are 0, 1, or 2. The symbols transmitted from 'Tx 0' are the output symbols and those transmitted from 'Tx 1' are the input symbols.

When a state diagram is expressed in $t(l, i, d)$ the number of paths of length l, input weight i, and output weight d, the corresponding transfer function is defined by

$$T(L, I, D) = \sum_{l \geq 0} \sum_{i \geq 0} \sum_{d \geq 0} L^l I^i D^d t(l, i, d). \tag{6.7}$$

Applying Mason's gain formula in [59][69] to the state diagram of Figure 6.4, the transfer function starting from state 0 and ending at state 0 is obtained as

$$\begin{aligned}T(L,I,D) &= (4L^3I^3D^3 - 6L^4I^4D^4 + 2L^3I^4D^4 + LI^2D^2 - L^2I^3D^3)/(1 - LI^2D^2 \\ &-2LID - L - 5L^3I^3D^3 - L^3I^3D^4 - 3L^3I^2D^2 - 3L^3I^4D^4 + 2L^2I^3D^3 \\ &+2L^2I^2D^2 + 2L^2ID + 7L^4I^4D^4).\end{aligned} \tag{6.8}$$

If we multiply both sides of Equation (6.8) by the denominator of the right hand side, and take the coefficient of $t(l,i,d)$ of both sides of the resulting equation, the following recursion determining $t(l,i,d)$ for $l \geq 0$, $i \geq 0$, $d \geq 0$ is obtained:

$$\begin{aligned}t(l,i,d) &= t(l-1,i-2,d-2) + 2t(l-1,i-1,d-1) + t(l-1,i,d) \\ &+5t(l-3,i-3,d-3) + t(l-3,i-3,d-4) + 3t(l-3,i-2,d-2) \\ &+3t(l-3,i-4,d-4) - 2t(l-2,i-3,d-3) - 2t(l-2,i-2,d-2) \\ &-2t(l-2,i-1,d-1) - 7t(l-4,i-4,d-4) + 4\delta(l-3,i-3,d-3) \\ &-6\delta(l-4,i-4,d-4) + 2\delta(l-3,i-4,d-4) + \delta(l-1,i-2,d-2) \\ &-\delta(l-2,i-3,d-3),\end{aligned} \tag{6.9}$$

where $\delta(l,i,d) = 1$ if $l = i = d = 0$ and $\delta(l,i,d) = 0$ otherwise, and with initial conditions that $t(l,i,d) = 0$ if any index is negative. At the following Section, *Derivation of the Bound*, the input-output weight enumerator $t(l,i,d)$ is used to obtain a union bound on the probabilities of bit error, over an assumed AWGN channel with symbol SNR (E_s/N_0).

6.2.2 Derivation of the Bound

The ISTTC scheme shown in Figure 6.3 is identical to a scheme constructed as a parallel concatenation of its three code fragments, each output of which is information symbol, parity check symbol, and its interleaved version of parity check symbol. Since the trellis of ISTTC has block length N, there are $t(N,i,d)$ symbol fragments of input weight i and output weight d from the two parity symbol fragments.

Denoting $p(d|i)$ to be the conditional probability of producing a symbol fragment of

weight d given a randomly selected input sequence of weight i, we obtain [68]:

$$p(d|i) = \frac{t(N,i,d)}{\binom{N}{i}}, \tag{6.10}$$

where $\binom{N}{i} = \frac{N!}{i!(N-i)!}$.

For the uncoded information fragment, $p_(d|i) = \delta(i,d)$, where

$$\delta(i,d) = \begin{cases} 1 & \text{if } d = i \\ 0 & \text{otherwise} \end{cases} \tag{6.11}$$

Assuming the interleaver to be random, the probability $\tilde{p}(d_0, d_1, d_2|i)$ that any input sequence with weight i will be mapped into the uncoded information fragment of weight d_0, parity check symbol fragment of weight d_1, and the interleaved version of parity check symbol fragment of weight d_2 is

$$\tilde{p}(d_0, d_1, d_2|i) = p_1(d_0|i)p(d_1|i)p(d_2|i). \tag{6.12}$$

The conditional probability that a maximum-likelihood decoder might prefer a particular symbol of total weight $d = d_0 + d_1 + d_2$ to the symbol with hamming weight 0 is $Q\left(\sqrt{\frac{2dE_s}{N_0}}\right)$, where $Q(.)$ is the complementary unit variance Gaussian distribution function. Hence, the information bit-error probability P_b is upper bounded by [68]

$$P_b \leq \sum_{i=1}^{N} \frac{i}{N} \binom{N}{i} E_{d|i}\left\{ Q\left(\sqrt{\frac{2dE_s}{N_0}}\right)\right\}, \tag{6.13}$$

where the conditional expectation $E_{d|i}\{.\}$ is over the probability distribution $\tilde{p}(d_0, d_1, d_2|i)$.

6.3 Performance and Analytic Results

The following sub-Sections provide the evaluation of the performance bound in addition to the simulation results of ISTTC.

6.3.1 Simulation Results

The frame error rate (FER - the frame size 128 bits) performance comparison between ISTTC and STBC with 3 transmitters is shown in Figure 6.5. The G_3 scheme shown in Equation 2.23 is used for our STBC scheme to be compared with ISTTC. The G_3 scheme requires 3 antennas to transmit, which achieves the rate 1/2 and thus, the throughput of 1 bit/sec/Hz. On the other hand, two transmitters, 4-state trellis, and QPSK symbols are used for the ISTTC simulation. One, two, or eight iterations between two constituent decoders are performed for the ISTTC scheme over Rayleigh fading channel with $f_d T_s$, 10^{-2}. The trellis length for ISTTC is 1024 trellis times, and the block interleaver of the same length is used for this scheme. In order to avoid the round-off errors occuring from numerical values with limited precision that the exponential computation in the MAP decoding algorithm causes, the Max-Log-MAP algorithm which turns the exponential computation into a simple selection algorithm is used for our simulation of ISTTC.
The ISTTC with two receivers obtains 5 dB gains over the ISTTC with one receiver at the FER of 10^{-2}. The large performance gap between one iteration and two iterations for ISTTC reflects the typical performance of iterative decoding. For the FER of 10^{-2}, the ISTTC achieves about 1.5 dB gain over the STBC in G_3 method for both one and two corresponding receivers, with the same throughput attained. This gain is obtained even with one less transmitters than the STBC scheme. Hence, we can easily see that the ISTTC achieves a competitive performance over other space-time codes with equal data rate.

The FER (with the frame size 128 bits) performance comparison between ISTTC and turbo codes is shown in Figure 6.6. Two transmitters, 4-state trellis, and QPSK symbols are used for our ISTTC simulation. The 4-state recursive systematic constituent encoders with the overall rate 1/3 are employed for turbo code simulation. One, two, and eight iterations between two constituent decoders are performed for both ISTTC and turbo code schemes over Rayleigh fading channel with $f_d T_s$, 10^{-2}. The trellis length

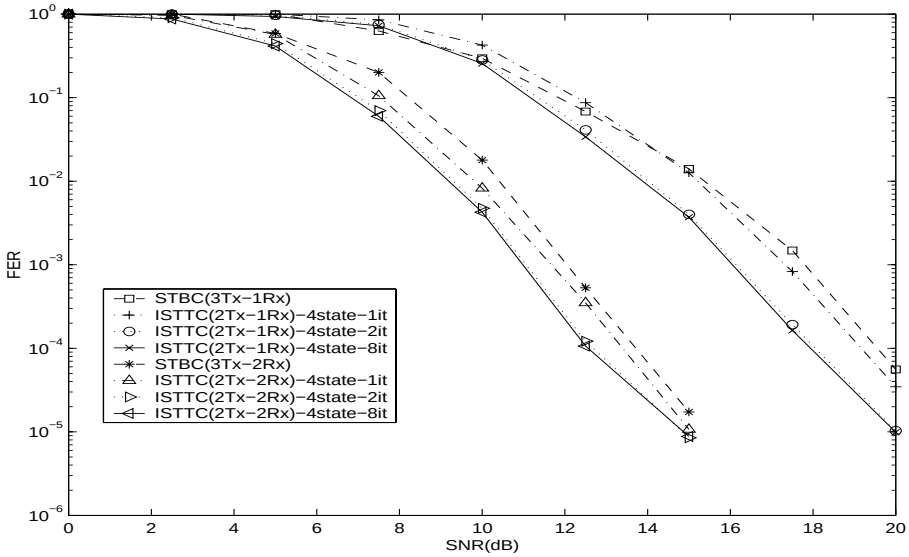

Figure 6.5: BER performance comparison between ISTTC (4-state trellis) with 1, 2, or 8 iterations and STBC with 3 transmitters designed to achieve rate 1/2 over Rayleigh fading channel with $f_d T_s$, 0.01.

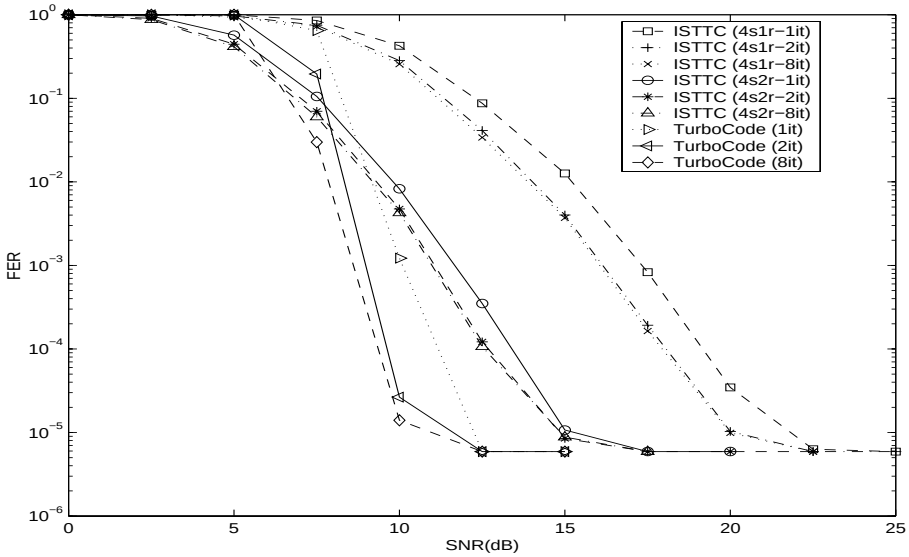

Figure 6.6: FER performance comparison among ISTTC (2Tx-1Rx), ISTTC (2Tx-2Rx) and Turbo codes simulated in 1, 2, and 8 iterations over Rayleigh fading channel with $f_d T_s$, 0.01.

for both ISTTC and turbo codes is equal as 1024, and a block interleaver is used for both schemes. The Max-Log-MAP algorithm is used for our simulation for both ISTTC and turbo codes.

The ISTTC with two receivers obtains 5 dB gains over the ISTTC with one receiver for a FER of 10^{-3}. The large performance gap between one iteration and two iterations for both ISTTC and turbo codes reflects the typical performance of iterative decoding. The error floor formed at a FER of $6\text{x}10^{-6}$ is another natural property of turbo code performance. The ISTTC with two receivers is just 2 dB worse than turbo codes at a FER, 10^{-3} with twice as faster data transmission rate as turbo codes. Hence, we can conclude that the proposed ISTTC scheme achieves the combined performance of both channel codes and space-time codes with less system complexity.

The aforementioned idea of our ISTTC scheme is that the STTC trellis can be used as a constituent code of a turbo code. The usual trellis codes make a transition in a trellis by an input data bit, but the transition in the STTC trellis is determined by an input symbol which is composed of k bits for 2^k-PSK system. Thus, it was necessary to implement passing the extrinsic information between two constituent decoders for all k bits composing a symbol, which was described in the previous Section 6.1.

The reduced throughput caused from the parallel concatenated STTC scheme can be compensated by combining ISTTC with an STBC in four transmitters. This is illustrated in the following Chapter 7.

6.3.2 Performance Bound

In order to plot the bound on P_b in (6.13), we need to compute the recursion (6.9) starting from $l = i = d = 0$ to $l = i = d = N$, and then save only the $t(l, i, d)$ values for $l = N$ and from $i = d = 0$ to $i = d = N$. These $t(N, i, d)$ values are applied forward to compute P_b. For $N = 100$, a diverged and unacceptable bound greater than 1 occurs. As N becomes larger, this divergence of bound becomes more serious [68]. The abrupt

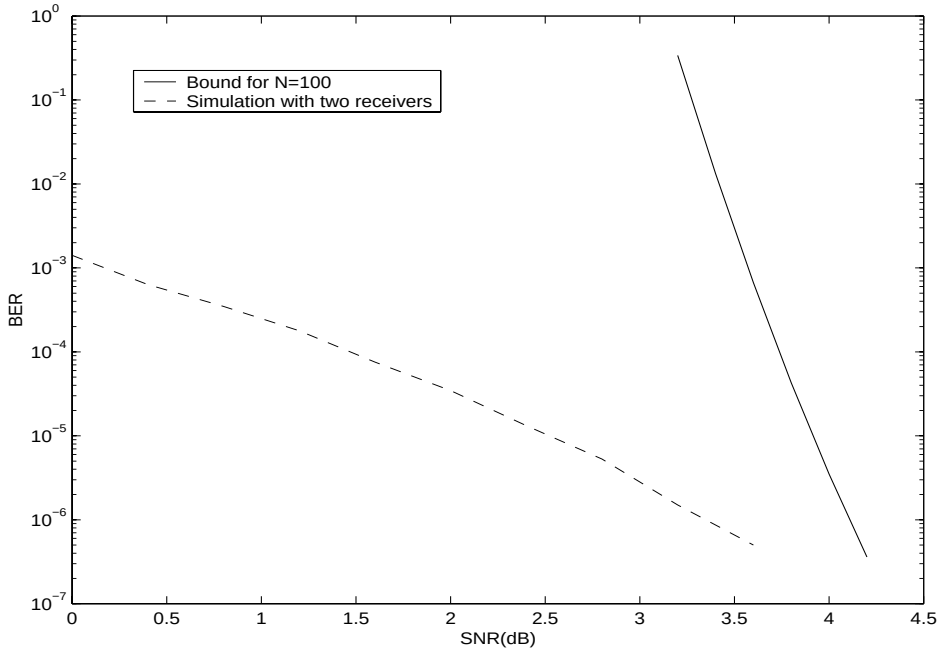

Figure 6.7: Transfer function bound versus simulated BER for the ISTTC with two receivers.

transition happens when the information SNR drops below the threshold determined by the computational cutoff rate R_0, i.e., when SNR $< -ln\,(2^{1-r} - 1)$ for a code with rate r [68][70]. Figure 6.7 shows the comparison between the computed bounds and the simulated BER performance for ISTTC with 2 receivers. The simulation of ISTTC is performed under the AWGN environment just like the computed bound case. We observe that, above the R_0 threshold of 3 dB, the simulated BER for ISTTC asymptotically approaches the error rate predicted by the transfer function bound. From the actual simulation data, an error floor which is a natural property of iterative decoding was formed. However, we cut off the tail of error floor to verify the right performance trend of both simulated and computed error rates.

Chapter 7

Iterative Decoding of Space-Time Trellis Codes Combined with Space-Time Block Codes

The space-time trellis codes combined with space-time block codes (STTC-STBC) provides an improved BER over the performance of space-time trellis codes (STTC) only. In this chapter, we propose iteratively decoded STTC-STBC (ISTTC-STBC) schemes. That is, the ISTTC proposed in Chapter 6 is serially combined with STBC. The reduced transmission rate from the iterative decoding can be compensated by combining the STBC scheme with more transmitters. Design schemes of ISTTC-STBC are illustrated and their performance results are shown via simulation.

7.1 Implementation of ISTTC-STBC

Space-time trellis code (STTC) was introduced in [7] to improve both spectral and power efficiency over the multiple-input-multiple-output (MIMO) fading channels. It is achieved due to the exploitation of the inherent parallelism and diversity within the MIMO channel [67]. The STTC can be concatenated with STBC that has the same number of transmit antennas without changing transmission rate. About 1 dB performance

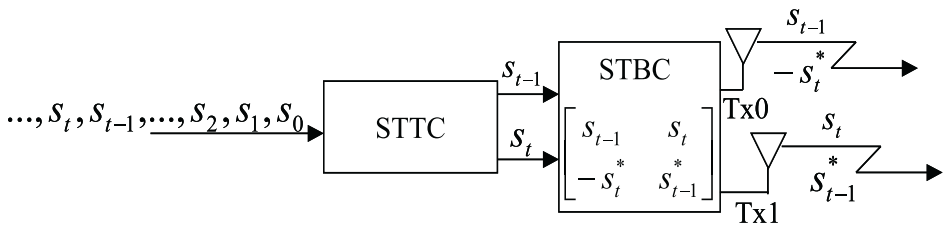

Figure 7.1: Block diagram of STTC combined with Alamouti scheme.

advantage at the BER of 10^{-3} is observed by combining STTC (2 transmitters) with the Alamouti scheme proposed in [21]. Furthermore, we propose to combine ISTTC with STBC. The number of outputs from ISTTC is equal to the number of transmitters for STBC in order not to change the overall transmission rate. The following sub-sections describe the design of STTC-STBC and ISTTC-STBC in detail.

7.1.1 Space-Time Trellis Codes Combined with Space-Time Block Codes

The received signal $r_{t,m}$ at the receiver m and time t is given by

$$r_{t,m} = \sum_{n=0}^{N-1} \alpha_{n,m} S_{t,n} + \eta_{t,m}, \tag{7.1}$$

where the parameter $\eta_{t,m}$ is AWGN. The symbol, $S_{t,n}$ is transmitted at time t from transmitter n. At a symbol period t, the N symbols in N transmitters are sent out at the same time. The channel path gain $\alpha_{n,m}$ between the n^{th} transmitter and the m^{th} receiver is assumed to be independent of different paths.

Figure 7.1 shows that the outputs of STTC are linearly arranged according to the Alamouti scheme. The Alamouti scheme is an STBC scheme designed in the orthogonal method with two transmitters, achieving full diversity and full transmission rate. The STTC with two transmitters and QPSK modulation achieves the throughput of 2 bits/s/Hz. The detail code construction for the STTC is illustrated in Section 2.3.

Since the STTC is combined with the Alamouti scheme, the STTC outputs are grouped to two symbols and linearly arranged according to the matrix (7.2) before transmission.

$$G_2 = \begin{bmatrix} S_{t-1} & S_t \\ -S_t^* & S_{t-1}^* \end{bmatrix}. \tag{7.2}$$

Columns and rows of the matrix (7.2) represent transmitters and symbol periods, respectively. That is, those two elements in a row are transmitted from 'Tx0' and 'Tx1' at the same symbol period. The soft decision information for the received signals as in (7.1) is obtained as follows [8][20][21][26],

$$\begin{array}{rcl} \tilde{S}_{t-1} & = & \sum_{m=0}^{1} \left\{ r_{t-1,m} \alpha_{0,m}^* + r_{t,m}^* \alpha_{1,m} \right\}, \\ \tilde{S}_t & = & \sum_{m=0}^{1} \left\{ r_{t-1,m} \alpha_{1,m}^* - r_{t,m}^* \alpha_{0,m} \right\}. \end{array} \tag{7.3}$$

After obtaining soft decision outputs $\tilde{S}_t$, we apply the Viterbi algorithm (VA) where the branch metric is computed by $\left|\tilde{S}_t - S_t\right|^2$. It is different from the branch metric of the VA for STTC, which is computed by $\sum_{m=0}^{1} \left| r_{t,m} - \sum_{n=0}^{1} \alpha_{n,m} S_{t,n} \right|^2$, where $S_{t,n}$ is the symbol supposed to be transmitted at the symbol period t from the nth transmitter according to the trellis scheme. Thus, the branch metric in VA of the STTC-STBC decoder becomes simpler than the STTC one, because the channel path gains and the symbols transmitted from 'Tx0' are already taken into account in (7.3) before computing the branch metric of the VA. Hence, channel path gains $\alpha_{n,m}$ do not have to be retrieved each time computing the branch metric in VA.

The performance of STTC-STBC is shown in Figure 7.2, compared with the performance of STTC over the Rayleigh fading channel with $f_d T_s$ 10^{-2}. The STTC-STBC is better performed for one receiver system. The STTC-STBC is 1 dB better than STTC using 1 receiver at BER 10^{-3}. However, for 2 receivers, the performance gets closer between STTC-STBC and STTC over the region above SNR 10 dB. The matrix G_2 of (7.2) is used for the STBC scheme, which does not change the overall transmission rate but improves the performance by 1 dB for 1 receiver system.

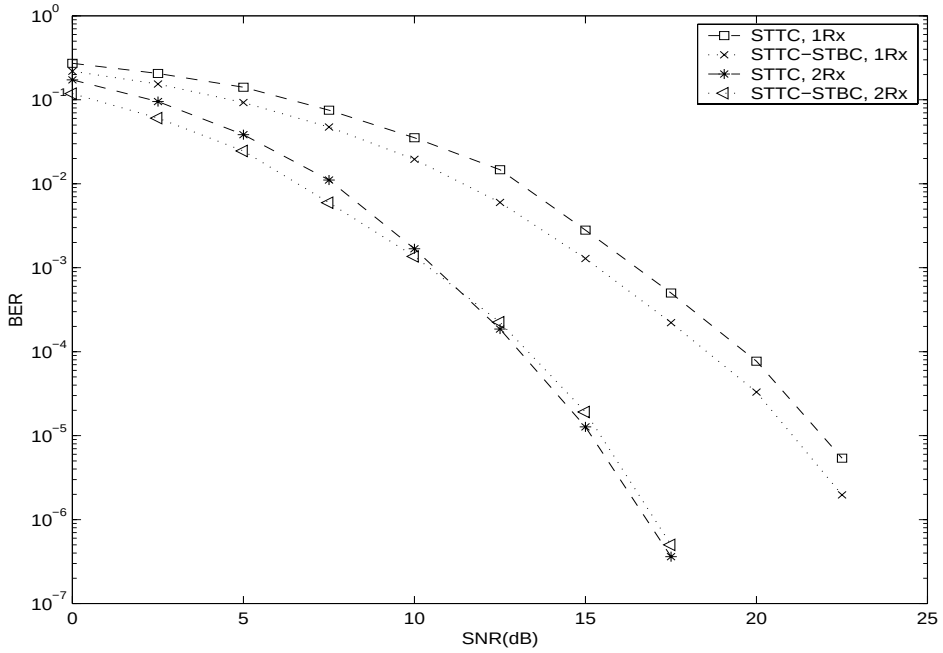

Figure 7.2: BER performance comparison between STTC and STTC-STBC over Rayleigh fading channel with $f_d T_s$, 0.01.

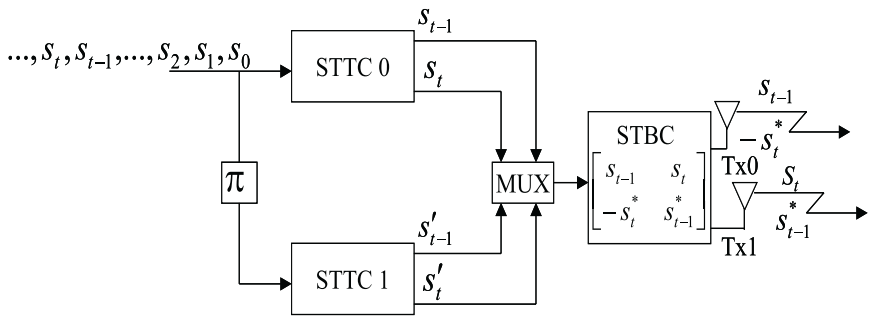

Figure 7.3: Encoder block diagram for iterative decoding of STTC-STBC with two transmitters.

7.1.2 Iterative Decoding of Space-Time Trellis Codes Combined with Space-Time Block Codes

The encoder block diagram for the iteratively decoded STTC-STBC (ISTTC-STBC) whose STBC is designed in Alamouti scheme is shown in Figure 7.3. The parallel concatenation of two constituent STTC reduces the overall throughput to 1 bit/sec/Hz. Thus, we propose to combine the ISTTC with an STBC designed in the quasi-orthogonal method of [22] in order to increase the rate of ISTTC-STBC to 2 bits/sec/Hz. This is achieved with increasing the number of transmitters. Whereas the codes designed in orthogonal methods illustrated in Section 7.1.1 use the orthogonal property of the codes [8][20], the reference [22] proposed structures that are not orthogonal but rather divided into groups. The columns within each group are not orthogonal to each other, but different groups are orthogonal among each other. This structure is called a quasi-orthogonal design.

Let us illustrate the schemes in Figure 7.3 and 7.4 in detail. For the STTC with 4-state trellis illustrated in [7], the symbols $s_t(s_t^{'})$ instead of $s_{t-1}(s_{t-1}^{'})$ in Figure 7.3 and 7.4 make a decision on the transition of trellis, thus only those symbols making a trellis-transition are interleaved for the constituent encoder 'STTC 1' of Figure 7.3

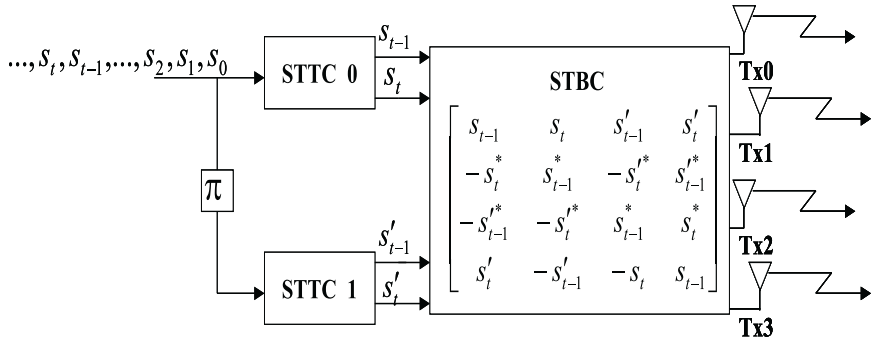

Figure 7.4: Encoder block diagram for iterative decoding of STTC-STBC with four transmitters.

and 7.4. For the system in Figure 7.3, the source data and the interleaved data are encoded through each constituent encoder respectively according to the STTC-STBC design method illustrated in Section 7.1.1. For the system in Figure 7.4, we take the following STBC with N=T=K=4, achieving full rate with a diversity of $2M$ as an example designed in the quasi-orthogonal method,

$$G_4 = \begin{bmatrix} S_{t-1} & S_t & S'_{t-1} & S'_t \\ -S^*_t & S^*_{t-1} & -S'^*_t & S'^*_{t-1} \\ -S'^*_{t-1} & -S'^*_t & S^*_{t-1} & S^*_t \\ S'_t & -S'_{t-1} & -S_t & S_{t-1} \end{bmatrix}. \tag{7.4}$$

It achieves the full rate with a diversity of $2M$. The number of transmitters (N) which is the number of columns in matrix (7.4), the symbol periods (T) which is the number of rows, and the number of symbols (K) in matrix (7.4) are all equal to 4. The S^*_t represents the complex conjugate of S_t. It is clear from the statement above that the diversity gain ($2M$) increases in proportion to the number of receivers (M). In our ISTTC-STBC scheme in Figure 7.4, two symbols each from 'STTC 0' and 'STTC 1' comprise the STBC matrix. The soft decision information for the received signals represented in (7.1)

is obtained as follows [26],

$$\begin{array}{rcl} \tilde{S}_{t-1} & = & \sum_{m=0}^{M-1}(r_{t-1,m}\alpha_{0,m}^{*} + r_{t,m}^{*}\alpha_{1,m} + r_{t+1,m}^{*}\alpha_{2,m} + r_{t+2,m}\alpha_{3,m}^{*}), \\ \tilde{S}_{t} & = & \sum_{m=0}^{M-1}(r_{t-1,m}\alpha_{1,m}^{*} - r_{t,m}^{*}\alpha_{0,m} + r_{t+1,m}^{*}\alpha_{3,m} - r_{t+2,m}\alpha_{2,m}^{*}), \\ \tilde{S}_{t-1}^{'} & = & \sum_{m=0}^{M-1}(r_{t-1,m}\alpha_{2,m}^{*} + r_{t,m}^{*}\alpha_{3,m} - r_{t+1,m}^{*}\alpha_{0,m} - r_{t+2,m}\alpha_{1,m}^{*}), \\ \tilde{S}_{t}^{'} & = & \sum_{m=0}^{M-1}(r_{t-1,m}\alpha_{3,m}^{*} - r_{t,m}^{*}\alpha_{2,m} - r_{t+1,m}^{*}\alpha_{1,m} + r_{t+2,m}\alpha_{0,m}^{*}), \end{array} \tag{7.5}$$

where $r_{t-1,m}$, $r_{t,m}$, $r_{t+1,m}$, and $r_{t+2,m}$ represent the received signals for the first, the second, the third, and the fourth row of matrix (7.4). Since S_{t-1} and S_t came from 'STTC 0', and $S_{t-1}^{'}$ and $S_t^{'}$ are fed from 'STTC 1', the $\tilde{S}_t$ and $\tilde{S}_t^{'}$ dictate the trellis-transition of 'STTC 0' and 'STTC 1', respectively. According to the following references [5][26][56], these soft outputs, $\tilde{S}_t$ and $\tilde{S}_t^{'}$ are passed to the constituent STTC decoders, '# 0' and '# 1' in Figure 7.5.

The decoder block diagram for ISTTC-STBC is shown in Figure 7.5. Different from the STTC-STBC scheme, the decoders of ISTTC-STBC require a MAP-type of algorithm for the iterative operation. Since an input symbol consisting of two bits for a QPSK modulation makes the trellis-transition just like the case for ISTTC, the *a priori* probability information which will be passed between two constituent decoders is composed of two independent information, Z_0 and Z_1 shown in Figure 7.5. The *a priori* probability for a symbol is given in Equations (6.2) - (6.3). Two likelihood ratios are also obtained in the same procedures as the ISTTC scheme. These are given in Equations from (6.4) through (6.6). After a certain set of iterations, the final log-likelihood ratios of the second constituent decoder are passed through the deinterleaver and the decisions for m_0 and m_1 at each trellis time are made.

7.2 Performance Results

The performance of ISTTC-STBC using G_2 is shown in Figure 7.6. Two transmitters, 4-state trellis, and QPSK symbols are used for our ISTTC simulation. One, two, and eight iterations between two constituent decoders are performed for the iteratively decoded

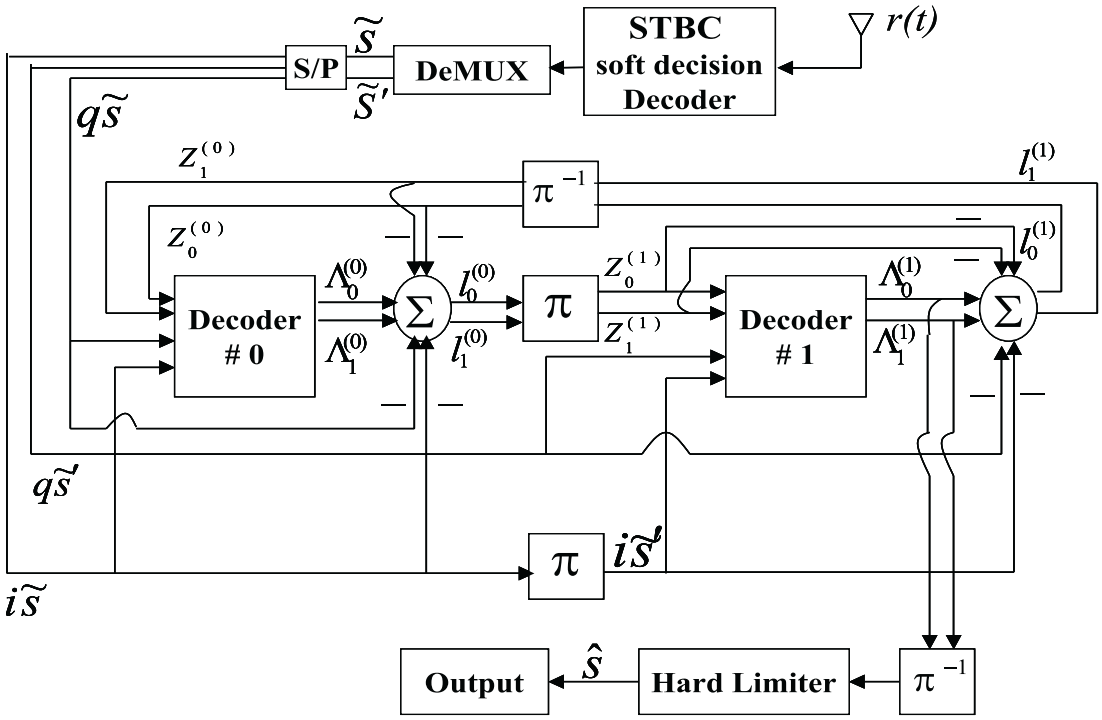

Figure 7.5: Decoder block diagram for iterative decoding of STTC-STBC.

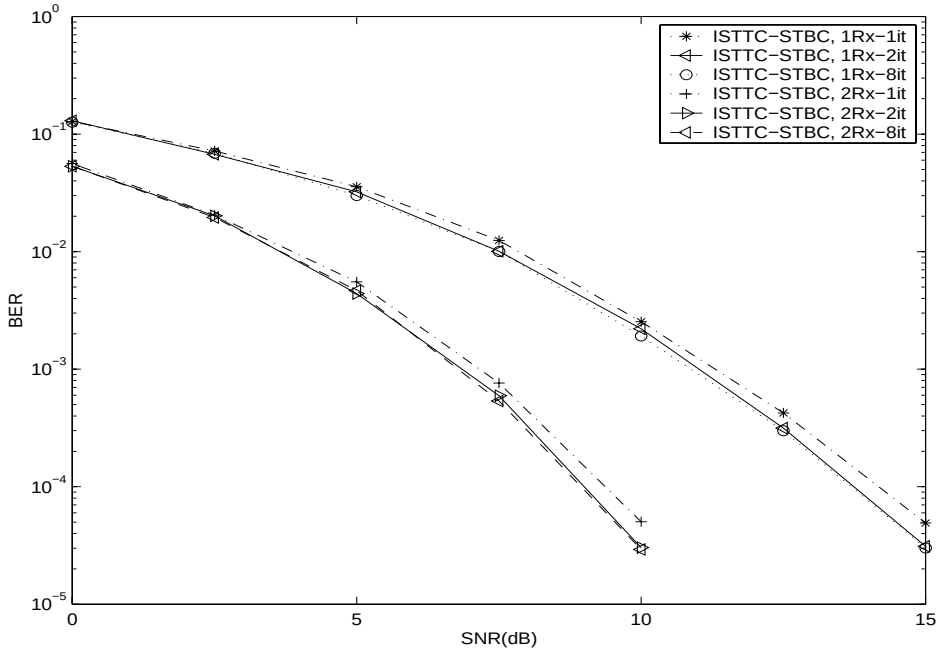

Figure 7.6: BER performance of ISTTC-STBC using G_2 with 1 or 2 receivers run in 1, 2, or 8 iterations between two constituent decoders over Rayleigh fading channel with $f_d T_s$, 0.01.

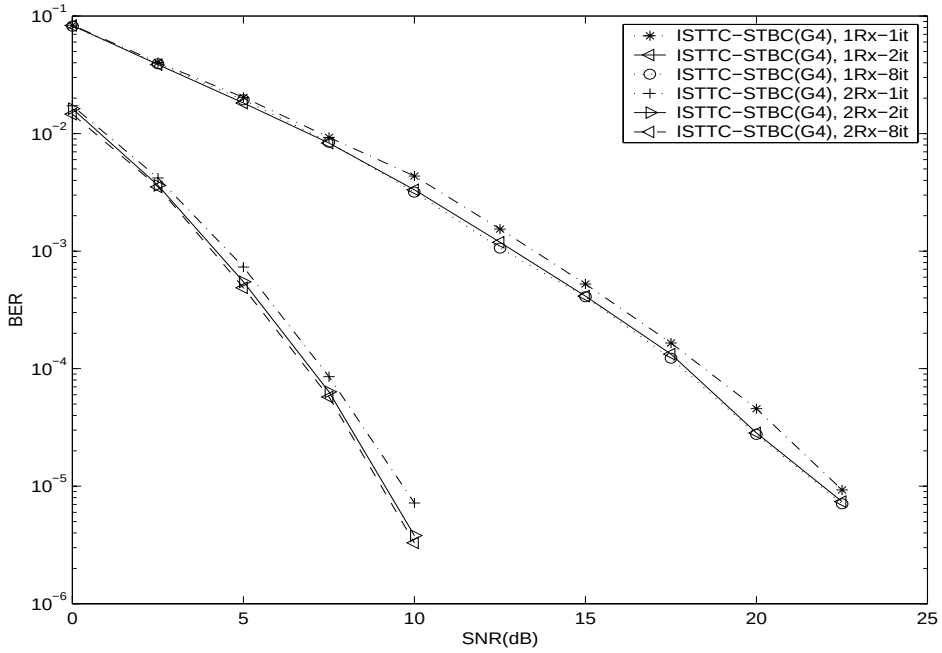

Figure 7.7: BER performance of ISTTC-STBC using G_4 with 1 or 2 receivers run in 1, 2, or 8 iterations between two constituent decoders over Rayleigh fading channel with $f_d T_s$, 0.01.

STTC (ISTTC) in this article. The trellis length for ISTTC is 1024 symbol periods, and the block interleaver of the same length is used for all the ISTTC schemes in this paper. The Max-Log-MAP decoding algorithm is used for each constituent decoder.

The ISTTC-STBC (G_2) with two receivers obtains 3.5 dB gains over the ISTTC-STBC (G_2) with one receiver for the BER of 10^{-3}. The relatively large performance gap between one iteration and two iterations reflects the typical performance of iterative decoding. Figure 7.7 shows the BER performance of ISTTC-STBC designed in quasi-orthogonal method (G_4). The ISTTC-STBC (G_4) scheme with two receivers achieves 7 dB gains over the ISTTC-STBC (G_4) with one receiver for the BER of 10^{-3}. That is, the ISTTC-STBC (G_4) is better performed with two receivers. The performance comparison between ISTTC-STBC designed in quasi-orthogonal method (G_4) and Alamouti

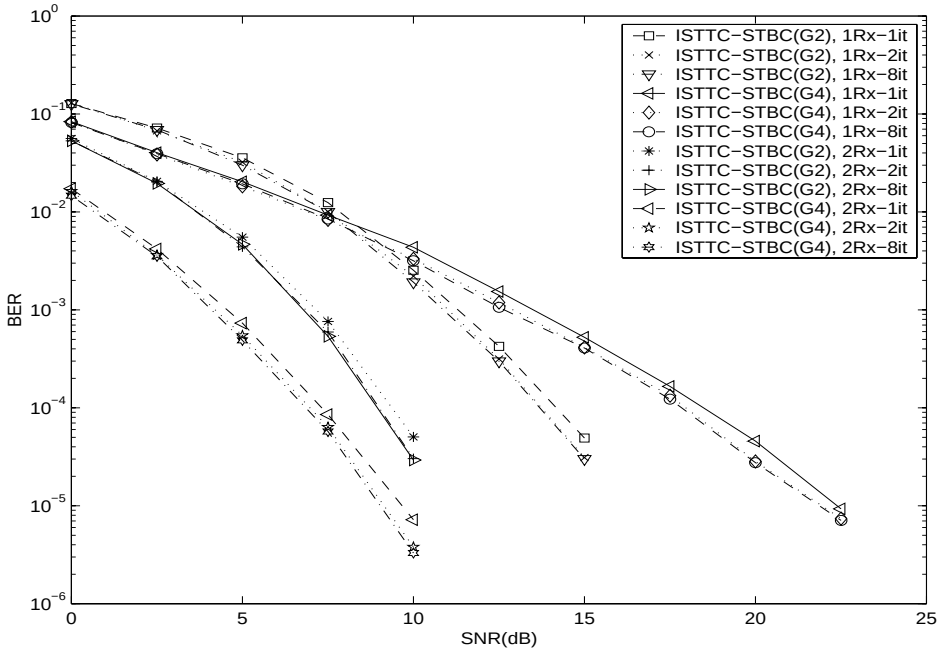

Figure 7.8: BER performance comparison between ISTTC-STBC (G_4) and ISTTC-STBC (G_2) over Rayleigh fading channel with $f_d T_s$, 0.01.

scheme (G_2) are shown in Figure 7.8. The performance of two schemes in Figure 7.8 shows little difference for one receiver system, but shows about 2.5 dB difference at the BER of 10^{-3} for two receivers system. This gain for ISTTC-STBC (G_4) is achieved even with twice as fast data rate as ISTTC-STBC (G_2).

The performance of ISTTC-STBC is comparable with turbo codes serially concatenated with STBC [26][56][65]. But, the inherent advantage of symbol-by-symbol MAP algorithm for ISTTC over the bit-by-bit MAP algorithm of turbo codes achieves better spectral efficiency. The achievement is assessed even excluding the increased capacity by employing multiple transmitters [6]. Hence, we can conclude that the proposed ISTTC scheme achieves the combined performance of both channel codes and space-time codes with relatively simpler system complexity. The ISTTC-STBC (G_2) outperforms turbo codes concatenated with STBC in terms of, at least, spectral efficiency. Furthermore,

the spectral efficiency can be more improved by having four transmitters using the STBC designed in quasi-orthogonal method (G_4). The transmission rate of ISTTC-STBC (G_4) is twice as good as the ISTTC-STBC (G_2), achieving even better BER performances.

Chapter 8

Iterative Decoding of Space-Time Trellis Codes Combined with Differential Space-Time Block Codes

The iteratively decoded space-time trellis codes (ISTTC) was developed in Chapter 6. In this chapter, we propose to combine a differential space-time block code (DSTBC) scheme with ISTTC, and show that a decent performance can be achieved over flat fading channels without channel estimation and error correction codes. The DSTBC will be briefly reviewed, and design schemes of the ISTTC combined with DSTBC (ISTTC-DSTBC) will be described in detail. This chapter presents the details of computing the extrinsic information shared between two constituent decoders and computing branch metrics using soft-outputs out of DSTBC. Its performance results will be shown via simulation.

8.1 Review of DSTBC

The channel state information (CSI) is necessary for coherent detection in both STTC and STBC. However, CSI is generally hard to obtain in fading channel environments. Thus, a differential STBC (DSTBC) was proposed to detect the information at the re-

ceiver without CSI. When the CSI is not available at the receiver, the STBC can be decoded by the transmission of pilot symbols [83]. A differential detection scheme which does not even require pilot symbols already exists for one transmit antenna [15]. The generalization of differential detection scheme for the case of multiple transmit antennas was researched in [23]-[25], but these schemes require the transmission of symbols known to the receiver at the beginning and hence are not truly differential. But, recently, differential space-time block coding (DSTBC) was proposed to achieve diversity advantage with no channel estimation [27]-[30]. Whereas the schemes in [29][30] are designed with unitary matrices, the differential schemes in [27][28] are based on orthogonal design with low differential detection complexity. The disadvantage of [27][28] is 3-dB performance degradation compared to the coherent detection. We design a DSTBC according to [27] in this dissertation.

We take the STBC scheme with two transmitters in [21] to describe DSTBC here, so that two symbols are linearly arranged according to the following matrix (8.1).

$$G_2 = \begin{bmatrix} S_{t-1} & S_t \\ -S_t^* & S_{t-1}^* \end{bmatrix}. \tag{8.1}$$

Columns and rows of the matrix (8.1) represent transmitters and symbol periods, respectively. That is, those two elements in a row are transmitted from 'Tx0' and 'Tx1' at the same symbol period.

For 2^b-PSK constellation, blocks of $2b$ bits are mapped to differential encoding coefficients (DEC) as follows. The first b bits are mapped to a constellation S_2 and the second b bits are mapped to a constellation S_3 using Gray mapping. If we assume initial two symbols, S_0 and S_1 to be dummy but known to receivers, then two DEC, A and B are defined as [27]

$$\begin{aligned} A &= S_2 S_0^* + S_3 S_1^*, \\ B &= -S_2 S_1 + S_3 S_0. \end{aligned} \tag{8.2}$$

Table 8.1: DEC Mapping for a QPSK scheme

Input Bits			
$m_0 m_1$	$m_2 m_3$	DEC A	DEC B
0 0	0 0	$-1+j0$	$0+j0$
0 0	1 0	$-.5-j.5$	$.5-j.5$
0 0	0 1	$-.5+j.5$	$.5+j.5$
0 0	1 1	$0+j0$	$1+j0$
1 0	0 0	$-.5-j.5$	$-.5+j.5$
1 0	1 0	$0-j$	$0+j0$
1 0	0 1	$0+j0$	$0+j$
1 0	1 1	$.5-j.5$	$.5+j.5$
0 1	0 0	$-.5+j.5$	$-.5-j.5$
0 1	1 0	$0+j0$	$0-j$
0 1	0 1	$0+j$	$0+j0$
0 1	1 1	$.5+j.5$	$.5-j.5$
1 1	0 0	$0+j0$	$-1+j0$
1 1	1 0	$.5-j.5$	$-.5-j.5$
1 1	0 1	$.5+j.5$	$-.5+j.5$
1 1	1 1	$1+j0$	$0+j0$

The procedures in (8.2) will be repeated over the entire data. Conversely, given A and B, the pair (S_2 S_3) is recovered by

$$(S_2 \;\; \mathrm{S}_3) = \mathrm{A}(\mathrm{S}_0 \;\; \mathrm{S}_1) + \mathrm{B}(-\mathrm{S}_1^* \;\; \mathrm{S}_0^*). \tag{8.3}$$

The original b bit information is decoded by inverse Gray mapping of S_2 and S_3. In this paper, we implemented the above differential encoding scheme with QPSK constellation, $\frac{1}{\sqrt{2}}$, $j\frac{1}{\sqrt{2}}$, $-\frac{1}{\sqrt{2}}$, and $-j\frac{1}{\sqrt{2}}$ for two input bits, 00, 10, 11, and 01, respectively, where j=$\sqrt{-1}$. We set S_0=S_1=$-\frac{1}{\sqrt{2}}$. According to (8.2), a DEC is computed from four input bits and summarized in Table 8.1. The next two symbols S_2 and S_3 are computed with the obtained DEC, A and B according to (8.3). Since S_0, S_1 and -S_1^*, S_0^* are transmitted at the first and second symbol period, the S_2, S_3 and -S_3^*, S_2^* are transmitted at the third and fourth symbol period. The S_4 and S_5 will be obtained in the same procedure

as we get S_2 and S_3. Thus, S_4, S_5 and -S_5^*, S_4^* are transmitted at the fifth and sixth symbol period. This process will continue until the entire data are transmitted.

The received signal is expressed mathematically in (6.1). For one receive antenna, it still holds with the receiver subscript omitted for simplicity purpose. According to [27], the coefficients corresponding to DEC, based on received signals, are computed as follows.

$$\begin{aligned} R_A &= r_{2t+1}r_{2t-1}^* + r_{2t+2}^* r_{2t}, \\ R_B &= r_{2t+1}r_{2t}^* - r_{2t+2}^* r_{2t-1}, \end{aligned} \tag{8.4}$$

where signals r_{2t-1}, r_{2t}, r_{2t+1}, and r_{2t+2} are assumed to be received. Now the receiver computes the closest DEC pair (A B) to the (R_A R_B) pair. Once this is computed, the inverse mapping of Table 8.1 is applied and the transmitted bits are recovered. The same procedure can be used for more than one receive antenna. For each receive antenna m, we compute $R_{A,m}$ and $R_{B,m}$ with only the mth receiver considered. Then the closest DEC pair (A B) to the ($\sum_{m=0}^{M-1} R_{A,m}$ $\sum_{m=0}^{M-1} R_{B,m}$) pair is computed. Here M is the number of receive antennas. Subsequently, the transmitted bits are computed by applying the inverse mapping of Table 8.1. Since the diversity gain is the number of transmitters times the number of receivers, it is easily deduced that $2M$-level diversity is achieved.

8.2 Implementation of ISTTC-DSTBC

Figure 8.1 shows a block diagram of ISTTC-DSTBC transmitter. Two outputs, S_{t-1}, S_t and S'_{t-1}, S'_t out of 'STTC 0' and 'STTC 1', respectively are alternately fed into 'DSTBC' through 'MUX'. Two most important encoding procedures of DSTBC which were described in Equations (8.2) and (8.3) can be written in the multiplication of three matrices,

$$\left[\begin{array}{cc} S_{t+1}(S'_{t+1}) & S_{t+2}(S'_{t+2}) \end{array} \right], \left[\begin{array}{cc} S_{t-1}^*(S_{t-1}^{*\prime}) & -S_t(-S'_t) \\ S_t^*(S_t^{*\prime}) & S_{t-1}(S'_{t-1}) \end{array} \right],$$

and

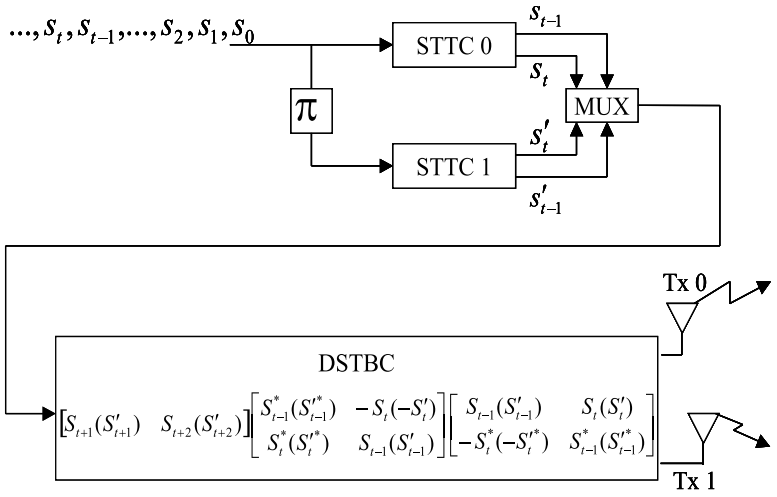

Figure 8.1: ISTTC-DSTBC transmitter block diagram.

$$\begin{bmatrix} S_{t-1}(S'_{t-1}) & S_t(S'_t) \\ -S^*_t(-S^{*'}_t) & S^*_{t-1}(S^{*'}_{t-1}) \end{bmatrix}.$$

The symbols within parentheses represent the interleaved version of signals, that is, the outputs out of 'STTC 1'. These are alternately processed in the DSTBC encoder as mentioned above. We set the initial two symbols, S_0 and S_1 to be known at the receiver and both to be equal as $-\frac{1}{\sqrt{2}}$. Since the ISTTC trellis starts always at 'State 0', initial two symbols are zero. Thus, initial four bits mapped into two symbols according to Table 6.1 should be all bit 1, and bit 11 corresponds to $-\frac{1}{\sqrt{2}}$ from our Gray mapping in Section 8.1. The multiplication of three matrices generates two symbols. These are encoded according to Alamouti scheme, and transmitted through two transmitters.

Figure 8.2 shows the receiver block diagram of ISTTC-DSTBC. The received symbols are stored over the entire trellis through the serial to parallel converter ('S/P'), because the iterative decoding which will be performed subsequently is processed in a block of data. Since R_A, R_B and R'_A, R'_B are soft information, we can use this information to compute the branch metric of ISTTC decoder. Because DEC were clearly defined by the input bits, the 'MAP' algorithm within our ISTTC scheme still generates the same

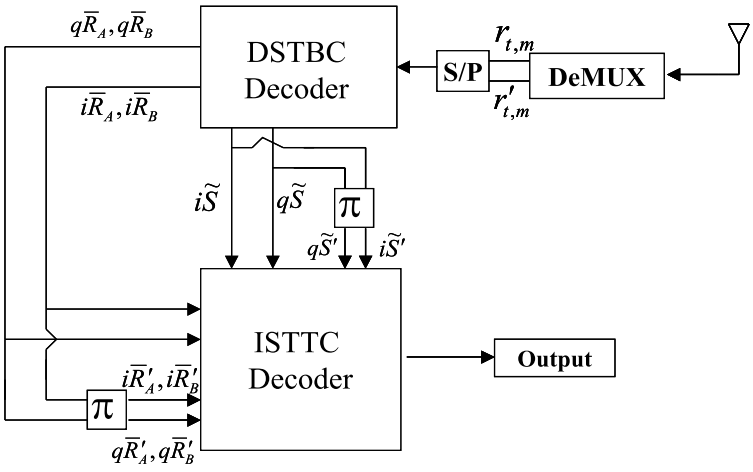

Figure 8.2: ISTTC-DSTBC receiver block diagram.

output as the one using soft-information of input data. However, we pass the initially decoded information out of 'DSTBC Decoder' to the 'ISTTC Decoder' as extrinsic information. The iR_A, qR_A and iR_B, qR_B represent the in-phase and quadrature-phase information of R_A and R_B, respectively. The superscript *prime* represents the interleaved version of each data. The initially decoded information out of 'DSTBC Decoder' is denoted in the figure as $i\tilde{S}$, $q\tilde{S}$ and $i\tilde{S}'$, $q\tilde{S}'$. Again, the i and q represent the in-phase and quadrature-phase of each data. Therefore, the Equation (6.6) turns into following,

$$\begin{aligned} \Lambda_0 &= i\tilde{S} + Z_0 + l_0, \\ \Lambda_1 &= q\tilde{S} + Z_1 + l_1. \end{aligned} \tag{8.5}$$

8.3 Performance Results

In this Section, we show the performance of our proposed scheme, ISTTC-DSTBC, comparing with other various schemes via simulation. Figure 8.3 shows the BER performance comparison between ISTTC-DSTBC and ISTTC-STBC. Both of these schemes compared are designed in 2 transmitters and 1 receiver. These are performed with the same number of iterations, 1, 2, and 8 over the same fading channel environment. The

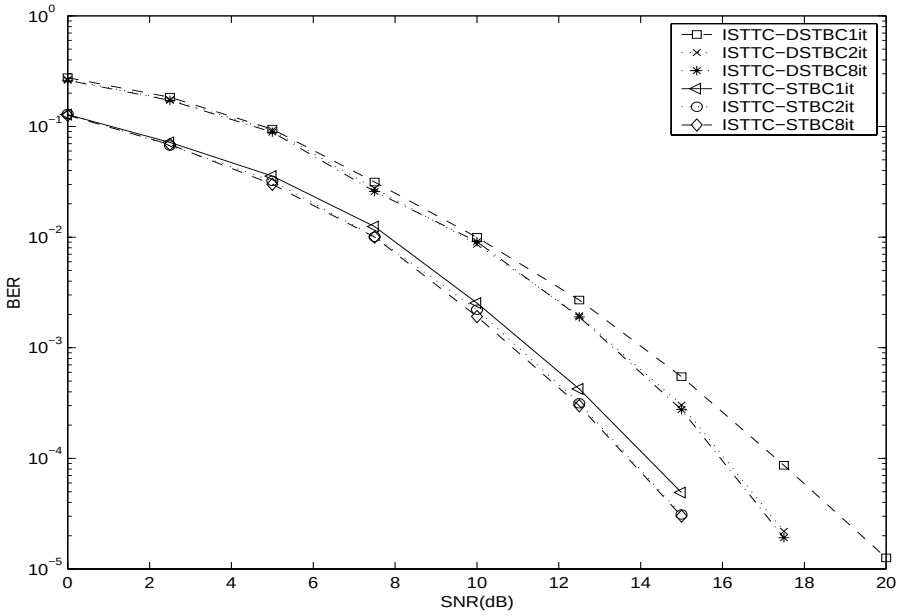

Figure 8.3: BER performance comparison between ISTTC-DSTBC and ISTTC-STBC, with 2 transmitters and 1 receiver.

normalized Doppler frequency ($f_d T_s$) of the channel is set to be 10^{-2}. The Alamouti scheme of (8.1) is used for both STBC and DSTBC. The trellis length for ISTTC is 1024 symbol periods, and the block interleaver of the same length is used for this scheme. The Max-Log-MAP decoding algorithm is used for each constituent decoder. As we can expect from the general coherent and non-coherent detection systems, the ISTTC-DSTBC is observed to have 3dB performance degradation against the ISTTC-STBC at the BER, 10^{-3}. The relatively larger performance gap between one iteration and two iterations for ISTTC reflects the typical performance of iterative decoding.

Figure 8.4 shows the BER performance comparison between ISTTC-DSTBC and turbo codes serially concatenated with the Alamouti scheme (Turbo-STBC). Both of these schemes are designed in 2 transmitters and 1 receiver, and run with 2 iterations. The same trellis length, decoding scheme, and interleavers as those used for Figure 8.3 are

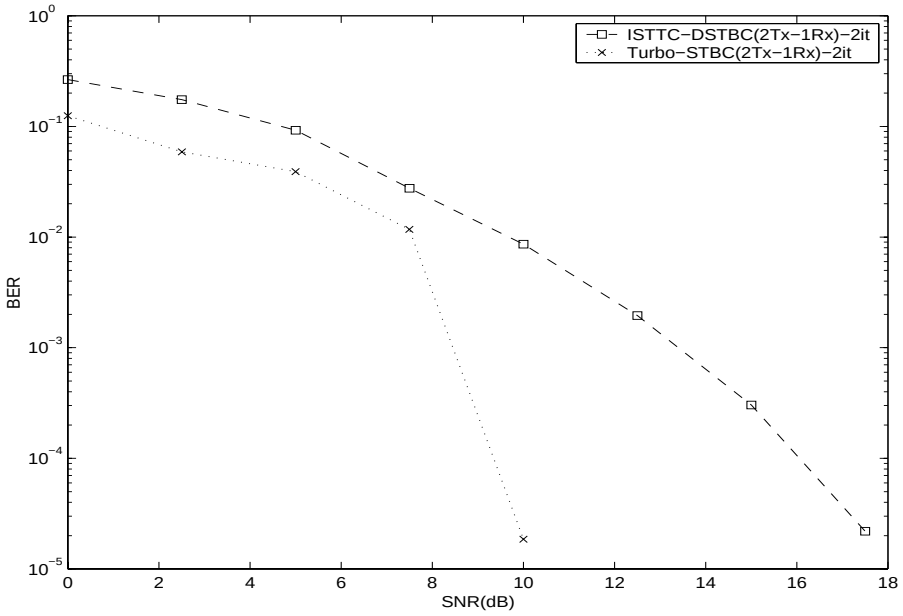

Figure 8.4: BER performance comparison between ISTTC-DSTBC and Turbo-STBC, with 2 transmitters and 1 receiver.

employed for both schemes in Figure 8.4. The identical channel environments are applied to all three figures in this paper. The usual trellis of turbo codes make a transition in a trellis by an input data bit, but the transition in the STTC trellis is determined by an input symbol which is composed of k bits for 2^k-PSK system. Thus, the difference between ISTTC and turbo codes is to share the extrinsic information between two constituent decoders for all k bits in a symbol, which increases the data transmission rate. Even if Turbo-STBC is designed with coherent detection, the ISTTC-DSTBC is observed to have only 2dB degradation in lower SNR region at BER, 10^{-2}. It is achieved even with the increased data rate, and still keeping the advantage of no channel estimation.

Figure 8.5 shows some disadvantage of having two receivers for ISTTC-DSTBC. Combining ISTTC with DSTBC for two receivers does not improve the BER performance much and even cause a serious error floor problem. It is obviously different phenomenon

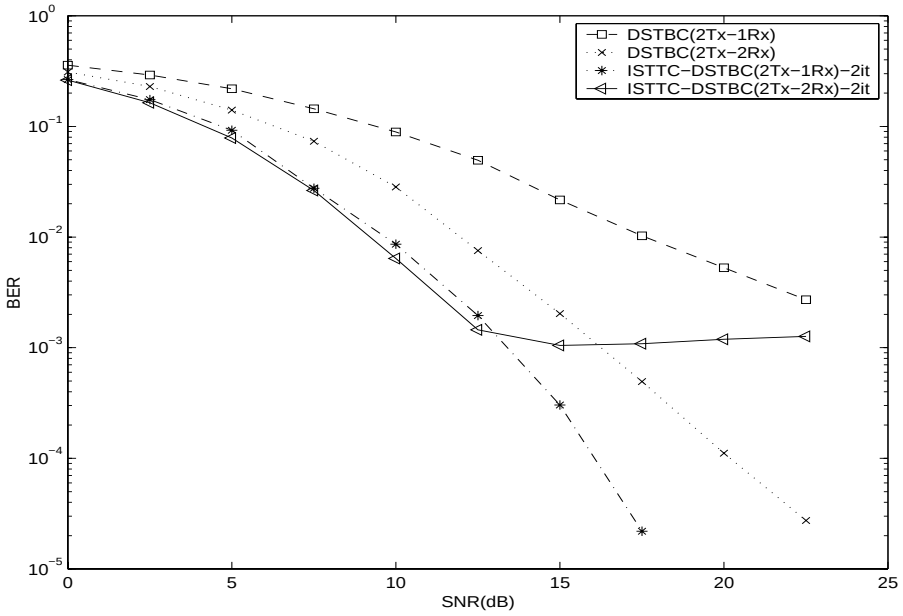

Figure 8.5: BER performance comparison between ISTTC-DSTBC and DSTBC with various number of receivers.

from DSTBC only with one receiver. It is a future research topic to clarify and cure the problems.

In this chapter, we showed design schemes of ISTTC-DSTBC, especially regarding how to pass the extrinsic information between the constituent ISTTC decoders under the difficult concatenation situation. It is a clever idea to use the soft outputs out of DSTBC for the branch metric computation. We also showed the DSTBC design schemes for a QPSK symbol mapping in detail.

Our proposed ISTTC-DSTBC without channel estimation achieves only 3dB degradation against the ISTTC-STBC with coherent detection. Our scheme without extra channel codes also shows a comparable performance against Turbo-STBC. The ISTTC-DSTBC has advantage in data transmission rate and system complexity compared with Turbo-STBC. Therefore, we can summarize the advantage of our scheme as follows. First of all,

the system complexity is reduced with channel estimation omitted and with using less complex trellis. The increase of data rate is another advantage over the typical turbo codes concatenated with space-time codes.

Chapter 9

Iteratively Decoded Space-Time Trellis Codes Combined with OFDM

Wireless communications experience multipath fading. The multipath channels can be characterized with the maximum delay spread, τ_{max} and symbol period, T_s. In time domain point of view, there is no inter symbol interference (ISI) for $\tau_{max} < T_s$. This is the frequency non-selective fading in frequency domain. However, when τ_{max} is larger than T_s for broadband, high speed transmission, the received signals are under the influence of ISI. It is called the frequency selective fading channel (FSFC) in frequency domain. The FSFC requires the equalizer at the receiver to remove ISI in case of coherent detection. As the data transmission rate increases, the complexity of equalizers also increases. The orthogonal frequency division multiplexing (OFDM) scheme was proposed to solve the complexity issue of equalizers [71]-[75].

We design the ISTTC scheme combined with the OFDM (ISTTC-OFDM) system to combat frequency selective channels. The OFDM is briefly reviewed in Section 9.1, and the modeling of FSFC is studied in Section 9.2. Design procedures of ISTTC-OFDM is described in Section 9.3. In addition, the ISTTC implemented together with the quasi-orthogonal STBC (ISTTCQ) is designed in combination with the OFDM system (ISTTCQ-OFDM). It is described in Section 9.4.

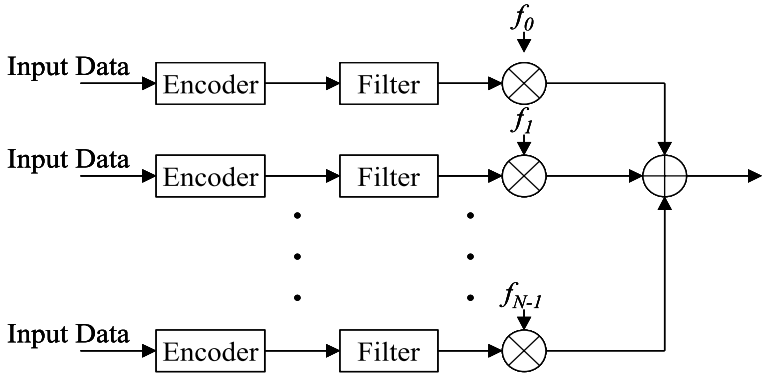

Figure 9.1: Transmitter Block Diagram for Multicarrier System.

9.1 OFDM Review

9.1.1 Multicarrier Transmission

The OFDM is a communication system that takes input data in parallel according to the number of carriers and transmits the input data modulated with those multicarriers. This multicarrier transmission basically belongs to the frequency division multiplexing method. Thus, the transmission period increases in accordance with the number of carriers, and the frequency selective channels which occur from broadband transmission over wireless channels can be approximately converted into a non-frequency selective fading channel equivalent where the ISI is removed [71][72]. Regarding this, one principle that the bandlimited signals can be transmitted simultaneously without ISI over multi-channels were introduced in 1966 [76], and one year later, the orthogonal QAM (Quadrature Amplitude Modulation) which uses both baseband filters preventing from the inter-channel interferences and banks of oscillator were proposed in [77]. Figure 9.1 and 9.2 show a transmitter and a receiver block diagram for multicarrier system. There are N modulators in Figure 9.1, which consists of encoders, filters, and carrier multipliers. In case the overall data transmission rate is R bps, the rate of each channel has R/N

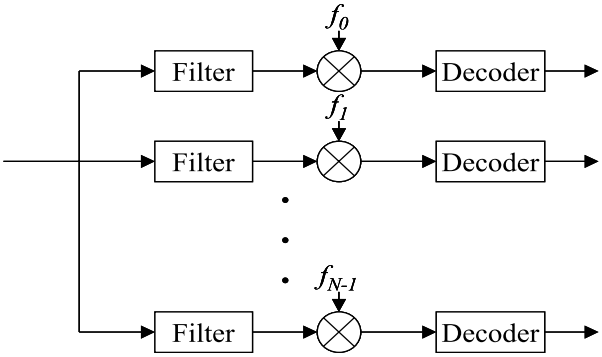

Figure 9.2: Receiver Block Diagram for Multicarrier System.

bps. The filters are used to prevent the input data from ICI. The same filters are used in the receiver end. But the use of filters and carrier oscillators increases the complexity of systems. In 1971, Weinstein and Ebert succeeded implementing the modulation and demodulation using DFT (Discrete Fourier Transform) and IDFT (Inverse DFT), and this became the fundamental structure of current OFDM systems [78]. Figure 9.3 shows transmitter and receiver block diagram for basic OFDM system structure. Input bits are turned into symbols in 'Encoder', and stored up to the size equal to the number of carriers in 'S/P' for parallel process. These parallel data are modulated with corresponding carriers and added in one OFDM symbol before transmission. Thus, for N-carriers and 2^k-ary symbols, the total bits are Nk. Here, each carrier and channel in Figure 9.3 is called as 'sub-carrier' and 'sub-channel'. The OFDM symbols at the transmitter in passband are expressed as

$$s(t) = Re\left\{ \sum_{p=-\infty}^{\infty} \sum_{k=0}^{N-1} S_{p,k} \Psi_{p,k}(t) \right\}, \tag{9.1}$$

where $S_{p,k}$ is the symbol transmitted through the kth carrier at the pth symbol period. The $\Psi_{p,k}(t)$ is given as

$$\Psi_{p,k}(t) = \begin{cases} e^{j2\pi f_k (t - pT_{sym})} & 0 \le t < T_{sym} \\ 0 & \text{otherwise} \end{cases} . \tag{9.2}$$

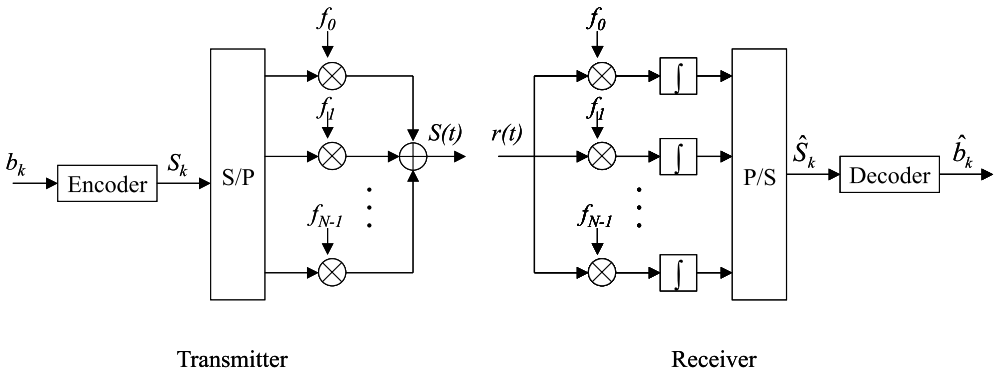

Figure 9.3: Transmitter and Receiver Block Diagram for Basic OFDM System.

The T_{sym} is the OFDM symbol period. The equation (9.2) should satisfy the following orthogonality to detect $S_{p,k}$ among the received signals.

$$\int_{-\infty}^{\infty} \Psi_{p,k}(t)\Psi^*_{p,k'}(t) = \begin{cases} T_{sym} & \text{for } k' = k \\ 0 & \text{for } k' \neq k \end{cases} . \tag{9.3}$$

The signal transmitted through each sub-channel is limited to T_{sym} in time-domain, and this can be seen as multiplying a rectangular window to the transmit signal. Thus, the spectrum is a sync function at each sub-channel. The center frequency of each sync function corresponds to the sub-carrier of the sub-channel. Since the zero-crossing occurs at $i/T_{sym}(i = \pm 1, \pm 2, ...)$, the orthogonality of (9.3) is met by setting the interval between the adjacent sub-carriers to be $1/T_{sym}$, and the demodulation without distortion is possible. Hence, the f_k in (9.2) is determined as

$$f_k = f_c + k/T_{sym}, \quad k = 0, 1, ..., N-1, \tag{9.4}$$

where f_c is the center frequency of each sub-carrier. The passband signal of (9.1) can be converted in baseband at the pth symbol period as follows,

$$s(t) = \sum_{k=0}^{N-1} S_{p,k} e^{j2\pi k(t-pT_{sym})/T_{sym}}. \tag{9.5}$$

If we sample the $s(t)$ at $t = pT_{sym} + nT_s(T_s = T_{sym}/N)$,

$$s_{p,n} = \sum_{k=0}^{N-1} S_{p,k} e^{j2\pi kn/N}, \quad n = 0, 1, ..., N-1. \tag{9.6}$$

The equation (9.6) is the IDFT, thus the baseband modulation of $s_{p,n}$ is performed through the IDFT. The demodulation at the receiver is easily achieved through the DFT. Since the DFT and IDFT are simply implemented by FFT (Fast Fourier Transform) and IFFT (Inverse FFT), the high-speed modulation and demodulation is possible. The one advantage of OFDM using FFT and IFFT is in its high spectral efficiency, and the fact that the bandpass filters at the receiver are unnecessary is another advantage.

Succeeding the Weinstein and Ebert's research, Peled and Ruiz solved the orthogonality issue between sub-carriers by using of the cyclic prefix as a guard band [79]. In 1981, Hirosaki succeeded in transmitting QAM signals using DFT [80], and Cimini applied the OFDM scheme to wireless channels and proposed a channel estimation scheme using the pilot tone [81].

9.1.2 Cyclic Prefix

Even though OFDM symbols are processed in a block of data, these symbols are influenced by the previously transmitted symbols during the transmission over multipath channels. Thus, we require a guardband to be inserted between the blocks of data in order to prevent the ISI. The length of the guardband (T_G) should be made longer than the maximum multipath delay (τ_{max}) to avoid ISI. That is, we set the length of the guardband to be $T_G \geq \tau_{max}$. The T_{sym} in Equation (9.2) becomes $T_{sub} + T_G$, where T_{sub} is the period of actual data. If we set all signals during T_{sub} to be '0', the ISI does not occur any more. But, the interference between sub-channels (ICI: Inter-carrier Interference) still exists. The ICI is solved by inserting cyclic prefix (CPX) for the guardband period [82]. The CPX causes, however, the bandwidth efficiency to be reduced by $T_{sub}/(T_{sub} + T_G)$. Thus, it is recommended that the T_G shouldn't be longer than one

fourth of T_{sub}. With CPX inserted, the equation (9.2) is redefined as

$$\Psi_{p,k}(t) = \begin{cases} e^{j2\pi f_k(t-pT_{sym})} & -T_G \leq t < T_{sub} \\ 0 & \text{otherwise} \end{cases} . \tag{9.7}$$

Hence, equations (9.5) and (9.6) can be replaced by followings

$$s(t) = \sum_{k=0}^{N-1} S_{p,k} e^{j2\pi \frac{k}{T_{sub}}(t-pT_{sym})}, \tag{9.8}$$

$$s_{p,n} = \sum_{k=0}^{N-1} S_{p,k} e^{j2\pi kn/N}, \quad n = 0, 1, ..., N-1, \tag{9.9}$$

where (9.9) is obtained by sampling (9.8) at $t = pT_{sym} + \frac{nT_{sub}}{N}$. The received baseband signal $r(t)$ over multipath channels is

$$r(t) = s(t) * h(t) + w(t), \quad pT_{sym} \leq t \leq pT_{sym} + T_{sub}, \tag{9.10}$$

where '*' is the convolution operation. The $h(t)$ is the impulse response of multipath channels, whose magnitude and phase are Rayleigh and uniform distributed respectively. The $w(t)$ is AWGN with zero mean and variance σ^2. The sampled received signals are,

$$r_{p,n} = \sum_{k=0}^{N-1} S_{p,k} H_{p,k} e^{j2\pi kn/N} + w_{p,n}, \quad n = -N_G, ..., -1, 0, 1, ..., N-1. \tag{9.11}$$

The $H_{p,k}$ is the frequency response at the pth symbol period and the kth sub-channel. The CPX is stripped off, then $r_{p,n}$ is demodulated after passing through FFT as follows

$$R_{p,m} = S_{p,m} H_{p,m} + W_{p,m}, \quad m = 0, 1, ..., N-1. \tag{9.12}$$

The $W_{p,m}$ is the AWGN in frequency domain. Therefore, under the ideal synchronization and the condition $T_G \geq \tau_{max}$, we can draw an OFDM equivalent over N independent flat fading channels as in Figure 9.4.

Several new parameters are introduced in this chapter. First of all, we denote the modulated signal $s(t)$, $s_{p,n}$, and the received signal $r(t)$, $r_{p,n}$ to be OFDM symbols. All the signals between the IFFT of transmitter end and the FFT of receiver end are

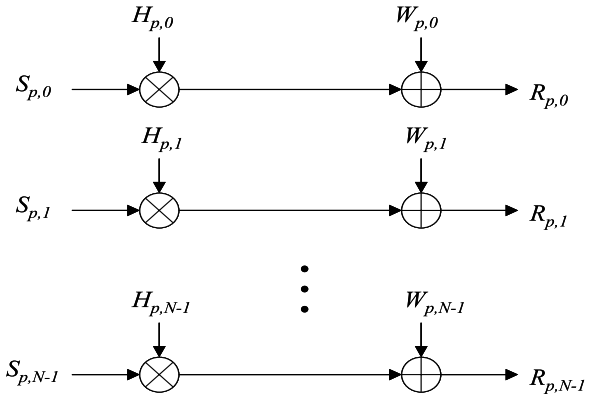

Figure 9.4: OFDM Equivalent Model.

in time-domain, and these are denoted in the lower case letters. For continuous time signals $s(t)$, $r(t)$, the t is the continuous time index, whereas for sampled signals $s_{p,n}$, $r_{p,n}$, the n is the sampled time index. All the signals before taking the IFFT and after taking the FFT are in frequency domain, and they are denoted in capital letters. The subscript k and m represent the subchannel indexes. Finally, the subscript p of OFDM symbol period is denoted whenever it is necessary.

9.2 Frequency Selective Fading Channel

The Rayleigh fading simulator based on Clarke's model was reviewed in Section 2.1.2. The Rayleigh fading simulator may be used in conjunction with variable gains and time delays to generate frequency selective fading effects [51]. It is shown in Figure 9.5. The impact of more than one multipath component is modeled by a convolution between the information signal and the channel state information.

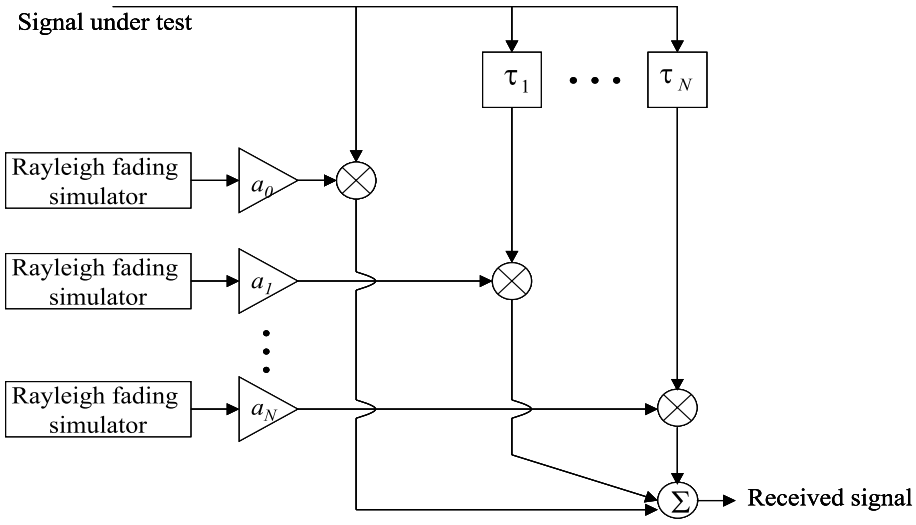

Figure 9.5: Frequency selective fading channel model according to gain and time delay setting.

9.3 ISTTC-OFDM

The ISTTC scheme introduced in Chapter 6 requires an OFDM system to perform over FSFC. For the same constituent STTC scheme of Figure 6.1, we can design the ISTTC-OFDM as in Figure 9.6. Figure 9.6 shows the block diagram for the transmitter end of ISTTC-OFDM. We assume that a total bandwidth of F Hz is available and it is divided into l sub bands. The constituent encoder, 'STTC 0' gives outputs, S_{k-1} and S_k, when it takes S_k as an input symbol at the kth sequence. The encoder 'STTC 1' takes interleaved version of data $S_k^{'}$ as an input and gives out $S_{k-1}^{'}$ and $S_k^{'}$. Those S_{k-1} and S_k are conveyed to the transmitter 0 (Tx 0) and transmitter 1 (Tx 1), respectively at one symbol sequence through 'MUX'. The interleaved data $S_{k-1}^{'}$ and $S_k^{'}$ are also conveyed to each respective transmitter at the next symbol sequence. These interleaved and non-interleaved data are alternately transmitted and stored in 'S/P' up to the size

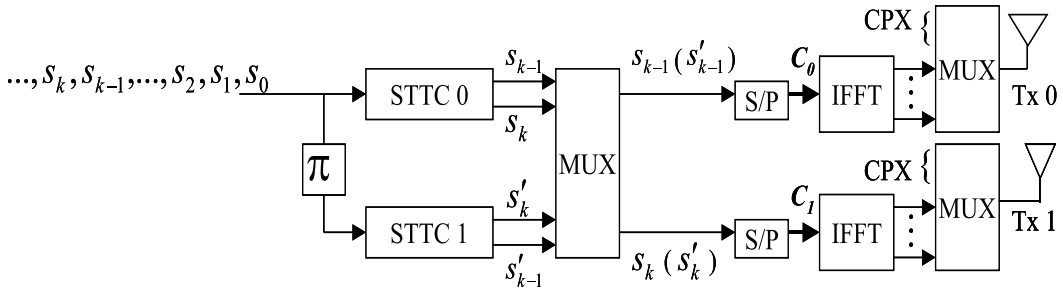

Figure 9.6: ISTTC-OFDM transmitter block diagram.

(l) of 'IFFT'. The output of 'S/P' is a codeword of the form

$$\begin{aligned} C_0 &= S_0, S_1, S_2, S_3, ..., S_{k-1}, S_k, ..., S_{l-2}, \\ C_1 &= S_1, S_2, S_3, ..., S_{k-1}, S_k, ..., S_{l-2}, S_{l-1}, \end{aligned} \tag{9.13}$$

where S_k belongs to a constellation such as M-PSK. We append a cyclic prefix (CPX) to each OFDM frame, C_0 or C_1 to avoid any ISI possibly due to the delay spread of the channel.

We assume that the fading remains constant during the transmission of an OFDM frame and it changes from a frame to another. The channel corresponding to each pair of transmit and receive antennas is modeled by a two-ray equal-power delay profile. The signal at each receiver is the superposition of the faded N transmitted signals added with AWGN, where N is 2 for the system of Figure 9.6. Figure 9.7 shows the block diagram for the receiver end of ISTTC-OFDM. After CPX is stripped off each frame and 'FFT' is applied to the incoming received signals, the output passed to the ISTTC decoder is given by:

$$R_{k,m} = \sum_{n=0}^{N-1} H_{n,m}^{k} C_n^k + W_m^k, \tag{9.14}$$

where $H_{n,m}^{k}$ are the frequency response of the channel between the n-th transmitter and the m-th receiver at k-th multi carrier frequency (kF/l). In this paper, it is assumed that the perfect channel state information is available to the decoder. The W_m^k is an independent samples of a Gaussian random variable with variance N_0. The $R_{k,m}^{'}$ is the

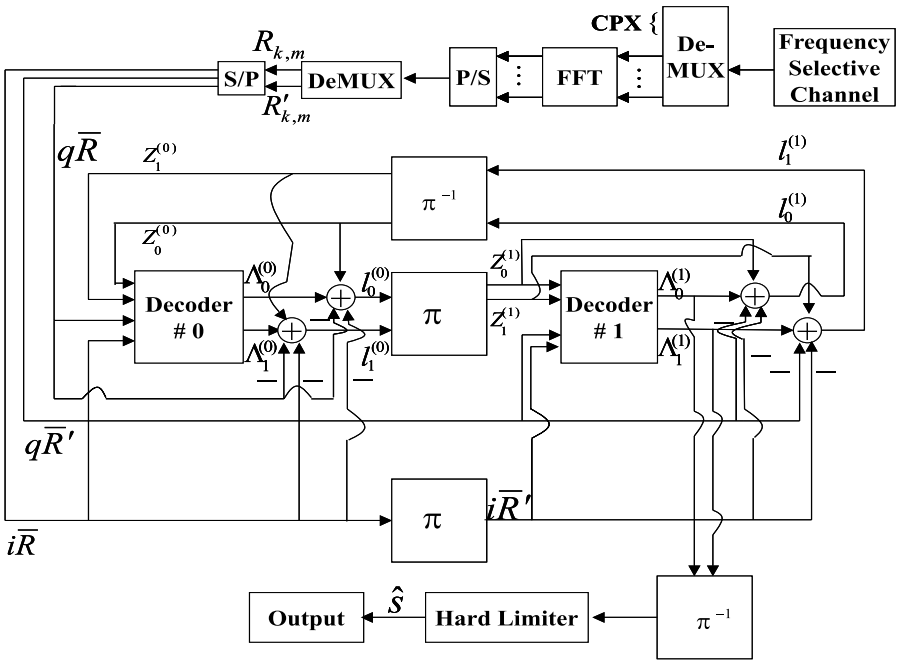

Figure 9.7: ISTTC-OFDM receiver block diagram.

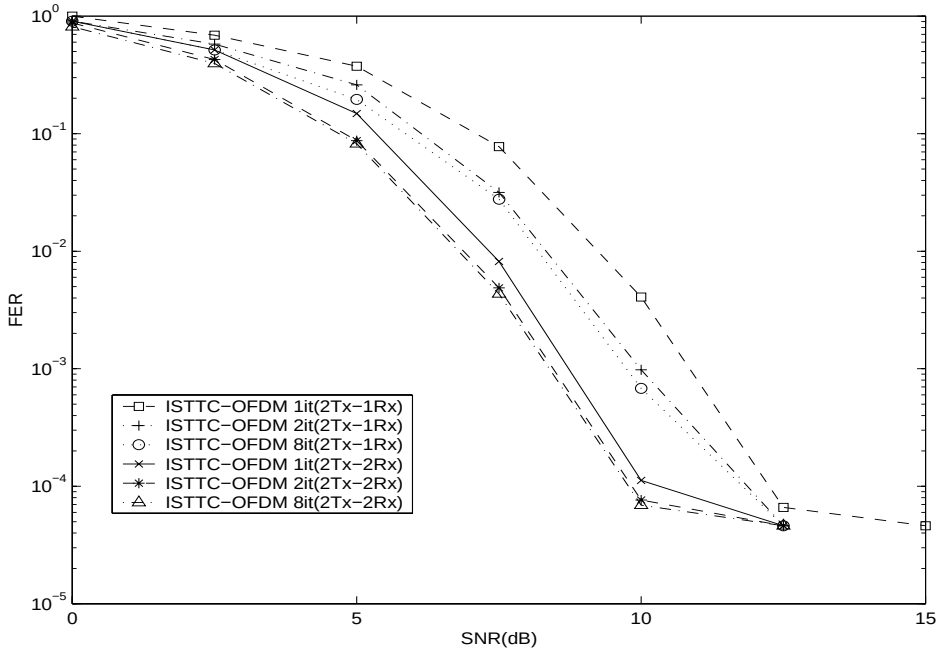

Figure 9.8: FER performance of ISTTC-OFDM with 1 or 2 receivers run in 1, 2, or 8 iterations between two constituent decoders over frequency selective channel.

interleaved version of $R_{k,m}$.

The serial-to-parallel ('S/P') converter stores the incoming data, $R_{k,m}$ and $R'_{k,m}$ over the duration of trellis length. The trellis length is an integer multiple of OFDM frames. Those blocks of incoming data are denoted as $\bar{R}$ and $\bar{R}'$ in the Figure. The parameters $i\bar{R}$, $q\bar{R}$, $i\bar{R}'$, and $q\bar{R}'$ in Figure 9.7 represent the in-phase or quadrature-phase components of $\bar{R}$ and $\bar{R}'$. These are fed to the MAP decoder '# 0', or '# 1' in Figure 9.7. Then the rest of the decoding procedures are equal to the ISTTC scheme.

The FER performance of ISTTC-OFDM is shown in Figure 9.8. The results are obtained over the frequency selective fading channel. The channel is modeled in a two-ray equal-power delay profile. The frame size of FER is 256 bits, which is equal to the number of carrier tones (l). For each constituent STTC, the same STTC scheme with 4-state as the ISTTC one illustrated in Chapter 6 is used. Each symbol in this STTC corresponds

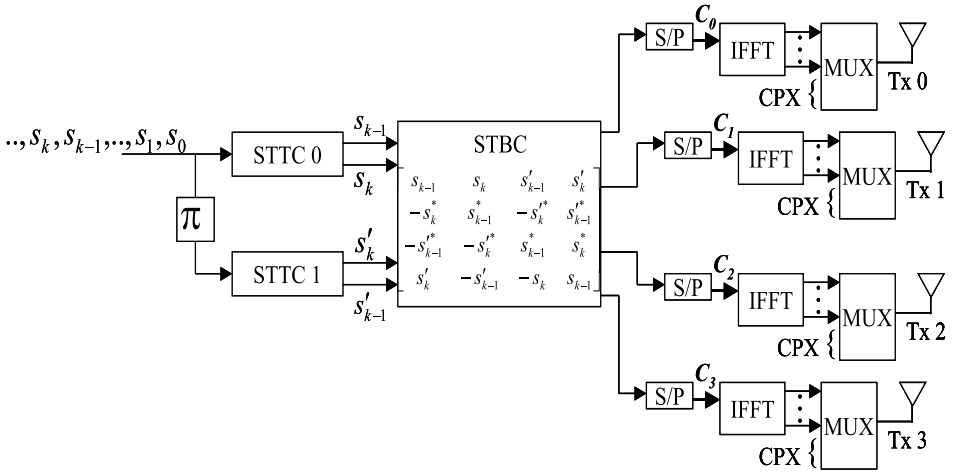

Figure 9.9: ISTTCQ-OFDM transmitter block diagram.

to a path of length 4096 in the trellis which can be chosen by a block of 8192 bits. The trellis length is an integer multiple of the number of carrier tones (l). We can observe about 2 dB advantage for 2 receivers. For SNR 7.5 dB, the FER of 0.04 is obtained for ISTTC-OFDM (1 receiver) with two iterations between constituent STTC decoders. From the given simulation results, under the assumption that the perfect channel estimation is available to the receiver, we can see that ISTTC-OFDM is capable of reliable transmission over frequency selective channels.

9.4 ISTTCQ-OFDM

In this Section, we add an OFDM system to ISTTC-STBC. The design scheme of ISTTC-STBC was described in Chapter 7. The encoder block diagram for the iteratively decoded STTC combined with STBC and OFDM systems is shown in Figure 9.9. The STBC in Figure 9.9 is designed in quasi-orthogonal method [22]. We name the system as ISTTCQ-OFDM in this dissertation. For the system in Figure 9.9, we take the STBC of G_4 (2.38). The S_k^* represents the complex conjugate of S_k. Two symbols each from

'STTC 0' and 'STTC 1' comprise the STBC matrix. That is, S_{k-1} and S_k came from 'STTC 0', and S'_{k-1} and S'_k are fed from 'STTC 1', respectively. The 'S/P's in Figure 9.9 store the incoming data upto the size (l) of 'IFFT'. The outputs of 'S/P's are codewords C_0, C_1, C_2, and C_3. The C_0 are sequences of symbols in the first column of the matrix (2.38). The C_1, C_2, and C_3 correspond to the second, third, and the fourth column, respectively. The CPX are appended to each OFDM frame, C_0 through C_3. The codewords are transmitted over the frequency selective channel environment. We assume that the fading remains constant during the transmission of an OFDM frame and it changes from a frame to another. The channel corresponding to each pair of transmit and receive antennas is modeled by a two-ray equal-power delay profile. The signal at each receiver is the superposition of the faded N transmitted signals added with AWGN, where N is 4 for the system of Figure 9.9.

Figure 9.10 shows the receiver block diagram of ISTTCQ-OFDM. After the received signals whose CPX is stripped off each frame, pass through 'FFT' and 'P/S', they are taken to the 'STBC soft decision Decoder'. Then, the output, $R_{k,m}$, $R'_{k,m}$ is given as (9.14), and the rest of the procedures are identical to the ISTTC-OFDM scheme.

The FER performance of ISTTCQ-OFDM is shown in Figure 9.11. The results are obtained over the frequency selective fading channel. The channel environment is identical to the channel of ISTTC-OFDM scheme in Section 9.3. The same trellis, FFT size, and STTC scheme as ISTTC-OFDM one in Section 9.3 are used for the ISTTCQ-OFDM scheme. The ISTTCQ-OFDM scheme with two receivers achieves 6.5 dB gains over the ISTTCQ-OFDM with one receiver for the FER of 10^{-2}. The ISTTCQ-OFDM is better performed with two receivers. Under the assumption that the perfect channel estimation is available to the receiver, it is observed that the ISTTCQ-OFDM provides the reliable performance over frequency selective channels.

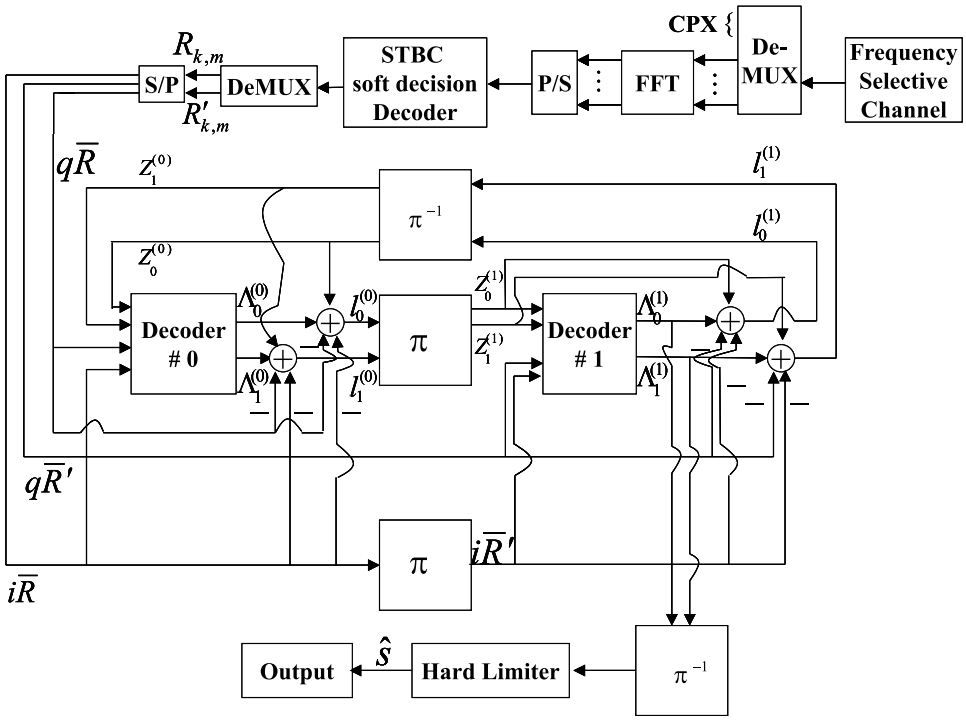

Figure 9.10: ISTTCQ-OFDM receiver block diagram.

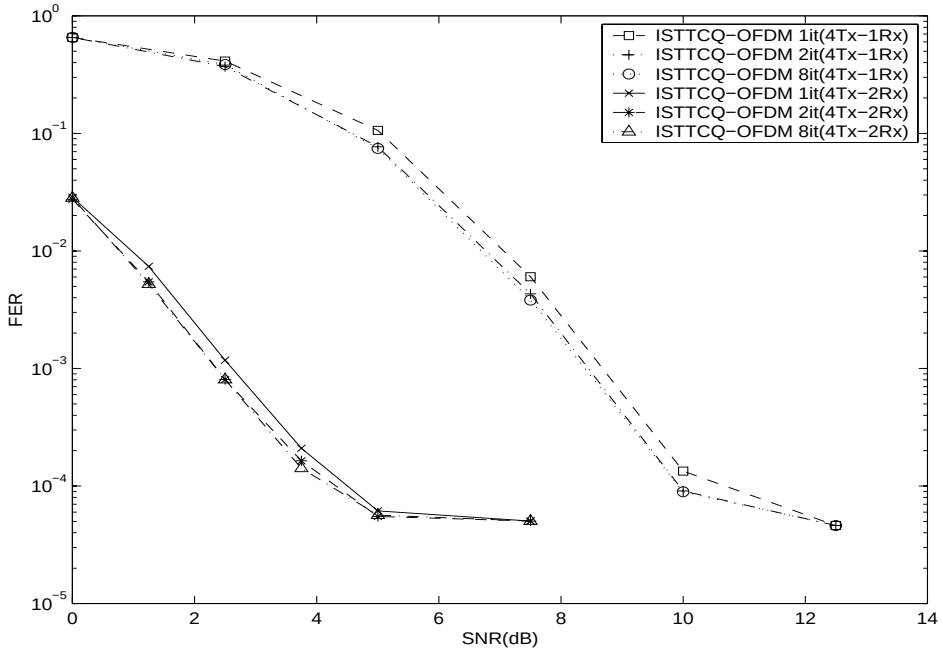

Figure 9.11: FER performance of ISTTCQ-OFDM with 1 or 2 receivers run in 1, 2, or 8 iterations between two constituent decoders over frequency selective channel.

Chapter 10

Research Contributions and Future Works

Hostile channel environments, limited bandwidth, and power resources are impairments in the modern digital communications. These problems became our research goals to overcome. Standalone existing schemes like STC and turbo coding principle cannot overcome the above limitations. Developing new schemes based on the STC and turbo code is the contribution of the research. We proposed new schemes, derived their necessary theoretical results, and showed their performance via simulations. We also analyzed the existing schemes and derived the performance bounds of our proposed schemes.

10.1 Research Contributions

The original contributions are summarized as follows, where the related publications are also listed.

A. The equations for soft decision made at decoders of various STBC systems including the quasi-orthogonal method were derived. (Sections 2.2.2 and 4.1)

B. The formula to compute the channel state information (CSI) for any STBC scheme was introduced so that decoding of STBC can be performed without the extra

channel estimation scheme. (Section 5.1)

C. Serial concatenations of turbo codes to STBC with or without channel estimations were accomplished to improve coding gains and diversity gains together. (Sections 4.1 and 5.2)

D. The iteratively decoded STTC (ISTTC) was proposed, that is, the STTC schemes were used as constituent codes of a turbo code scheme. (Section 6.1)

E. The BER performance upper bound on ISTTC was derived using the transfer function bounding technique. (Section 6.2)

F. Using the fact that it improves BER performance to combine STTC and STBC together, we combined the ISTTC with STBC to observe more performance gains. (Section 7.1)

G. The DSTBC scheme was implemented in a QPSK modulation, and combined with ISTTC to achieve better performance without extra channel codes and channel estimation. (Section 8.2)

The A and C were summarized and published in the IEEE VTC, 2001 [26]. Some of the design schemes listed in A, B, and C were reported in the IEEE VTC, 2001 [25]. The design schemes of [25] were extended to any STBC scheme in [24]. The D, E, and F were summarized and published in the IEEE WCNC, 2004 [16], and also these materials were written for a Journal publication and submitted to the IEEE Transactions on Vehicular Technology. The DSTBC combined with ISTTC in G were submitted to the IEEE GLOBECOM, 2004 and IEEE MILCOM, 2004, and they are under review now.

10.2 Future Works

Our dissertation research was focused mostly on the system over flat fading channels, although frequency selective channels (FSC) were briefly studied in Chapter 9. The

orthogonal frequency division multiplexing (OFDM)is one of the widely used solutions to overcome FSC. Most of our studied schemes can be combined with OFDM for FSC channels.

This dissertation has focused on the analytical and simulation based results. These simulation-based results can be verified via hardware implementation. A hardware description language such as VHDL can be used to simulate and synthesize it on a specific target field programmable gate array (FPGA). The VHDL is a low-level programming language closer to the hardware than C-program or MATLAB that we used for simulations and system-level designs through the entire dissertation research. Currently, there are several ways developed to generate the VHDL more easily from the higher-level languages such as C or MATLAB. Hence, we can summarize a possible future work plan as follows.

First, we need to develop the interface to combine an OFDM system with ISTTC-DSTBC. Even though the OFDM systems require accurate channel estimations, by combining ISTTC-DSTBC, we can achieve an OFDM system without channel estimation. The ISTTC-DSTBC combined with OFDM might provide coding gains in addition to diversity gains over FSC.

Second, since the OFDM systems need accurate channel estimations, sophisticated channel estimators are needed to be developed.

Finally, presently the information theorists, the system design engineers, and the hardware designers work independently to design and integrate communication hardware systems, and the process takes long time to develop. Software defined radio (SDR) integrates all these independent works and develop a hardware communication systems efficiently using some of the tools like Simulink, Real-Time Workshop, Xilinx System Generator, etc. Our work can provide the necessary simulated results for a SDR based design.

Bibliography

Bibliography

[1] G. Ungerboeck, "Channel coding with multilevel phase signals," *IEEE Transactions on Information Theory*, vol. IT-28, pp. 5666, Jan. 1982.

[2] G. Ungerboeck, "Trellis coded modulation with redundant signal sets, part I : Introduction," *IEEE Communications Magazine*, vol.25, no.2, pp. 511, 1987.

[3] G. Ungerboeck, "Trellis coded modulation with redundant signal sets, parts II : State of the art," *IEEE Communications Magazine*, vol.25, no.2, pp. 1221, 1987.

[4] E. Biglieri, D. Divsalar, P. McLane, and M. Simon, *Introduction to Trellis-Coded Modulation with Applications*, MacMillan, 1991.

[5] A. Naguib, N. Seshadri, and A. Calderbank, "Increasing data rate over wireless channel," *IEEE signal processing magazine*, pp. 76-92, May 2000.

[6] G. Foschini and M. Gans, "On limits of wireless communications in a fading environment when using multiple antennas," *Wireless Comm. Magazine*, vol. 6, pp. 311-335, Mar. 1998.

[7] V. Tarokh, N. Seshadri, and A. Calderbank, "Space-time codes for high data rate wireless communication: Performance criterion and code construction," *IEEE Transactions on Information Theory*, vol. 44, No. 2, pp. 744-765, Mar. 1998.

[8] V. Tarokh, H. Jafarkhani, and A. Calderbank, "Space-time block coding for wireless communications: Performance results," *IEEE Journal on Selected Areas in Comm.*, vol. 17, No. 3, pp. 451-460, Mar. 1999.

[9] Yufei Wu, "Implementation of parallel and serial concatenated convolutional codes," Ph.D Dissertation, Bradley Dept. of Elect. & Comp. Eng., Virginia Tech, Apr. 2000.

[10] I. Brodsky, *Wireless: The Revolution in Personal Telecommunications*, Boston, MA: Artech House Publishers, 1995.

[11] P. Rooyen, M. Lotter, and D. Wyk, *Space-time processing for CDMA mobile communications,* Norwell, Massachusetts: Kluwer Academic Publishers, 2000.

[12] W. C. Y. Lee, "Smaller cells for greater performance", *IEEE Communication Magazine*, pp. 19-23, Nov. 1991.

[13] Ran Gozali, "Space-time codes for high data rate wireless communications," Ph.D Dissertation, Bradley Dept. of Elect. & Comp. Eng., Virginia Tech, Apr. 2002.

[14] R. Mostafa, F. Alam, and K. Bae, "3G-around the world and back again," *RF Design*, pp. 52-66, Feb. 2002.

[15] J. Proakis, *Digital communications*, third edition, McGraw-Hill Inc., 1995.

[16] Junghoon Suh, and Mostofa K. Howlader, "Iteratively decoded space-time trellis codes," IEEE WCNC, Mar. 2004.

[17] D. Cui, and A. Haimovich, "Performance of parallel concatenated space-time codes," *IEEE Communications Letters*, vol. 35, No. 20, , pp. 1707-1708, Sep. 1999.

[18] W. Firmanto, Z. Chen, B. Vucetic, and J. Yuan,"Design of space-time turbo trellis coded modulation for fading channels," IEEE Globecom, vol. 2, pp. 1093-1097, Nov. 2001.

[19] D. Agarwal, V. Tarokh, A. Naguib, and N. Seshadri, "Space-time coded OFDM for high data rate wireless communication over wideband channels," IEEE VTC, pp. 2232-2236, May 1998.

[20] V. Tarokh, "Space-time block codes from orthogonal designs," *IEEE Transactions on Information Theory*, vol. 45, No. 5, pp. 1456-1467 Jul. 1999.

[21] S. Alamouti, "A simple transmit diversity technique for wireless communications," *IEEE Journal on Select Areas in Comm.*, vol. 16, No. 8, pp. 1451-1458, Oct. 1998.

[22] H. Jafarkhani, "A Quasi-Orthogonal Space-Time Block Code," *IEEE Transactions on Communications*, vol. 49, No. 1, pp. 1-4, Jan. 2001.

[23] V. Tarokh, S. Alamouti, and P. Poon,"New detection schemes for transmit diversity with no channel estimation," IEEE ICUPC, pp. 917-920, Oct. 1998.

[24] J. Suh and M. Howlader, "Concatenation of Turbo codes to space-time block codes with no channel estimation," IEEE MILCOM, vol. 1, pp. 726-731, Oct. 2002.

[25] Junghoon Suh and M.M.K. Howlader, "Concatenation of turbo codes with transmit diversity without channel estimation," IEEE VTC, pp. 1228-1232, May 2002.

[26] Junghoon Suh and M.M.K. Howlader, "Design schemes of space-time block codes concatenated with turbo codes," IEEE VTC, pp. 1030-1034, May 2002.

[27] V. Tarokh, and H. Jafarkhani, "A differential detection scheme for transmit diversity," *IEEE Journal on Select Areas in Comm.*, vol. 18, No. 7, pp. 461-471, Jul. 2000.

[28] H. Jafarkhani, and V. Tarokh, "Multiple transmit antenna differential detection from generalized orthogonal designs," *IEEE Transactions on Information Theory*, vol. 47, No. 6, pp. 2626-2631, Sep. 2001.

[29] B. Hughes, "Differential space-time modulation," *IEEE Transactions on Information Theory*, vol. 46, pp. 2567-2578, Nov. 2000.

[30] B. Hochwald and W. Sweldens, "Differential unitary space-time modulation," *IEEE Transactions on Communications*, vol. 48, pp. 2041-2052, Dec. 2000.

[31] C. Shannon, "A mathematical theory of communication," *Bell Sys. Tech. J.*, vol. 27, pp. 379-423 and 623-656, 1948.

[32] R. Hamming, "Error detecting and correcting codes," *Bell Sys. Tech. J.*, vol. 29, pp. 147-160, 1950.

[33] M. Golay, "Notes on digital coding," *Proc. IEEE*, vol. 37, pp. 657, 1949.

[34] S. Wicker, *Error Control Systems for Digital Communications and Storage*, Englwood Cliffs, NJ: Prentice Hall, Inc., 1995.

[35] R. Bose and D. Ray-Chaudhuri, "On a class of error correcting binary group codes," *Information and Control*, vol. 3, pp. 68-79, Mar. 1960.

[36] I. Reed and G. Solomon, "Polynomial codes over certain finite fields," *SIAM Journal on Applied Mathematics*, vol. 8, pp. 300-304, 1960.

[37] W. Peterson, "Encoding and error correction procedures for the Bose-Chaudhuri codes," *IRE Trans. Inform. Theory*, vol. IT-6, pp. 459-470, Sep. 1960.

[38] R. Chien, "Cyclic decoding procedures for Bose-Chaudhuri-Hocquenghem codes," *IEEE Trans. Inform. Theory*, vol. IT-10, pp. 357-363, Oct. 1964.

[39] G. Forney, "On decoding BCH codes," *IEEE Trans. Inform. Theory*, vol. IT-11, pp. 549-557, Oct. 1965.

[40] E. Berlekamp, "Non-binary BCH decoding," in *IEEE Int. Symp. on Inform. Theory*, (San Remo, Italy), 1967.

[41] E. Berlekamp, *Algebraic Coding Theory*, New York: McGraw-Hill, 1968.

[42] P. Elias, "Coding for noisy channels," in *IRE Convention Record*, vol. 3, pp. 37-46, 1955.

[43] A. Viterbi,"Error bounds for convolutional codes and an asymptotically optimum decoding algorithm," *IEEE Trans. Inform. Theory*, vol. IT-13, pp. 260-269, Apr. 1967.

[44] Bahl L.R., Cocke J., Jelinek F., and Raviv J., "Optimal Decoding of Linear Codes for Minimizing Symbol," *IEEE Transactions on Information Theory*, pp. 284-287, Mar. 1974.

[45] G. Berrou, A. Glavieux, P. Thitmajshima, "Near Shannon limit error-correcting coding: Turbo Codes," Proc. of International Conf. on Comm., pp1064-1070, Geneva, May 1993.

[46] J. Hagenauer, and P. Hoeher, "Optimal Decoding of Linear Codes for Minimizing Symbol," *IEEE Transactions on Information Theory*, pp. 284-287, Mar. 1974.

[47] P. Robertson, P. Hoeher, and E. Villebrun, "Optimal and sub-optimal maximum a posteriori algorithms suitable for turbo decoding," *European Trans. on Telecommun*, vol. 8, pp. 119-125, Mar. 1997.

[48] D. Divsalar, and F. Pollara, "Serial and hybrid concatenation codes with applications," in *Proc., Int. Symp. on Turbo Codes and Related Topics*, (Brest, France), pp. 80-87, Sep. 1997.

[49] P.W. Wolniansky, G.J. Foschini, G.D. Golden, and R.A. Valenzuela,"V-BLAST: an architecture for realizing very high data rates over the rich-scattering wireless channel," URSI International Symposium on ISSSE, pp. 295-300, 29 Sep. - 2 Oct. 1998.

[50] R.H. Clarke, "A Statistical Theory of Mobile-radio Reception," *Bell Systems Technical Journal*, vol. 47, pp. 957-1000, 1968.

[51] Theodore S. Rappaport, *Wireless communications: Principles & Practice*, Prentice Hall, Inc. 1996.

[52] S.O. Rice, "Mathematical Analysis of Random Noise," *Bell Systems Technical Journal*, vol. 23, pp. 282-332, Jul. 1944.

[53] S.O. Rice, "Statistical Properties of a Sine Wave Plus Random Noise," *Bell Systems Technical Journal*, vol. 27, pp. 109-157, Jan. 1948.

[54] M.J. Gans, "A Power Spectral Theory of Propagation in the Mobile Radio Environment," *IEEE Transactions on Vehicular Technology*, vol. VT-21, pp. 27-38, Feb. 1972.

[55] J.I. Smith, "A Computer Generated Multipath Fading Simulation for Mobile Radio," *IEEE Transactions on Vehicular Technology*, vol. VT-24, No. 3, pp. 39-40, Aug. 1975.

[56] Roger Gaspa and Javier R. Fonollosa, "Space-Time Coding for UMTS. Performance Evaluation in Combination with Convolutional and Turbo Coding," IEEE VTC, pp. 92-98, Sep. 2000.

[57] D. Divsalar and F. Pollara, "Turbo codes for deep-space communications," *TDA Progress Report 42-120, October-December 1994*, Jet Propulsion Lab., Pasadena, California, pp. 29-39, Feb. 15, 1995.

[58] D. Divsalar and F. Pollara, "Multiple turbo codes for deep-space communications," *TDA Progress Report 42-121, January-March 1995*, Jet Propulsion Lab., Pasadena, California, pp. 66-77, May 15, 1995.

[59] Shu Lin and Daniel J. Costello Jr., *Error Control Coding: Fundamental and Applications*, Prentice-Hall Inc., 1983.

[60] J. Wozencraft and B. Reiffen, "Sequential Decoding", MIT Press, Cambridge, Mass., 1961.

[61] J. Massey, "Threshold Decoding", MIT Press, Cambridge, Mass., 1963.

[62] Bernard Sklar, *Digital Communications: Fundamentals and Applications*, Prentice-Hall Inc., 1988.

[63] S. Benedetto, D. Divsalar, G. Montorsi, and F. Pollara, "Soft-output decoding algorithms in iterative decoding of turbo codes," *JPL TDA Progress Report 42-124*, Feb. 15, 1996.

[64] Eric K. Hall and Stephen G. Wilson, "Design and Analysis of Turbo Codes on Rayleigh Fading Channels," *IEEE Journal of Selected Areas in Comm.*, pp. 160-174, Feb. 1998.

[65] G. Bauch and I. Hagenauer,"Analytical Evaluation of Space-Time Transmit Diversity with FEC-Coding," IEEE Globecom, vol. 2, pp. 435-439, Nov. 2001.

[66] G. Bauch, "Concatenation of Space-Time Block Codes and Turbo-TCM," *ICC'99*, pp. 1202-1206, Jun. 1999.

[67] D. Bevan, and R. Tanner, "Performance comparison of space-time coding techniques," *IEE Electronics Letters*, vol. 35, No. 20, , pp. 1707-1708, Sep. 1999.

[68] D. Divsalar, S. Dolinar, F. Pollara, and R. McEliece, "Transfer Function Bounds on the Performance of Turbo Codes," *JPL TDA Progress Report 42-122*, pp. 44-55, Aug. 1995.

[69] S. Mason, and H. Zimmermann, "Electronic Circuits, Signals, and Systems," *JPL TDA Progress Report 42-122*, Wiley, New York, 1960.

[70] S. Benedetto, E. Biglieri, and V. Castellani, *Digital Transmission Theory*, Englewood Cliffs, New Jersey: Prentice-Hall, Inc., 1987.

[71] J. Bingham, "Multicarrier modulation for data transmission: an idea whose time has come," *IEEE Communications Magazine*, vol. 28, pp. 17-25, Mar. 1990.

[72] H. Sari, G. Karam, and I. Jeanclaude, "Transmission Techniques for digital terrestrial TV broadcasting," *IEEE Communications Magazine*, vol. 33, pp. 100-109, Feb. 1995.

[73] G. Stuber, and M. Russell, "Terrestrial digital video broadcasting for mobile reception using OFDM," IEEE Globecom, pp. 2049-2053, Nov. 1995.

[74] K. Maxwell, "Asymmetrical digital subscriber line: interim technology for the next forty years," *IEEE Communications Magazine*, vol. 34, pp. 100-106, Oct. 1996.

[75] L. Cimini, Jr., J. Chuang, and N. Sollenberger "Advanced cellular internet service (ACIS)," *IEEE Communications Magazine*, vol. 36, pp. 150-159, Oct. 1998.

[76] R. Chang, "Synthesis of band-limited orthogonal signals for multichannel data transmission," *Bell System Technical Journal*, vol. 46, pp. 1775-1796, Dec. 1966.

[77] B. Saltzberg, "Performance of an efficient parallel data transmission system," *IEEE Transactions on Communications*, vol. 15, pp. 805-811, Dec. 1967.

[78] S. Weinstein, and P. Ebert, "Data transmission by frequency division multiplexing using the discrete Fourier transform," *IEEE Transactions on Communications*, vol. 19, pp. 628-634, Oct. 1971.

[79] A. Peled, and A. Ruiz, "Frequency domain data transmission using reduced computational complexity algorithms," IEEE ICASSP, pp. 964-967, Nov. 1980.

[80] B. Hirosaki, "An orthogonally multiplexed QAM system using the discrete Fourier transform," *IEEE Transactions on Communications*, vol. 29, pp. 982-989, Jul. 1981.

[81] S. Weinstein, and P. Ebert, "Analysis and simulation of a digital mobile channel using orthogonal frequency-division multiplexing," *IEEE Transactions on Communications*, vol. 33, pp. 665-675, Jul. 1985.

[82] M. Engels, *Wireless OFDM Systems,* Norwell, Massachusetts: Kluwer Academic Publishers, 2002.

[83] V. Tarokh, A. Naguib, N. Seshadri, and A. R. Calderbank, "Space-time codes for high data rates wireless communications: Performance criteria in the presence of channel estimation errors, mobility, and multiple paths," *IEEE Transactions on Communications*, vol. 47, pp. 199-207, Feb. 1999.

[84] P. Ho and D. Fung, "Error performance of multiple-symbol differential detection of PSK signals transmitted over correlated Rayleigh fading channels," *IEEE Transactions on Communications*, vol. 40, pp. 25-29, Oct. 1992.

[85] D. Divsalar and M. Simon, "Maximum-likelihood differential detection of uncoded and trellis coded amplitude phase modulation over AWGN and fading channels-Metrics and performance," *IEEE Transactions on Communications*, vol. 94, pp. 76-89, Jan. 1994.

[86] F. Adachi, "Adaptive differential detection using linear prediction for M-ary DPSK," *IEEE Transactions on Vehicular Technology*, vol. 47, pp. 909-918, Aug. 1998.

[87] R. Schober, W. Gerstacker, and J. Huber, "Decision-feedback differential detection of MDPSK for flat Rayleigh fading channels," Communication Theory Mini-Conference, pp. 135-140, Jun. 1999.

[88] R. Schober and W. Gerstacker, "Decision-feedback differential detection based on linear prediction for MDPSK signals transmitted over Ricean fading channels," *IEEE Journal on Selected Areas in Comm.*, vol. 18, pp. 391-402, Mar. 2000.

[89] C. Cozzo, D. Mohile and B. Hughes, "Multiple-symbol detection of differential space-time modulation," IEEE PCISS, Princeton, NJ, Mar. 2000.

[90] R. Schober and L.H.-J. Lampe, "Noncoherent receivers for differential space-time modulation," *IEEE Transactions on Communications*, vol. 50, pp. 768-777, May 2002.

[91] P. Fan, "Multiple-symbol detection for transmit diversity with differential encoding scheme," *IEEE Transactions on Consumer Electronics*, vol. 47, pp. 96-100, Feb. 2001.

[92] C. Gao and A. Haimovich, "Multiple-symbol differential detection for space-time block codes," IEEE PCISS, Princeton, NJ, Mar. 2002.

[93] E. Chiavaccini and G. Vitetta, "Further results on Tarokh's space-time differential technique," IEEE ICC, vol. 3, pp. 1778-1782, Apr. 2002.

[94] J. Beek, O. Edfors, M. Sandell, S. K. Wilson, and P. O. Borjesson, "On channel estimation in OFDM systems," IEEE VTC, pp. 815-819, Jul. 1995.

[95] O. Edfors, M. Sandell, J. Beek, S. K. Wilson, and P. O. Borjesson, "OFDM channel estimation by singular value decomposition," *IEEE Transactions on Communications*, vol. 46, pp. 931-939, Jul. 1998.

[96] V. Mignone and A. Morello, "CD3-OFDM: A novel demodulation scheme for fixed and mobile receivers," *IEEE Transactions on Communications*, vol. 44, pp. 1144-1151, Sep. 1996.

[97] Y. Li, L. J. Cimini, Jr., and N. R. Sollenberger, "Robust channel estimation for OFDM systems with rapid dispersive fading channels," *IEEE Transactions on Communications*, vol. 46, pp. 902-915, Jul. 1998.

[98] Y. Li, N. Seshadri, and S. Ariyavisitakul, "Channel estimation for OFDM systems with transmitter diversity in mobile wireless channels," *IEEE Journal on Select Areas in Comm.*, vol. 17, No. 3, pp. 461-471, Mar. 1999.

Vita

Junghoon Suh was born in Daegu, a south eastern city of South Korea on January, 10, 1969. He entered the Electronics Engineering department of Kyungpook National University with the full scholarship which was determined by the score of national entrance examination. After completing the sophomore, he joined the army, KATUSA (Korean Augmentation Troops to US Army) for 27 months to complete the mandatory army service. He resumed his B.E. degree on the March of 1992 and finished the B.E. degree on the February of 1994. He received his Master of Science in Engineering degree from the Arizona State University at Tempe in the Spring of 1997.

He started his Ph.D. study as a graduate teaching assistant in the University of Tennessee, Knoxville in the Fall of 1999. Currently, he works at the Wireless Communication Research Group (WCRG) under the supervision of Dr. Mostofa K. Howlader. He has been working in the areas of space-time coding and turbo coding for his Ph.D. research, and has scheduled to have the defense of dissertation on April, 2, 2004.

His future primary research interests are channel coding, modulation design, array signal processing, channel modeling, and most digital communication systems design areas which need to be jointly researched.